Photodissociation of Simple Molecules in the Gas Phase

Hiroyasu Sato*

Laser Photochemistry Research Group, Department of Chemistry for Materials, Faculty of Engineering, Mi'e University, 1515 Kamihamacho, Tsu 514-8507, Japan

Received May 31, 2000

Contents

I. Introduction

A. Motivation

What is central to chemistry? Of course the answer is by no means unique. There are so many ways of

* Present address: 750-15 Nagaokacho, Tsu 514-0064, Japan. E-mail: satlaser@ztv.ne.jp.

10.1021/cr990403l CCC: $36.00
Published on Web 09/12/2001

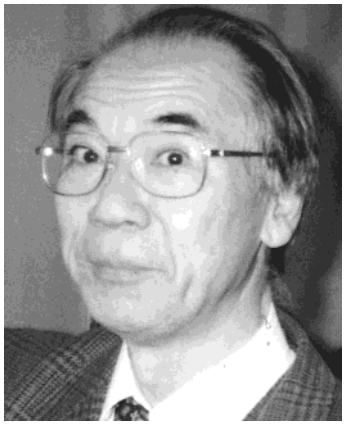

Hiroyasu Sato is born in Tokyo in 1937. He received his D.Sc. degree in 1966 from the Faculty of Science, Osaka University. He was a Research Associate in Osaka University from 1964, moved to Kagoshima University as Associate Professor in 1969, was promoted to Professor in 1977, and moved to Mi'e University in 1978. He was Adjunct Professor at the Institute for Molecular Science (1994–95). Beginning with preparative organometallic chemistry, his research interests span a rather wide field: UV and IR spectroscopy of charge-transfer complexes and adsorbed species, energy and electron transfer in (pre)micelles, Langmuir–Blodgett films and multilayers in relation to solar energy utilization, photodissociation mechanisms of small molecules and organometallic compounds related to laser CVD studied by laser-induced fluorescence and multiphoton ionization, dye aggregates and metal microparticles, magnetic field effects on photochromic dyes, photochemistry mediated by solid surfaces, reactions of metal ions with clusters by the laser ablation-molecular beam (LAMB) method, laser ablation of polymers, and more. He has received a Laser Society (Japan) Award (1994) and was Secretary of the Japanese Photochemistry Association (1992–93). He has also been the regional editor of *Applied Organometallic Chemistry* (Wiley) since 1991.

thinking: preparation of novel compounds, discovery of rules governing molecular compositions and structures, elucidation of structure−function relationships, etc. However, everyone will agree that the single fact which is really exceptional to chemistry is that molecules *react*, i.e., they reorganize themselves into another set of atom(s) and molecule(s). Then, *how* and *why* do chemical reactions occur? What is their motive force? This constitutes the motivation for the investigation on *reaction mechanisms*. Particularly, it is called *reaction dynamics* when studied in the microscopic, i.e., atomic and/or molecular level following the time evolution of every microscopic reaction step, as far as possible.

On the other hand, it has been an everlasting challenge to chemists and chemical physicists to have control over the route of chemical reactions by driving them in the desired directions. To this end one must have exact knowledge about the true nature of chemical reactions as thoroughly as possible. Eyring[1] and Evans and Polanyi[2] developed absolute reaction rate theory, in which the essential role of *the transition state* is stressed

$$\text{reactant(s)} \rightarrow \text{transition state} \rightarrow \text{product(s)} \quad (1)$$

The molecular structure of a transition state together with its energetic contents as a function of its internal coordinates determines the fate of the reaction.

When one plots the potential energy (PE) for a bimolecular reaction

$$\text{A−B + C} \rightarrow \text{[A−B−C]} \rightarrow \text{A + B−C} \quad (2)$$

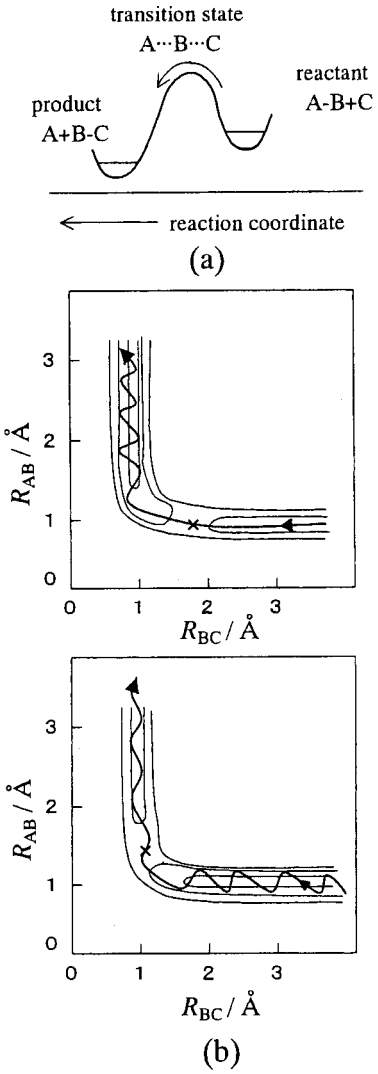

Figure 1. (a) Potential energy curve (PEC) along the reaction path. (b) Potential energy surface (PES) for the reaction A−B + C → (A···B···C) → A + B−C. (See text. Adapted from ref 3.)

along the "reaction coordinate", one obtains a potential energy curve (PEC) as shown in Figure 1a. The activation barrier is the energy difference of the transition state measured from the reactant. When one plots the PE as a function of the lengths of the ruptured and created bonds (R_{AB} and R_{BC}, respectively), one obtains the potential energy surface (PES) as schematically drawn in Figure 1b.[3] The reactant (on the left-hand side of eq 2) and the product (on the right-hand side of eq 2) correspond to a trough on the PES, respectively, and the transition state [A−B−C] to the saddle point, i.e., the point highest along the reaction path and the lowest in the direction perpendicular to it. Let us imagine that we play with a tiny ball (a representative point) rolled along the valley on the PES. As the reaction proceeds, the representative point moves on, from the entrance region (R_{AB} = const., $R_{BC} = \infty$) to the exit region ($R_{AB} = \infty$, R_{BC} = const.) along the valley on the PES. The PEC depicted in Figure 1a corresponds to the cut-through of the PES along this valley. When the transition state is on the entrance side (the barrier is called the early barrier or entrance barrier; large

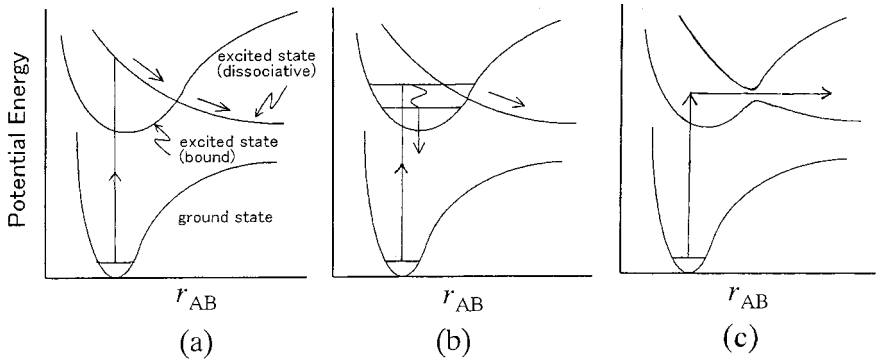

Figure 2. Potential energy curves relevant to photodissociation: (a) direct photodissociation, (b) predissociation (diabatic representation, through an intersection of two excited states), (c) predissociation (adiabatic reprentation, through an avoided crossing of two potential energy surfaces).

translational energy of A−B vs C helps the reaction in this case), the ball takes a zigzag path after it surmounts the barrier-top, i.e., the product B−C is vibrationally excited. On the contrary, when the barrier is on the exit side (late barrier or exit barrier), the ball moves quickly down the exit valley. (Large vibrational excitation of the A−B bond helps the reaction in this case.) The products A and B−C are highly translationally excited, with little vibrational excitation of the B−C bond.

A photodissociation reaction is a unimolecular reaction driven by light energy. The photodissociation reaction, e.g.

$$\mathrm{ABC} + h\nu \rightarrow \mathrm{ABC}^* \rightarrow \mathrm{A} + \mathrm{B{-}C} \qquad (3)$$

corresponds to the latter half of the bimolecular reaction. (The asterisk (*) denotes electronically excited species.) Molecules have a large number of (almost infinite) PESs corresponding to excited electronic states in addition to that of the ground electronic state. Actually the ground state simply means the electronic state that is the lowest in energy.

Although we are accustomed to the ball (an atom) and stick (a chemical bond) picture of a molecule, the world of chemistry looks, if viewed in terms of potential energy, as if many ponds (stable molecules) are separated by mountains (transition states). In such a chemistry landscape, in addition to the ground surface (the PES of ground electronic state), there are many transparent surfaces hanging in the sky (the PESs of excited electronic states). Some of the PESs cross each other, making a "seam" of surfaces. This is the landscape in which electrons (quantum mechanical wave packets) play.

Electronic transitions bring the molecule on the PES of the electronic ground state onto the PES of a particular excited electronic state (see Figure 2, which shows PECs of a diatomic molecule AB or sections of PESs along the reaction coordinate R_{AB} of a polyatomic molecule). The shape of every PES is different from all others. Because the transition occurs "instantaneously", i.e., much faster than the nuclear motion, the molecule does not change its shape during the transition. Therefore, immediately after a molecule is brought onto the PES of a particular excited state, the shape of the molecule is, in general, *not* the equilibrium one of that particular excited state. In other words, the molecule is not at the bottom of the PES. Sometimes the molecule finds itself on the steep slope of an excited state, which can lead to dissociation (as in Figure 2a). Then *direct* dissociation takes place. Even if the excited state in which the molecule is excited is a bound one and the molecule can undergo vibrations in the excited state, the molecule may either (1) cross over to a dissociative excited state through the intersection of two excited states and then dissociate (in the diabatic representation, as in Figure 2b), i.e., cross over to a dissociative region of PES through the avoided crossing of two excited states (in the adiabatic representation, as in Figure 2c), or (2) cross over to a (very high) continuum state of the ground (or one of the lower) electronic state above the latter dissociation threshold and then dissociate (*predissociation* in these cases), in competition with the radiative and nonradiative deactivation (without dissociation) to the ground electronic state.

The photodissociation reaction event occurs *under the constraint of energy and angular momentum conservation*. When the bond dissociation energy is D, the available energy

$$E_{\mathrm{AVL}} = h\nu - D \qquad (4)$$

is distributed among the translational energy (E_{T}) and internal energy (E_{INT}) of the fragments, the latter again among electronic, vibrational, and rotational energy (E_{el}, E_{V}, and E_{R}, respectively) of the photofragments. The fractions of E_{AVL} among these energies are denoted as f_{T}, f_{INT}, f_{el}, f_{V}, and f_{R}, respectively ($f_{\mathrm{T}} + f_{\mathrm{INT}} = 1$, $f_{\mathrm{INT}} = f_{\mathrm{el}} + f_{\mathrm{V}} + f_{\mathrm{R}}$). The way in which the available energy is distributed among the degrees of freedom is called *energy disposal*. Energy disposal can be very different for each case, as exemplified in Figure 3.[4−6] The most coarse-grained picture of a photodissociation reaction is manifested in such an energy disposal. More detailed dynamic characterization can be made by *vector correlation* between directional properties, electric field vector of light ($\boldsymbol{E}$), transition moment of the parent molecule ($\boldsymbol{\mu}$), velocity vector ($\boldsymbol{V}$), and angular momentum vector ($\boldsymbol{J}$) of recoiling fragments, as schematically shown in Figure 4.[7]

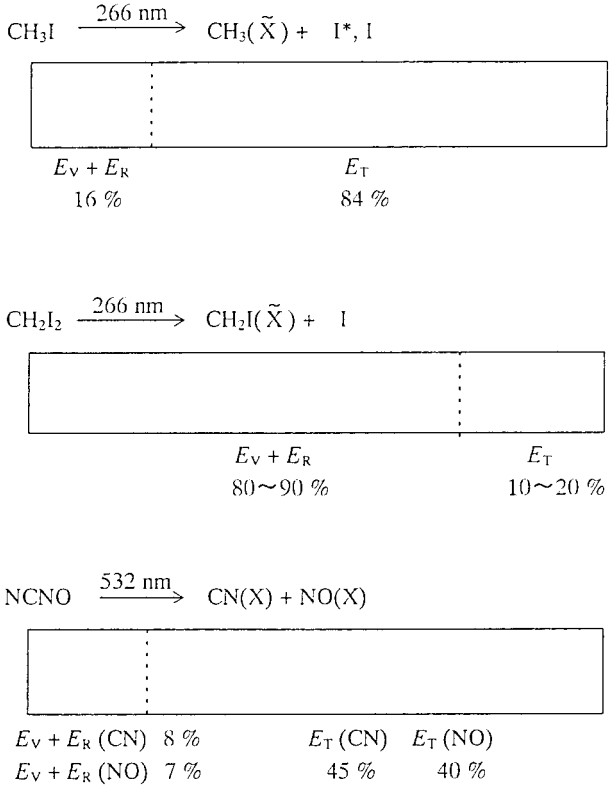

Figure 3. Examples of observed energy disposal (see text).[4−6]

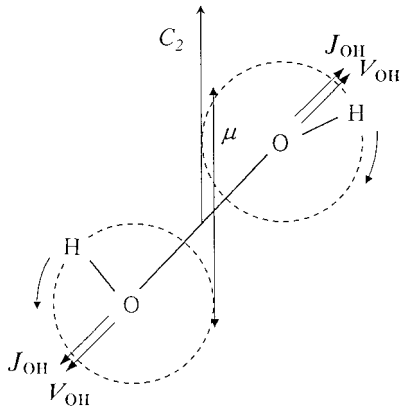

Figure 4. Vector correlations between transition dipole (***μ***), velocity of photofragment (***V***), rotational angular momentum of photofragment (***J***), taking H_2O_2 (Ã) → 2OH as an example. C_2 is the symmetry axis. (Adapted from ref 7.)

B. Rapid Progress in Photodissociation Dynamics Studies in 1970−1999

Photodissociation studies are both old and new, studied for a long time through the history of photochemistry. However, studies of photodissociation dynamics made great progress in the last three decades (1970−1999). The advent of lasers, together with the development of highly sensitive and/or fast-response detection methods, gave a large impetus to the investigation of photodissociation reaction dynamics. The year 1970 roughly corresponds to the dawn of a new era; application of lasers opened Aladdin's magic door to the secret of photodissociation. This is why the author is preparing this review at this time.

Applications of lasers have been very important to the studies of photodissociation dynamics for a variety of reasons. (1) Working in the energy (i.e., light frequency or wavelength) domain, the very narrow energy spread of laser light can be exploited in order to prepare parent molecules in a particular vibronic and even rotational−vibronic level. The fate of these molecules can be followed in a very clean way when studied in the gas phase in the absence of collisions causing energy exchange with other coexistent species.

(2) State-selective and highly sensitive detection of photofragments by laser-induced fluorescence (LIF), resonant multiphoton ionization (REMPI), etc. (described later in section II), provides a wealth of information on the distribution of photofragments among various internal states, including electronic, spin-fine structure, vibrational, rotational, and Λ-type doubling.

(3) Working in the time domain, pico- or femtosecond pulse lasers can be used to follow the time evolution of the course of reaction.

(4) Use of polarized laser light gives us a wealth of information on vectorial characteristics of photodissociation mechanisms (more details are given in sections II.G−I). Photofragment spectroscopy and a variety of its descendants as well as Doppler spectroscopy unravel vectorial correlations among many directional properties, such as transition moment of the parent (***μ***), velocity (***V***), and rotational angular momentum (***J***) of recoiling fragments. For example, the angular dependence of recoiling fragments with respect to the polarization of photodissociating laser light (***E***) gives anisotropy (the ***μ***−***V*** correlation) information. Analyses of the Doppler profile of rotational spectral lines provide us with ***μ***−***J***, ***V***−***J***, and ***μ***−***V***−***J*** correlations in addition to the ***μ***−***V*** correlation. These tell, for example, whether dissociating partners fly apart parallel or perpendicular to the transition moment of the parent molecule and whether they fly apart rotating in or out of the plane as determined by two velocity vectors.

(5) Novel laser-based methods, such as cavity ring-down spectroscopy, provide highly sensitive detection methods in addition to LIF and REMPI.

In addition to the use of lasers, the supersonic molecular beam (jet) technique enables studying the photodissociation of van der Waals molecules and clusters. These have a large significance in chemical reactions. Indeed, the direct observation of the transition PES has long been the dream of chemists. Although the observation of the transition state, per se, is not possible or a very hard task, studies of van der Waals molecules and clusters gave a most precious substitute for that before the development of femtosecond (fs) lasers (see section II.K). In another aspect, high-resolution studies of photodissociation are possible using supersonic molecular beams in conjunction with mass spectrometry. Action spectra of predissociation in the UV, visible, and IR regions give absorption spectra associated with the excited state relevant to the photodissociation process.

Although the present review intends to compile results of experimental studies, theoretical studies

also play a key role. From only experimental results (without consulting the theory), one cannot invert them back to first principles. One can have a real insight into the heart of photodissociation dynamics by comparison of experimental results with theoretical predictions. There are two types of theoretical studies: (a) those of molecular PESs by ab initio and other means and (b) those of reaction rates and the energy disposal under statistical or other assumptions. Citation of some theoretical papers in the category b is made in section III, and some papers related to category a are touched in section IV relevant to each molecule. However, these citations are restricted to the absolute minimum.

Photodissociation spectroscopy is one of the most powerful methods for the elucidation of the true nature of chemical reactions. Moreover, it leads to the clarification of a variety of (sometimes very subtle) interactions between every type of molecular freedom, which is very important in the detailed understanding of chemical bonding both in the static and dynamic context. Photodissociation spectroscopy has now become, so to speak, a new form of molecular absorption spectroscopy. Another point to be emphasized here is that such a study not only is relevant to pure science, but has many practical applications. For example, it is indispensable to studies of the global atmosphere, such as those related to the ozone hole and automobile exhaust gas issues, and interstellar chemistry. Photodissociation studies deserve, in the author's opinion, much more attention from general readers in the present and future.

C. Composition of Present Review

The present paper intends to give an overview of the dynamics of photodissociation reactions of simple molecules in the gas phase. Only photodissociation reactions of molecules composed of more than three atoms are considered because the main focus is on the interplay between internal and translational degrees of freedom and between the angular momenta of molecular rotation. The present review is meant to be general and comprehensive, providing a consistent view of this fascinating world to general interested readers, rather than to concentrate on every sophisticated detail.

The rest of this review is composed as follows. A concise description of experimental methods is given in section II. Theoretical models of reaction rates and energy disposal in molecular photodissociation are given in section III. In section IV some typical molecules (and classes of molecules) on which a large amount of research effort has been made are selected as examples. Only selected papers are cited in the text to provide highlights of research work made to date rather than to be complete. Readers are referred to the tables in the Supporting Information for more complete listings on these compounds.

There are several outstanding books and reviews, the latter being more or less concentrated on a particular aspect of interest.[8−18] The present author has published two books[19] which compiled experimental data on more than 400 simple molecules and

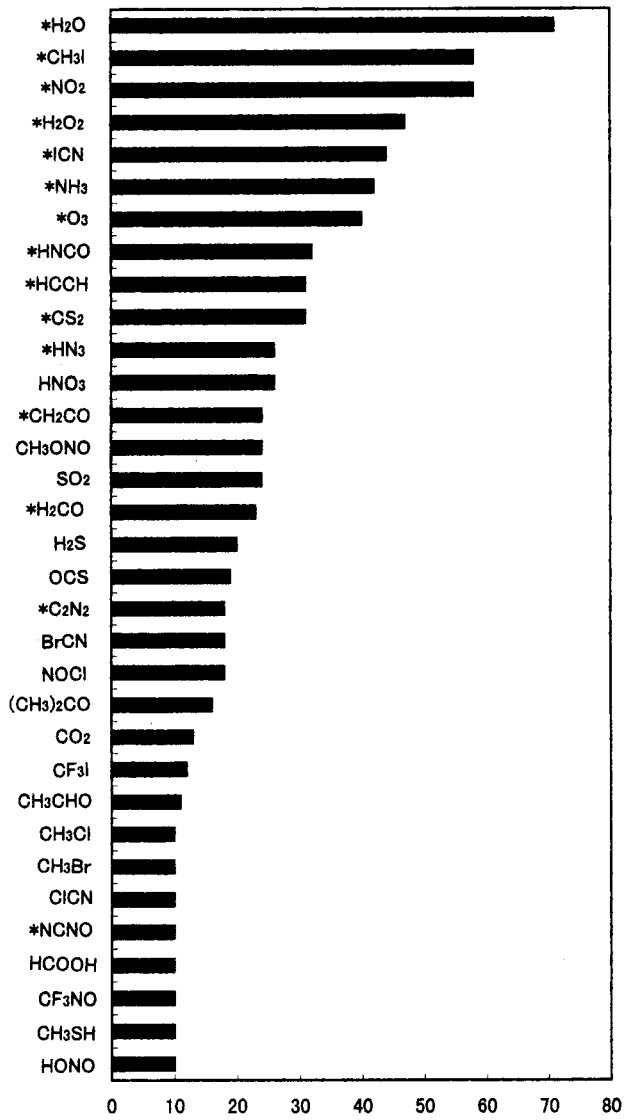

Figure 5. Numbers of papers listed in the author's compilations, ref 19, with a little addition. The numbers are only approximate because many papers may have inadvertently eluded the author's attention. Compounds marked with an asterisk (*) are in the present review.

130 van der Waals molecules/clusters taken from more than 1600 original papers published worldwide from 1970 to 1999. The compilation, meant to be exhaustive as far as possible, was originally published in *Research Reports of the Faculty of Engineering, Mie University*.[20] Figure 5 comprises a list of papers compiled in these two books by the present author, which should help readers find the general trends of this research field. The compounds with an asterisk are the ones treated in the present review.

The content of the present review is taken from original papers compiled in these two books,[19] but the purpose here is to be comprehensive and critical, while the books were meant to compile all the data *as published in the original articles*. Some papers which inadvertently were not included in the two books are now added. The coverage of the present review is from 1970 to approximately the end of 1999, although a few papers published in 2000 are newly added. Papers on infrared multiphoton dissociation (IRMPD) are not included. Papers on infrared pre-

dissociation of van der Waals molecules and clusters are included.

Interestingly, the history of photodissociation studies starts from the high-energy side, UV and vacuum UV, where emission measurements played the major role. Excimer lasers were used very conveniently for some time. As time went on, every delicate point near the photodissociation threshold attracted much attention, for which high-resolution tunable laser sources and highly sensitive and/or high-resolution measurements are the absolute prerequisite. Thanks to the development of many new strategies, viz. supersonic molecular beam, sub-Doppler measurement, velocity-aligned ion imaging, and double-resonance techniques like vibrationally mediated photodissociation, photodissociation studies on some molecules have now reached the highest possible scrutiny except, perhaps, for the aspect of coherence (memory of phase).

D. Briefs for Busy Readers

It may be relevant to collect the "essence" of photodynamics studies for busy readers who are not familiar with this field. Even if a reader does not want further readings, he or she may have a touch of the fragrance of this field.

1. Energy Balance

By knowing the balance of energy "income" and "outcome", one can grasp the most coarse-grained picture of the photodissociation process. The "surplus" energy, which is the input photoenergy minus the dissociation energy, is called available energy (E_{AVL}). The distribution of E_{AVL} among a variety of internal (electronic, vibrational, rotational, spin fine structure, Λ -type doubling) and "external" (translational) degrees of freedom is called "energy disposal".

2. Vector Correlations

While energy is a scaler quantity (without any directional property), there are many kinds of directional properties associated with the electronic transition, vibration, rotation, spin alignment, fragment recoil directions, etc. By probing the interplay between these directional properties manifested in the photodissociation event, one can have more detailed insight into the nature of reaction. Some of them are (1) the direction of photofragment recoil (velocity vector $\boldsymbol{V}$) vs the direction of light absorption (transition moment $\boldsymbol{\mu}$), (2) when some of the fragments fly apart as rotating, the direction of the rotation axis and rotational speed (rotational angular moment $\boldsymbol{J}$) vs $\boldsymbol{\mu}$ or $\boldsymbol{V}$.

3. How Fast Does the Dissociation Occur?

This is reflected in the lifetime of a particular excited state subject to photodissociation. The lifetime can be measured in real-time if molecules in that excited state emit. Alternatively, it can be deduced from the bandwidth of a rovibrational band belonging to the excited state (larger bandwidth for shorter lifetime because of the Heisenberg's uncertainty principle). The time scale of a particular dissociation event can be traced directly from the rise time of the photofragment signal detected by ultrafast (picosecond or femtosecond) pulsed lasers. The time scale of each molecule in the photodissociation is usually in the range of tens to hundreds of femtoseconds. In the case of predissociation (i.e., dissociation occurs after the excited molecule traverses to another excited state or to the ground state), molecules take more time before they are dissociated.

4. Statistical or Nonstatistical Internal Energy Distribution

Recent development of ultrasensitive detection methods enables the measurement of photofragments just after they are born, that is, before any collisions with other species leading to relaxation to a stable state. These fresh photofragments are said to be in the 'nascent' state. It is quite usual that the energy distributions of nascent photofragments are not statistical, when the dissociation event is fast enough. However, if the dissociation event is slow, relaxation to a stable state will compete with the accumulation of photoproducts to a measurable amount. Then the energy distribution of photofragments approaches a statistical one.

5. Fluctuations in the Internal Energy Distribution

Particularly for photodissociation at energies immediately above the dissociation threshold, the rotational distributions of photofragments sometimes fluctuate significantly, although on average they follow the statistical trend.

6. Branching Ratio between Photodissociation Channels

It frequently happens that two or more dissociation channels compete with each other. This can happen when a molecule is excited to a dissociative excited state (correlated to one of the products), which further out in the exit channel interacts with a second dissociative excited state (correlated to another product). It can also happen when the multidimensional PES of a molecule has two transition states, one along, for instance, a bond stretching coordinate and one along a concerted elimination coordinate. In the latter case, one can normally predict the branching between the two product channels by considering statistical transition-state theory and the two relative barrier heights. These theories assume that the change of electronic wave function immediately follows the nuclear motion (an adiabatic process). However, in some cases *nonadiabatic recrossing* between two PESs markedly reduces the rate of crossing the transition state and evolving to one set of products, affecting the branching ratio.[21,22]

7. Coherence (Memory of Phase)

To what extent does the original phase of the electronic wave packet survive during a photodissociation event? There are many mechanisms for the coherence (memory of phase) to be lost. However, coherence is kept in some favorable cases. Although this fact has been known for some time, experimental verification has only recently become possible. This aspect will be investigated more thoroughly soon,

because it is directly connected to "coherent control" on the outcome of chemical reactions.

8. Discovery of Ultraweak Transitions

Highly sensitive photodissociation studies led to the discovery of ultraweak transitions, such as those forbidden by symmetry or spin-conservation rules, that cannot be studied by conventional absorption spectroscopy. Such information can be very important. For example, an ultraweak transition of ozone may contribute to the high-altitude ozone-deficit problem in the long wavelength region where no ozone photodecomposition has been believed to occur.

9. Approach to Transition States

In an effort to approach transition states by spectroscopic means, several methods have been devised. (For early studies of bimolecular reactions, see ref 23.) Emission of molecules while they photodissociate was probed by Imre, Kinsey, et al.[24−26] Zewail and co-workers[27−29] probed the transition states in the photodissociation ICN → I + CN and IHgI* → HgI + I using a femtosecond laser. Butler and co-workers[30,31] found symmetric vibrations of molecules, and Neumark and co-workers[32−35] studied *antisymmetric* vibration of molecules in the *transition region* (see section II.K for details).

II. Experimental Methodology

A. State of Molecules

In the static cell (bulb) or flow experiments, the pressure of gaseous molecules should be low enough to ensure collision-free conditions. This may be very difficult to attain in the case of very low sensitivity measurements. In supersonic molecular beam (jet) experiments, target molecules are seeded in a rare gas such as helium, neon, or argon. The molecules become internally (i.e., vibrationally and rotationally) very cold, e.g., 5−10 K, by giving up the internal energy to the translational energy of rare-gas atoms. This eliminates hot bands to a large extent, substantially simplifying the spectral analyses. Supersonic molecular beams are imperative for the preparation of van der Waals molecules and clusters.

B. Light Sources

Since photodissociation of molecules occurs only when the light energy exceeds the bond dissociation energy, UV light is necessary except for a small number of molecules with very weak chemical bonds. In the early days discharge lamps for atomic resonance lines were the only available light sources.

The advent of lasers brought about a revolutionary improvement of our arsenal. Typical lasers (wavelength in nm) are Nd:YAG laser (fundamental 1064, second harmonic 532, third harmonic 355, fourth harmonic 266), N_2 laser (337.1), and excimer lasers (XeCl 308, KrF 248, KrCl 222, ArF 193, Xe_2 172, F_2 157). Tunable lasers are the dye laser, the Ti−sapphire laser, etc.

Nonlinear crystals can be used to produce the second, third, fourth harmonics, for the sum-frequency and difference-frequency generation (SFG and DFG, respectively), and for optically parametric oscillation (OPO).

Synchrotron orbit radiation (SR or SOR) can be used in the vacuum ultraviolet region where lasers cannot reach. Use of the free-electron laser (FEL) is still in its infancy.

The "intermolecular" chemical bonds in van der Waals molecules and clusters are so weak that IR lasers are used for their predissociation. Presently useful are OPO or DFG based on dye lasers.

The "mid-IR" region (5−20 μm) is chemically most informative. However, to chemists' deep regret, this region still remains essentially untouchable in the time of this writing (Dec 2000), except for limited spectral regions accessible by CO, CO_2, HF lasers, etc., and by diode lasers. The only possible tunable source in this region is the very weak laser obtained by DFG using such crystals as $AgGaS_2$. Is development of highly efficient and robust nonlinear crystals for OPO or DFG in this region at all possible? Free electron lasers (FELs) must be more easily accessible for chemists. Possibly the development of the quantum cascade laser[36] could supply the chemists' needs.

C. Emission Studies

When the fragments are formed in their electronically excited states and emit, emission spectroscopy is of course useful for its detection, identification, and measurement of internal (vibrational and rovibrational) state population distribution. When the pressure is low enough to realize a collision-free condition, i.e., the time between collisions leading to relaxation is long compared to the emitting lifetime, one can probe the nascent vibrational or rovibrational distribution. Polarization of emission gives stereochemical information.[7] Doppler measurement yields the velocity of the fragment. The lifetime of the emitting parent molecule shortened by competition with photodissociation gives important information on the photodissociation dynamics.

D. Laser-Induced Fluorescence

When the fragments are formed in the ground state and hence do not emit, they can be probed by laser-induced fluorescence (LIF), by bringing them into an emitting state by excitation using another laser (a probe laser). Usually the excitation wavelength is scanned, the resulting fluorescence is *not* dispersed, and all the fluorescence intensity is collected. The measurement of the fluorescence excitation spectrum (which is usually called laser-induced fluorescence (LIF) spectrum) corresponds to that of the absorption spectrum.[37] The principle and a schematic of experimental apparatus is given in Figure 6. Photodissociation laser light ($h\nu_d$) produces (usually nonstatistical) vibrational distribution of nascent photofragments. By scanning of a probe laser light ($h\nu_p$), photofragments in a particular vibrational level (v'') are excited to a particular vibrational level (v') in the electronic excited state when the energy of the

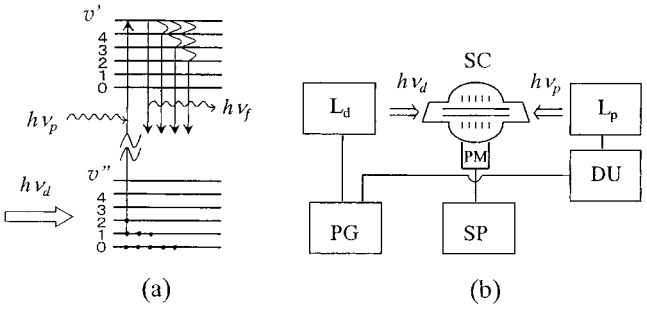

Figure 6. Laser-induced fluorescence (LIF) measurement. (a) Schematic drawing of energy levels (see text, $h\nu_d$, dissociation laser light; $h\nu_p$, probe laser light; $h\nu_f$, fluorescence light). (b) Example of experimental setup (L_d and L_p, dissociation and probe laser, respectively; SC, sample cell; PG, pulse generator; DU, delay unit; PM, photomultiplier; SP, signal processor).

laser light coincides with the energy separation between the two levels. All the fluorescence from the excited level to various levels ($h\nu_f$) is collected without energy dispersion. In the apparatus shown, two laser beams are collinear and counterpropagating for the efficient collection of LIF intensity. Doppler analysis can be performed in a similar fashion as done for emission spectroscopy. In this case, however, the Doppler profile appears on the LIF spectrum.

E. Single-Photon and Multiphoton Ionization, Resonance-Enhanced Multiphoton Ionization (REMPI)

Highly sensitive detection of photofragments is achieved when they are ionized and mass-analyzed. While electron bombardment is conveniently used, photoionization is another way to ionize. Single-photon ionization requires a short-wavelength (UV or vacuum UV) photon. The advent of lasers made multiphoton ionization (MPI) possible. MPI is very convenient because visible light from a wavelength-tunable dye laser can be utilized for ionization. There are two types of multiphoton ionization, simultaneous and sequential (stepwise), depicted in Figure 7a and b, respectively. The former does not involve the intermediate excitation of any real state(s), although a *virtual* intermediate state is assumed only for convenience. This is multiphoton ionization in the genuine sense. The latter, stepwise, involves a real intermediate state. For example, one-photon resonant

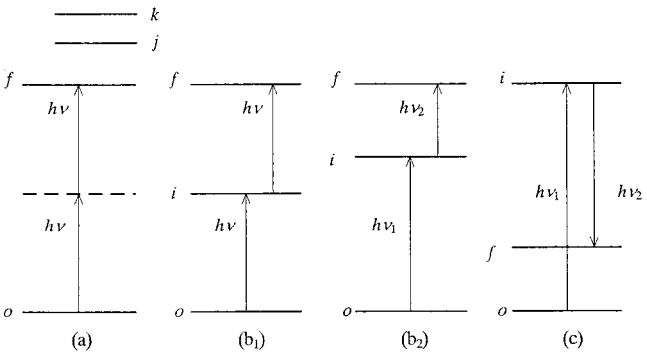

Figure 7. Multiphoton ionization (MPI) and stimulated emission pumping (SEP): (a) simultaneous MPI (- - - *virtual* intermediate state); (b) sequential (stepwise) MPI, (*i*, real intermediate state); (c) stimulated emission pumping (SEP).

two-photon ionization, or (1 + 1) photon ionization, is nothing but two one-photon excitation processes occurring in sequence. The first photon brings the molecule to an excited state, and the second photon ionizes it. In a two-photon resonant 3-photon ionization, or (2 + 1) photon ionization, the simultaneous (genuine) two-photon ionization brings the molecule to an excited state and the third photon ionizes it. When the first, second,..., photon in MPI is in resonance with a particular excited state of a molecule, the efficiency of MPI is enhanced by several orders of magnitude. This process, called resonance-enhanced multiphoton ionization (REMPI), is a highly sensitive and (because only those molecules preselected in the intermediate state can be ionized) highly state-selective method. Recently high Rydberg excited levels have been used as the intermediate state in REMPI for threshold ionization. The sequential (stepwise) multiphoton process shown in Figure 7c is called the pump−dump process or stimulated emission pumping (SEP) process. In this case the stimulated emission of the last photon *forces* a molecule to one of the low-lying excited states. This constitutes the only available effective means to bring the molecule to such a state not accessible by direct absorption.

F. Translational Spectroscopy

Photodissociation reactions are usually accompanied by the ejection of some amount of translational energy. The amount is large when the dissociation is a fast and direct process. Conservation of momentum ($\boldsymbol{P}$) requires that the sum of $\boldsymbol{P}$s of the sibling (born in coincidence) fragments should vanish (as viewed on the coordinate system moving with the center of gravity of the total system). When the parent molecule is dissociated into two fragments, the velocity measurement of one suffices. The velocity of the partner can be calculated from the conservation of momentum. Time-of-flight (TOF) mass spectroscopy is very convenient for this.[38] The photofragment spectroscopy of Wilson,[39] explained in the next section, combines polarized laser light with TOF mass spectroscopy to obtain the anisotropy ($\boldsymbol{\mu}-\boldsymbol{V}$ correlation), one of vector correlations discussed in the next section. When a H (or D) atom is released in the photodissociation process, H (D) atom photofragment translational spectroscopy[40] is very convenient to probe the detailed energy disposal, especially when LIF observation of the counterfragment is difficult because of, for example, predissociation. Doppler LIF strategy was used for some time. However, high-*n* Rydberg TOF (HRTOF) spectroscopy developed by Welge and co-workers greatly improved the resolution and sensitivity. In this method, $n = 2 \leftarrow n = 1$ excitation of H-atom products is performed by Lyman α radiation at 121.6 nm. This radiation is obtained by frequency tripling of dye laser light near 365 nm. Because the $n = 2$ level lies at an energy that is nearly 3/4 of the ionization potential, further absorption of one of the fundamental dye laser photons brings the H atom to high-*n* Rydberg levels (*n* around 50) close to the ionization threshold. After a rather long flight path (e.g., 1 m), H atoms are field

ionized at a mesh a few millimeterrs in front of the ion detector (MCP). The H photofragment flies as the *nascent neutral* species and is monitored *via the ion*.

G. Angular Distribution (Photofragment Spectroscopy)

Photofragment vector correlations provides very important information on reaction dynamics. The directional aspect of photodissociation was originally discussed by Zare.[41] Since then, several strategies have emerged to interrogate such correlations experimentally. In a very naive but pioneering experiment, Bersohn et al.[42] examined the angular distribution of Cd photofragments from $Cd(CH_3)_2$ with respect to the polarization of the light used for the dissociation (in their case a mercury lamp).

When lasers became available to the photodissociation community, Wilson et al.[39] devised photofragment spectroscopy. The basic feature of the experiment is shown in Figure 8a. A molecular beam of the parent molecule is crossed with a laser beam, where the photodissociation occurs. A detector (for example, a quadrupole mass spectrometer with electron impact ionization) is located in the *Z*-axis direction at a known distance from this crossing region. The electric field vector of the laser light ($\boldsymbol{E}$) is in the *XZ* plane, at a chosen angle (θ) to the *Z*-axis. The distribution of the time-of-flight (TOF) for the fragments to fly to the detector is converted to the kinetic energy distribution, and this is measured as a function of θ.

Suppose an ensemble of molecules with a transition dipole $\boldsymbol{\mu}$ (naturally in the molecule-fixed frame) is randomly oriented in the laboratory frame. When it

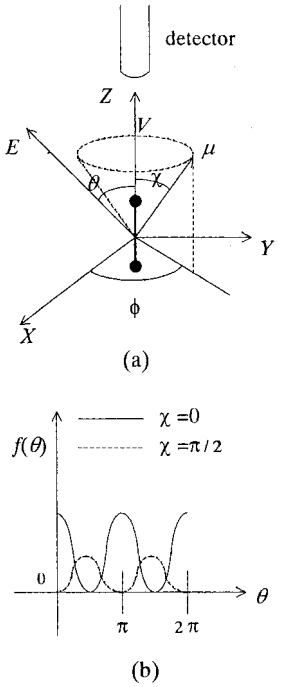

Figure 8. Photofragment spectroscopy. Axial recoil of a diatomic molecule is assumed. Detector (a quadrupole mass spectrometer with electron impact ionization) is in the *Z*-direction. $\boldsymbol{E}$: electric field of exciting laser light. $\boldsymbol{\mu}$: transition moment. $\boldsymbol{V}$: velocity vector of the photofragment.

is irradiated with light with an electric vector $\boldsymbol{E}$, the probability of excitation (P) is given as

$$P = |\boldsymbol{\mu}\cdot\boldsymbol{E}|^2 \tag{5}$$

Therefore, the distribution of excited molecules has a maximum in the direction parallel to $\boldsymbol{E}$, with a cylindrical symmetry about $\boldsymbol{E}$. This relationship establishes the relationship between the molecular frame and the laboratory axes. In the following, only the axial recoil of a diatomic molecule (fragments fly apart in the direction of molecular long axis) is considered for simplicity. Let us consider the general case that $\boldsymbol{\mu}$ makes an angle χ with the molecular long axis. A simple calculation leads to the angular distribution of the fragments[39,42,43]

$$f(\theta) = (1/4\pi)\int_0^{2\pi}|\boldsymbol{\mu}\cdot\boldsymbol{E}|^2\,\mathrm{d}\phi$$
$$= (1/4\pi)\mu E\,[1 + 2P_2(\cos\chi)P_2(\cos\theta)] \tag{6}$$

where the Legendre's polynomial $P_2(a) = (3/2)a^2 - (1/2)$. $\beta = 2P_2(\cos\chi)$ is called an anisotropy factor. In the general case that the recoil direction makes an angle a with the molecular long axis, β can be expressed as $\beta = 2P_2(\cos\chi)P_2(\cos\alpha)$ For axial recoil ($\alpha = 0$), one has $\beta = 2$ and -1 for the parallel transition (with $\boldsymbol{\mu}$ parallel to the molecular long axis, i.e., $\chi = 0$) and perpendicular transition (with $\boldsymbol{\mu}$ perpendicular to the molecular long axis, i.e., $\chi = \pi/2$), respectively. In these cases $f(\theta)$ is proportional to $\cos^2\theta$ and $\sin^2\theta$, respectively (Figure 8b).

The anisotropy is blurred if the dissociation is slow in comparison with the rotation time of the excited parent. The effect has been treated for diatomic molecules.[44] In that case β is to be multiplied by

$$f(\omega\tau) = [1 + (\omega\tau)^2]/[1 + 4\,(\omega\tau)^2] \tag{7}$$

where τ is the average excited-state lifetime before dissociation and ω is the average excited-state rotational angular velocity. For the ideal case of rapid dissociation, $f(\omega\tau) \rightarrow 1$.

Thus, one can tell from the experimentally determined value of β, (1) if the dissociation is *direct*, i.e., the molecule has little time to rotate before the dissociation act, and (2) if the relevant excited state is associated with a parallel or perpendicular transition.

Photofragment alignment is defined by[45,46]

$$A_0^{(2)} = \langle(3J_z^2 - \boldsymbol{J}^2)/\boldsymbol{J}^2\rangle \tag{8}$$

which is proportional to the second Legendre polynomial $2P_2(\cos\theta_J)$ of the angle θ_J between the angular momentum vector $\boldsymbol{J}$ and the *Z* axis. The alignment falls in the range $4/5 \geq A_0^{(2)} \geq -2/5$ in the limit of large J.

H. Doppler Strategy

When emitting molecules approach or retreat from the detector, the detected emission frequency is Doppler-shifted. If the flight path is at an angle to the direction to the detector, the velocity component in that direction is to be used. Even if the fragment

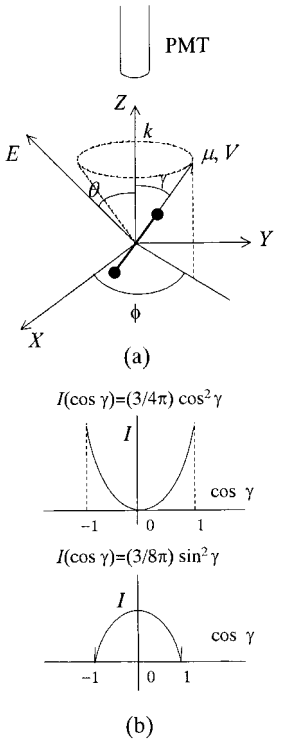

Figure 9. Doppler spectroscopy. Axial recoil of a diatomic molecule is assumed. Detector (a photomultiplier) is in the *Z*-direction. ***E***: electric field of exciting laser light. ***μ***: transition moment. ***V***: velocity vector of the photofragment.

is prepared in its ground state and therefore does not emit, the Doppler strategy can be used in a LIF measurement, in that the Doppler-shifted exciting light can bring the moving fragment to the relevant excited state. Narrow bandwidth laser excitation made possible the widespread use of the Doppler strategy.

As an introductory example, the case of parallel transition and axial recoil is considered in Figure 9a. Let us put the detector (a photomultiplier) on the *Z*-direction. That is, the vector of propagation of the light to be detected (***k***) is in the *Z* -direction. The electric field of the laser light (***E***) is in the *XZ* plane. ***E*** spans an angle θ with ***k***. (This angle θ is set by the experimenter.) When a fragment emitting at frequency ν_0 flies with a velocity ***V*** making an angle γ to the detector direction (*Z*-axis), the detector catches the Doppler-shifted frequency

$$\nu = \nu_0(1 + V\cos\gamma/c) \qquad (9)$$

Using the formal analogy to Figure 8a, it is straightforward to have the spectral profile

$$I(\cos\gamma) = (1/4\pi)\,[1 + 2P_2(\cos\gamma)P_2(\cos\theta)] \qquad (10)$$

In the general case of the direction of ***μ*** with respect to the molecular axis

$$I(\cos\gamma) \propto (1/4\pi)\,[1 + \beta P_2(\cos\gamma)P_2(\cos\theta)] \qquad (11)$$

If the experiment is done at $\theta = 90°$, we have $I(\cos\gamma) = (3/4\pi)\cos^2\gamma$ and $(3/8\pi)\sin^2\gamma$ for parallel ($\beta = 2$) and perpendicular ($\beta = -1$) transitions, respectively

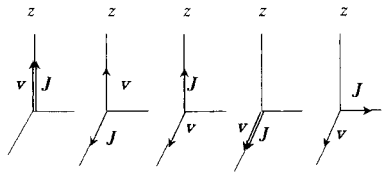

anisotropy (μ–v)	$\beta_0^2(20)$	+1	+1	$-\frac{1}{2}$	$-\frac{1}{2}$	$-\frac{1}{2}$
alignment (μ–J)	$\beta_0^2(02)$	+1	$-\frac{1}{2}$	+1	$-\frac{1}{2}$	$-\frac{1}{2}$
(v–J) correlation	$\beta_0^0(22)$	+1	$-\frac{1}{2}$	$-\frac{1}{2}$	+1	$-\frac{1}{2}$
μ–v–J correlation	$\beta_0^2(22)$	−1	$+\frac{1}{2}$	$+\frac{1}{2}$	$+\frac{1}{2}$	−1
		(a)	(b)	(c)	(d)	(e)

Figure 10. Values of bipolar moments for some limiting orientations of ***V*** and ***J*** of a photofragment in the body-fixed axes of the parent molecule. (Adapted from ref 47.)

(Figure 9b). These Doppler patterns appear in the emission or LIF spectrum as a band profile.

However, a more general treatment taking the polarization effects into account revealed that the profile of a Doppler-broadened line of a photoproduct depends not only on the direction of the emitted or absorbed photon, but also on the polarization(s) used to detect it. Dixon[47] gave a general formula to deduce various vector correlations from the analysis of the Doppler profile of emission and LIF spectra

$$g(\nu) = (2\Delta\nu_D)^{-1}\{\, g_0 + g_2P_2(x_D) + g_4P_4(x_D) + g_6P_6(x_D)\} \qquad (12)$$

where $\Delta\nu_D$ is the maximum Doppler shift, $x_D = \Delta\nu/\Delta\nu_D$, and each of the g_k terms is a linear combination of products of the $\beta_0^K(k_1k_2)$ bipolar moments and the angular moment coupling factors γ' and depends on the geometrical relationship between molecular and light beams and on the polarization of a particular branch (P, Q, R) in the rotational structure in the spectrum. Equation 12 effectively reduces to the form of eq 11 (but β is to be replaced by β_{eff}) when polarization effects are low.

The bipolar moments deduced are

β_0^2 (02): alignment (***μ***−***J*** correlation)

β_0^2 (20): anisotropy (***μ***−***V*** correlation)

β_0^0 (22): ***V***−***J*** correlation

β_0^2 (22): ***μ***−***V***−***J*** correlation

The first two are related to the quantities introduced in section II.G as β_0^2 (02) = $(5/4)A_0^{(2)}$ and β_0^2 (20) = $(1/2)\beta$. Figure 10[47] shows the values of these bipolar moments for some limiting orientations of ***V*** and ***J*** of a photofragment in body-fixed axes of the parent molecule. In this figure, the *Z* axis is the axis of the transition moment ***μ***. Detailed derivations of eq 12 are beyond the scope of this review. Interested readers are referred to Dixon's original paper[47] and, for example, papers by Houston[48] and Hall et al.[49] on its practical application. It may be relevant to add here that recent interests are on coherent and incoherent contributions to the angular momentum

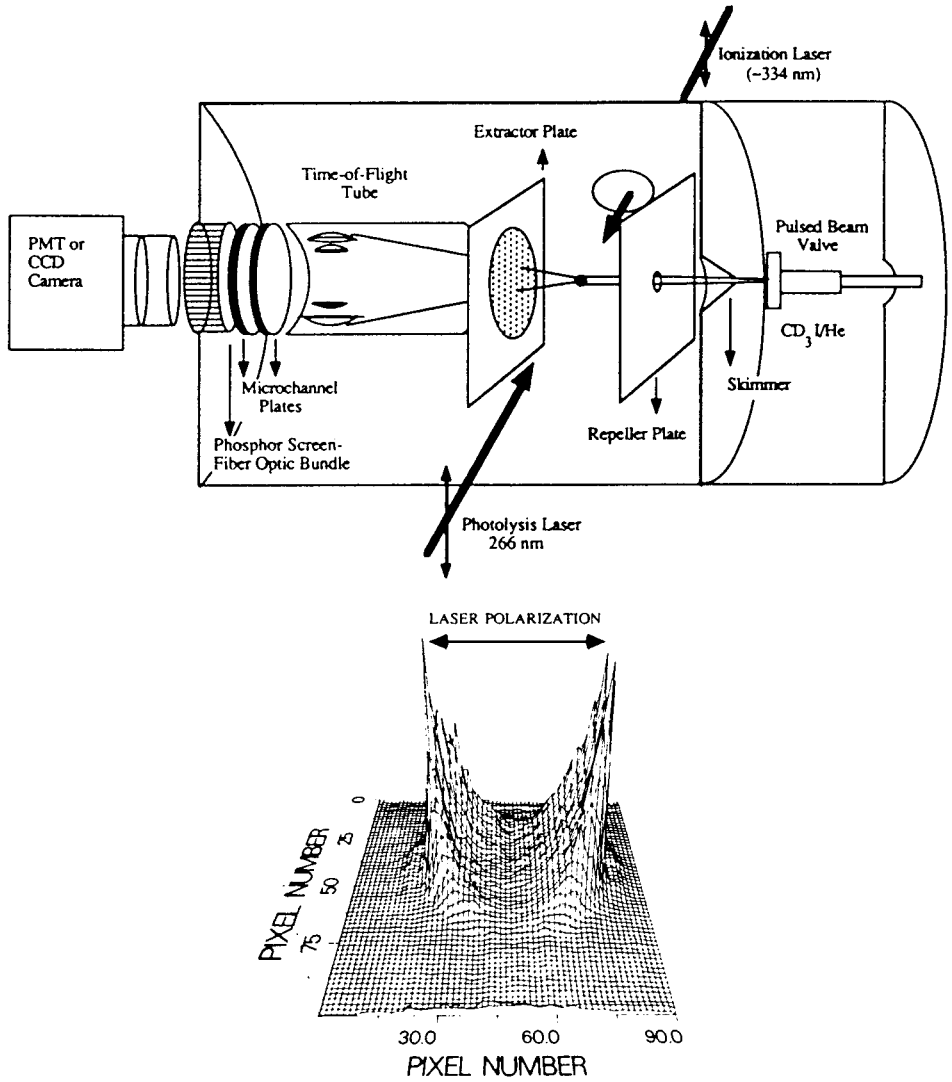

Figure 11. Photofragment imaging spectroscopy: (a) experimental apparatus (Reprinted with permission from ref 51. Copyright 1990 American Chemical Society), (b) two-dimensional distribution of CH_3 formed by the 266-nm photodissociation of CH_3I (Reprinted with permission from ref 50. Copyright 1987 American Institute of Physics.).

distribution of products to know the phase difference between many paths to the same final states.

I. Photofragment Imaging

Chandler, Houston, and co-workers[50] proposed the photofragment imaging method. It is essentially a combination of REMPI and two-dimensional imaging of fragment ions. See Figure 11. Two counterpropagating pulsed laser light beams photodissociate molecules in a molecular beam and ionize the resultant fragments by REMPI, respectively. Fragment ions generated in a small volume are extracted by an electric field toward the two-dimensional position-sensitive detector. The REMPI process ionizes only fragments in the preselected state. Directional (with respect to the polarization of the dissociation light pulse) and velocity information of the fragments is projected on the two-dimensional screen. Chandler and co-workers[51,52] showed that such information as the anisotropy (β) parameter, branching ratio, Doppler profile, and vector correlations can be extracted from the two-dimensional image using as examples the photodissociation of CD_3I at 266 nm and H_2S at 243 nm. This method is very convenient and has been used by many people. Many variations of the original method are presented. A wide variety of new techniques including the imaging method are reviewed by Houston.[53] Chandler and Parker[54] recently described velocity mapping of multiphoton excited states for two diatomic molecules D_2 and O_2.

J. Femtosecond Real-Time Probing and Femtosecond Transient Spectroscopy

By using femtosecond pulse lasers one can follow the course of reaction in real time. Zewail and coworkers applied this technique in photodissociation studies. They followed the build-up of photofragments CN from ICN and from NCNO by observing the rise in their LIF signal using a picosecond laser[55] and CN from ICN using a femtosecond laser (Figure 12).[56] The build-up time of CN was later redetermined to be 205 ± 30 fs, using multiphoton ionization of *N*,*N*-diethylaniline as a clock to determine time zero.[57] They were able to probe the transition state by probing CN fragments to the red (for example, 389.5 nm) of the free CN bandhead (388.5 nm) on the

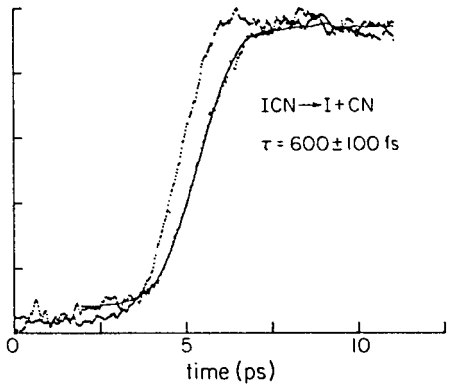

Figure 12. Femtosecond real-time probing of photodissociation. (Reprinted with permission from ref 56. Copyright 1985 American Chemical Society.)

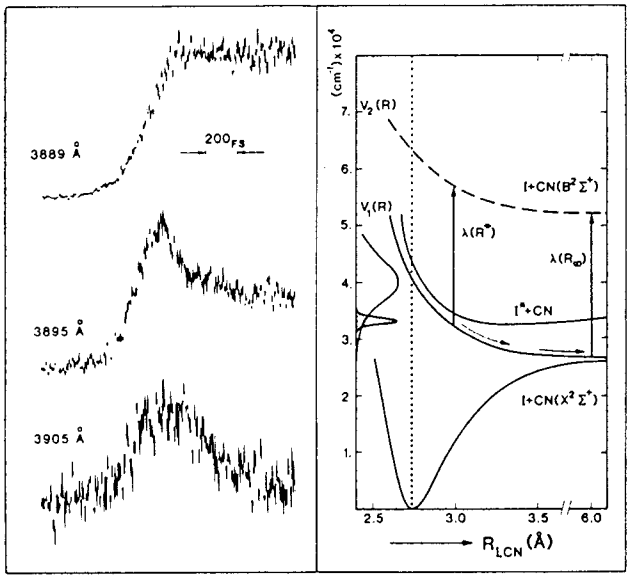

Figure 13. Femtosecond transition-state spectroscopy. (Reprinted with permission from ref 27. Copyright 1987 American Institute of Physics.)

femtosecond scale (femtosecond transient spectroscopy, FTS).[27,28] By doing so they detected the *rise and decay* of the LIF signal (Figure 13), while only the build-up of signal was detected when they probed at the edge of free CN handhead. The technique of femtosecond real-time probing of reactions is described by Rosker, Dantus, and Zewail.[58] Bernstein and Zewail[59] reported the inversion to the potential energy curve from the FTS transients. In the FTS of HgI_2,[29] Dantus et al. observed recurrences of the HgI LIF signal for fragments vibrating perpendicular (symmetric coordinate) and *along* (antisymmetric coordinate) the reaction coordinate I + HgI → IHg + I. The role of alignment and orientation in the femtochemistry is discussed by Zewail and co-workers.[60,61] Zewail also reviewed the development of femtochemistry.[62,63]

K. Approach to the Transition State

Several methods have been devised to interrogate the transition state and to probe the time evolution of dissociating fragments. Imre et al.[25] probed emission of CH_3I during the photodissociation at 266 nm. The emission spectrum is called "continuum resonance Raman scattering spectrum" or "dissociative resonance Raman scattering spectrum". As shown later in Figure 16, it was featured by a remarkably long (up to $v'' = 29$) progression of ν_3 (C−I stretch). The energy of $v'' = 29$ amounts to about 75% of the dissociation energy. This indicates that only the C−I stretching vibration is active in the initial stage of dissociation. This technique was also applied to O_3.[24] Johnson, Kinsey, and co-workers reviewed the development of this approach.[26] FTS of Zewail and co-workers[27−29] is described in the previous section, section II.J. Fragments vibrating perpendicular to (symmetric stretch) and along (antisymmetric stretch) the reaction coordinate were revealed by the recurrence in their FTS signal. Butler and co-workers[30,31] reported on transition-state spectroscopy. The vibrational progression in the absorption spectra of H_2O and H_2S can be assigned to recurrences in the motion along the symmetric stretch coordinate on the saddle point *region* of the first excited state, perpendicular to the reaction coordinate H + OH → HO + H. Neumark et al.[32−35] studied negative-ion photodetachment spectra of XHX^- (X = Cl, Br, and I). This provided a direct spectroscopic probe of the neutral XHX collision complex, as long as the geometry of the ion was similar to that of the neutral transition state. The spectra showed not only the structure associated with the symmetric stretching motion perpendicular to the reaction coordinate X + HX → XH + X, but also features in *antisymmetric* stretch, roughly corresponding to the bouncing of the H atom between the two X atoms. (The XHX molecules in the transition *region* are not only bound along directions perpendicular to the reaction coordinate, but also quasi-bound *along* the reaction coordinate, because reaction proceeds on many paths in the transition region, and many of these paths tunnel through the ridge that bisects the reactant side and product side, forming two shallow minima.)

L. Λ-Doubling

A few words on Λ-doubling are added here. In linear molecules with nonzero electronic orbital angular momentum, e.g., OH($X\,^2\Pi$) or NH($c^1\Pi$), there is a pair of closely separated energy levels, with the occupied pπ-lobe parallel and perpendicular to the molecular axis. In labeling two Λ-doublet levels various notations (Π^+ and Π^-, Π^∞ and Π,[8] A′ and A″) are used in the literature. In the present review the data are given in the form of Π^+ and Π^-. Readers are referred to the 29-author article[64] on the nomenclature for Λ-doublet levels in rotating linear molecules.

III. Theoretical Models

A variety of theoretical models have been developed not only to explain the experimental results, but also to predict the outcome of photodissociation reactions. Those of one class are on individual molecules with respect to the calculation of the shape of PESs and the crossing probability between these PESs, etc. Those of the other class address more generally reaction rates and the energy disposal. Some theoretical papers of the former class are listed in chapter

IV in the sections of each compound. The papers of the latter class are briefly cited here. However, citations are restricted to the absolute minimum directly needed to understand the listings in the text. Readers are referred to outstanding reviews and original papers for further information.[15,17,65−70]

When the dissociation is impulsive, the reaction occurs instantaneously. In other words, dissociation occurs faster than molecular rotation. In such a case, vectorial correlations as described in the previous section are well conserved. Distribution of available energy into many degrees of freedom of the photoproducts is usually far from statistical. Much of the available energy goes into translation. However, when the reaction occurs more or less statistically, as in the cases that photodissociation occurs close to the dissociation threshold, available energy is distributed over all the degrees of freedom. Several statistical models of unimolecular reactions can then be applied. What is to be predicted by these models are (1) the reaction velocity and (2) the distribution of products among accessible states. In the statistical theory, the reaction velocity is estimated by counting the number of open channels (reactant → product) at the transition state. Since the molecular system at the transition state moves into the reaction products with a high probability, counting the number density of attainable states at the transition states has a meaning close to the prediction of reaction velocity. If the transition state is properly located, i.e., the passage of the reactants through the transition state almost always means that the reaction will proceed to products, the prediction becomes successful. The other aspect of the models is to explain or predict the distribution of products among a variety of accessible states, or in other words, distribution of available energy among various degrees of freedom in the outcome of the photodissociation reactions. Product distributions are either statistical or nonstatistical. When they are statistical, all the accessible product states appear with the same probability. On the contrary, not all of the accessible states are reached in the nonstatistical cases.

The fundamental assumption in the statistical theory is that all the possible states are attained with the same probability. According to the microcanonical transition state theory, the reaction rate $k(E)$ is given by

$$k(E) = W/h\rho(E) \tag{13}$$

where W is the number of states in the transition state and $\rho(E)$ is the molecular density of states. There are several types of statistical models which differ in the way to estimate W and $\rho(E)$. Because the transition state is usually *not* observable, estimation of $k(E)$ depends on empirical data.

The most popular method is the RRKM (Rice−Ramsperger−Kassel−Marcus) theory.[65] In this theory, W is the number of open channels at the transition state $N^{\ddagger}(E - E_0)$ and

$$k(E) = N^{\ddagger}(E - E_0)/h\rho(E) \tag{14}$$

Difficulties encountered in the RRKM approach partly come from incomplete randomization of excess energy over the degrees of freedom of the system. In phase space theory (PST),[66,67] the collective motion of representative points (p_i, q_i) in the phase space (p, q) is considered. The passage of representative points through the critical surface (dividing the products from the reactants) corresponds to the reaction taking place. The PST uses the statistical weights for each set of product excitations at a very "loose" transition state. The only restrictions imposed are the conservation of energy and total angular momentum. In PST, the transition state is at the separated fragments and the product distribution in a specific rovibrational state can be obtained from

$$P(J_{KaKc}|v,s) = P(E,J \rightarrow v,\ J_{KaKc}) = W_s(E,J;v,\ J_{KaKc})/\sum_{J_{KaKc}} W_s(E,J;v,\ J_{KaKc}) \tag{15}$$

where $W_s(E,J;v,\ J_{KaKc})$ is the number of open channels leading to the particular (v, J_{KaKc}) state of the fragment. The denominator represents the total number of open channels summed over all possible product states. The distribution thus obtained is the most random possible one under the constraint of conservation of total energy and angular momentum. The PST yields rates that are uniformly faster than the experimental values.[15]

Some of the modifications of PST are the variational-RRKM,[68] statistical adiabatic channel models (SACM),[69] and separate statistical ensembles (SSE).[70] Variational-RRKM theory is based on the idea that the transition state should be placed at the position along the reaction coordinate which minimizes the number of open channels. SACM is based on PST but takes account of potential energy barriers to dissociation that arise due to angular interactions of the separating fragments.[15] Both the variational RRKM theory and SACM predict that the transition state "moves in" closer to the reactant side along the reaction coordinate as the total energy increases above threshold. The transition state becomes "tighter", and as the chemical bond is formed, energy level spacings increase greatly over these for free rotation of the fragments. This decreases the number of open channels at the transition state, and in some cases the number becomes an order of magnitude less than the PST. The adiabatic channel potentials of the SACM connect these transition-state energy levels smoothly and without crossings to the asymptotic levels of the freely rotating products. Open channels are only those with an energy maximum less than the total available energy, and these channels can contribute to the rate of the reaction. Since these channels are all closely parallel, the variational RRKM and SACM models result in the same predicted rate constants. In the actual cases nondiabatic transitions are caused by rotation−translation relaxation, i.e., interaction between motion along the reaction coordinate and product rotations occurs. The molecule jumps from one adiabatic channel to another.

If the vibrational quantum numbers of the product become well-defined before the system reaches its transition state, the number of open channels is

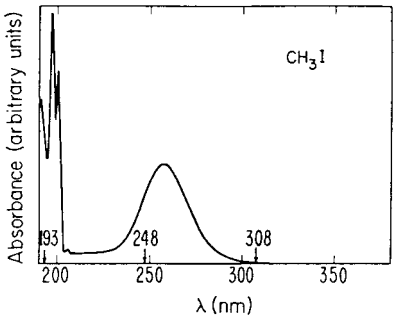

Figure 14. Absorption spectrum of CH_3I. (Reprinted with permission from ref 73. Copyright 1981 American Chemical Society.)

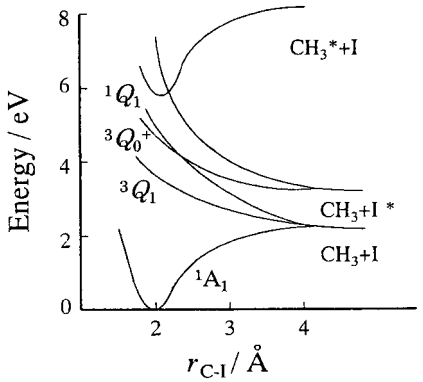

Figure 15. Schematic potential energy curves of CH_3I.

defined for independent vibrationally adiabatic potential energy surfaces, each with its own transition-state location. Higher product vibrational states have looser transition states because of the smaller amount of excess energy. The rate of formation is equal to the PST rate for the highest possible vibrationally excited product, i.e., that at the threshold, but the rate is much less for the ground-state product.

The separate statistical ensembles (SSE) theory of Wittig and co-workers[70] predicts PST-like rotational state distributions, but the probability of the formation of vibrational state v ($P(v)$) is proportional to the density of states of an ensemble of the disappearing oscillators. The resulting values are larger than the PST values by the factor $(E - E_v)^{1/2}$. Although the SSE contains no adjustable parameters, it predicts value of $P(v)$ at least as well as the much more complicated variational-RRKM calculations.

IV. Typical Molecules

A. Methyl Iodide CH_3I—Which Occurs First, the Scission of C–I Bond and the Flattening of Umbrella-like CH_3 Moiety?

Main points of interest in the photodissociation of CH_3I are (1) the I*/I branching ratio which reflects the curve crossing ($^1Q_1$ and $^3Q_0^+$) and (2) which occurs first the scission of C−I bond and the flattening of umbrella-like CH_3 moiety. The related molecule CF_3I is known by Kasper and Pimentel's chemical laser experiments,[71] where some of the iodine-atom fragments were found in the excited state ($I^*(^2P_{1/2})$) and emitted infrared light.

CH_3I in the ground state is a symmetric top composed of the "umbrella" of CH_3 and the "stock" of C−I. It belongs to the C_{3v} point group. The C−I bond length (r_e) is 2.132 Å. The angle ∠HCH is 111.2°.[72] The thermochemical dissociation energy $D_0°$ (H_3C−I) is only 55.0 ± 1 kcal mol^{-1}.[4] However, this molecule absorbs only in the UV. The absorption spectrum of CH_3I (Figure 14)[73,74] features a broad band in the range 350−210 nm (centered near 258 nm) and a sharp Rydberg band between 200 and 170 nm. The band is due to five transitions from the ground state into five excited states $^3Q_2$, $^3Q_1$, $^3Q_0^+$, $^3Q_0^-$, and $^1Q_1$ as designated by Mulliken,[75] three of which ($^3Q_1$, $^3Q_0^+$, and $^1Q_1$) have dipole-allowed transitions from the ground state.[73] Gedanken and Rowe[76] decomposed the Ã band into three components $^3Q_1$, $^3Q_0^+$, and $^1Q_1$ using magnetic circular dichroism.

These excited states produce methyl radical CH_3 via two exit channels

$$CH_3I + h\nu \rightarrow CH_3 + I(^2P_{3/2}),\ I^*(^2P_{1/2}) \quad (16)$$

where the asterisk denotes the excited state. The longest wavelength for photolysis was reported to be 333.45 nm.[77] An interesting feature of CH_3I is that the $^3Q_0^+(A_1)$ state which correlates with CH_3 + I* is predissociated by the $^1Q_1(E)$ state correlating to the ground-state fragments CH_3 + I, as schematically shown in Figure 15. The parallel transition probed at 248 or 266 nm excites the molecule to the $^3Q_0^+(A_1)$ state and produces $I^*(^2P_{1/2})$ as the main product, with a smaller amount of $I(^2P_{3/2})$. The latter correlates to a $^1Q_1$ excited state which is apparently formed via curve crossing with $^3Q_0^+$. The $I^*(^2P_{1/2})/I(^2P_{3/2})$ branching ratio, sometimes expressed in the form of "quantum yield" $\phi(I^*) = I^*(^2P_{1/2})/\{I^*(^2P_{1/2}) + I(^2P_{3/2})\}$ and the $^3Q_0^+ \rightarrow {}^1Q_1$ curve crossing probability as a function of photodissociation wavelength in the Ã band region have been the target of intensive research.

The reaction is essentially the purely axial recoil of a pseudotriatomic molecule H−C−I. Since the CH_3 radical has a planar equilibrium structure, the dissociation process must involve the flattening of the CH_3 moiety sooner or later within the time evolution of photodissociation. It is interesting to note which occurs first, flattening of CH_3 or breaking of the C−I bond. It can be reflected in the ν_2 "umbrella" out-of-plane bending vibrational distribution of the resulting CH_3 product. The parent to product carryover of rotational angular momentum may be manifest in the N,K-structure of CH_3. All of these can be different for the CH_3 product formed directly and through the curve-crossing.

Among pioneering work, Riley and Wilson applied photofragment spectroscopy at 266 nm.[4] The I*/I ratio was approximately 3.5. More than 80% of available energy was found in translation. Leone's group[73,78] obtained $\phi(I^*)$ values of 0.81 and ∼0.05 at 248 and 308 nm, respectively, by IR emission measurements. The extent of vibrational excitation of CH_3 has been the target of long sustained disagreement. Baughcum and Leone[78] reported IR fluorescence from the out-of-plane bend vibration (607 cm^{-1}) on 248-nm excita-

tion. Inverted vibrational distributions of ν_2 (umbrella out-of-plane bending) were reported in several earlier papers, including the pioneering time-of-flight mass spectrometry (TOFMS) experiment at 266 nm of Sparks et al.[79] It suggested the C−I cleavage preceding the flattening of CH_3. However, such an inverted distribution was not observed in later work, e.g., the MPI detection at 266 nm by Loo et al.[80] (Sparks et al.[79] used a heated nozzle to avoid dimerization of CH_3I. This gave rise to a warm methyl.) Suzuki et al.[81] used infrared diode laser kinetic spectroscopy and obtained a noninverted vibrational distribution at 248 nm. They suggested that the geometry of the CH_3 moiety in the precursor CH_3I is relaxed gradually to its equilibrium planar structure before the cleavage of the C−I bond. The high-resolution CARS of CH_3 radicals formed at 266 nm under near-nascent conditions (~3 to ~6 collisions) by Zahedi et al.[82] showed that most of the CH_3 product was in the ground vibrational state, with little excitation seen in the ν_2 vibration. Activity in the ν_2 vibrational distribution was reported in a very recent photofragment imaging work by Eppink and Parker,[83] although the distribution was noninverted. Their data at 266 nm were very close to that of Suzuki et al.[81] at 248 nm mentioned above. Eppink and Parker[83] additionally found some activity in the ν_1 (symmetric stretch) and ν_4 (asymmetric deformation). Results of ion imaging combined with hexapole state selection and orientation of CD_3I were reported by Janssen et al.[84]

The rotational distribution of the CH_3 fragment was highlighted by the peculiar behavior of the N,K-structure. Black and Powis[85,86] reported the predominance of $N = K$ bands (rotation parallel to the CH_3 C_3 top axis) using an effusive beam. On the contrary, cooled supersonic expansion experiments of Loo et al.[80] revealed a strong preference for $K = 0$ (rotation perpendicular to the CH_3 C_3 top axis). Assuming the relative velocity vector $\boldsymbol{V}$ lying along the top axis, velocity ($\boldsymbol{V}$) and rotation ($\boldsymbol{J}$) vectors tend to be perpendicular. They attributed the Black and Powis' results to initial CH_3I rotation. The CARS results of Zahedi et al.[82] were consistent with conservation of K during dissociation.

The emission spectrum of CH_3I during the photodissociation at 266 nm, called "continuum resonance Raman scattering spectrum", was probed by Imre et al.[25] (Figure 16). It had a remarkably long (up to $v'' = 29$) progression in the ν_3 (C−I stretch). The energy of $v'' = 29$ amounts to about 75% of the dissociation energy. This indicates that only the C−I stretching vibration is active in the initial stage of dissociation. Lao et al.[87] measured the perpendicular/parallel angular distribution of emitted photons, following the purely parallel excitation at 266 nm to the $^3Q_0^+$ state, to determine whether the molecule is emitting from the same electronic state to which it is excited ($^3Q_0^+$) or if it has crossed to an electronic state with a different orientation of the electric dipole transition moment ($^1Q_1$) before it emits. As the C−I bond stretches with time, molecules emit to eigenstates with higher and higher quanta in the C−I stretch in the electronic ground state. The fraction of photons

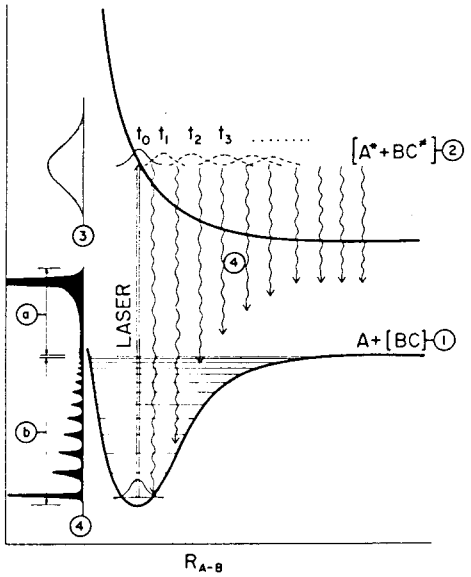

Figure 16. Emission of a dissociating molecule. (Reprinted with permission from ref 25. Copyright 1984 American Chemical Society.)

emitted via a perpendicular transition moment, i.e., after the curve crossing, increased with the number of quanta in C−I stretch, as expected.

Predissociation lifetimes of the $\tilde{C}$ state were studied by Campbell and Ziegler[88] with a polarization-resolved resonance hyper-Raman technique and those of $\tilde{B}$ and $\tilde{C}$ states by Syage[89] from lifetime-broadened line shapes via direct absorption and REMPI. The former group determined the $\tilde{C}$-state lifetime to be 180 ± 30 fs. The depolarization ratio dispersion indicated mode-specific predissociation effects. The latter group reported mode-specific lifetimes: 0.87 ps ($\tilde{B}$-state origin), 0.83 ps (ν_2), 0.92 ps (ν_3), 0.67 ps (ν_6), and 0.25 ps ($\tilde{C}$-state origin).

Picosecond direct monitoring of bond rupture was made by Zewail's group.[90−92] Knee et al.[90] monitored the appearance of I* and I on the 280-nm excitation of CH_3I in molecular beams. The photodissociation lifetime was shorter than 0.5 ps. Rydberg state femtosecond dynamics of CH_3I and CD_3I were probed in real-time in molecular beams.[91,92] These molecules were two-photon excited to 5pπ−6p Rydberg state using a 315-nm femtosecond laser. They were probed by one-photon (618 nm) femtosecond pulse ionization delayed by 0−2000 fs. The decay of the CH_3I or CD_3I signal was considered to be mainly due to dissociation into CH_3 and I fragments, which occurs following a diabatic crossing from the Rydberg-bound state to the dissociation continuum. The lifetime was 175 ± 10 and 325 ± 15 fs for CH_3I and CD_3I, respectively. This substantial isotopic difference was related to the mass effect for tunneling toward the dissociation continuum. The dissociation in this case is more likely to proceed along the C−H_3 coordinate at the very beginning of dissociation rather than along the C−I coordinate.

On the theoretical side, the PESs related to the $\tilde{A}$-band photodissociation dynamics were calculated by many groups. Shapiro[93] theoretically studied the photodissociation dynamics on two electronic states, $^3Q_0$ and $^1Q_1$, coupled with non-Born−Oppenheimer

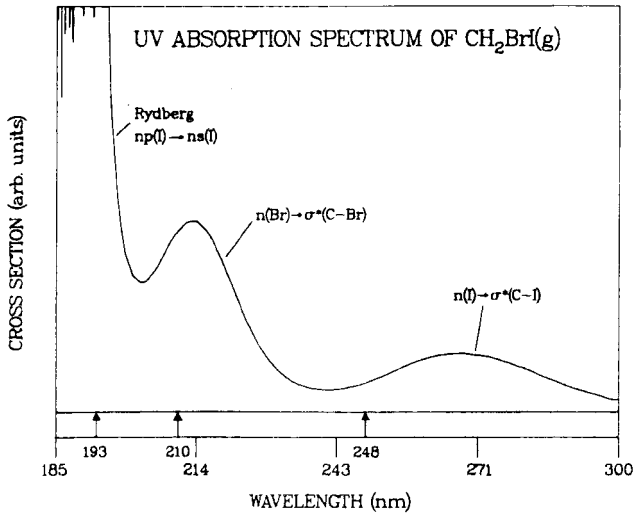

Figure 17. UV absorption spectrum of CH_2BrI. (Reprinted with permission from ref 98. Copyright 1987 American Institute of Physics.)

coupling terms. He solved the quantum dynamics of a dissociating collinear "pseudo-triatomic" made up of an I atom, a C atom, and a body representing the H_3 center of mass and obtained the intensity distributions of Raman lines CH_3I as it falls apart in good agreement with experiment of Imre et al.[24] Amatatsu, Morokuma, and Yabushita[94,95] calculated ab initio PESs of $^3Q_0$ and $^1Q_1$ excited states, and the results were fitted to three diabatic potential terms and their couplings. Then classical trajectory calculations were performed using these potential functions, taking into account the nonadiabatic transitions between the two surfaces. The results were, in general, in good agreement with the experimental findings.

B. Selective Bond Cleavage in CH_2BrI—Selective Scission of the Stronger C–Br Bond Rather than the Weaker C–I Bond

Selective bond cleavage in a molecule with two chromophores presents an interesting challenge. While thermal dissociation simply leads to the rupture of the weaker bond, selective scission of one of the two bonds is feasible with photodissociation. Lee and Bersohn[96] photodissociated CH_2BrI with a high-pressure Hg−Xe lamp. It was found that 14% of products were Br atoms resulting from the scission of the C−Br bond (stronger than the C−I bond), though 86% were I atoms. The anisotropy parameter β was 1.42. It was concluded that the Br atoms were formed as a result of a weaker absorption band (related to C−Br) hidden in the main absorption band (related to C−I). Butler et al. of Y. T. Lee's group[97,98] showed in photodissociation at 210 nm a bond-selective fragmentation process of breaking the C−Br bond rather than the C−I bond, with additionally some three-body dissociation into $CH_2 + Br + I$. At this wavelength, the absorption peak of the n(Br) → σ^*(C−Br) transition is clearly separated from the n(I) → σ^*(C−I) transition peaking near 270 nm (Figure 17).

C. Acetylene HC≡CH—Presence of an Exit Barrier Leads to C_2H ($\tilde{X}$) Rather than C_2H ($\tilde{A}$)

Acetylene in its ground state ($\tilde{X}^1\Sigma_g^+$) is linear. The C−C and C−H bond lengths (r_e's) are 1.203 and 1.060 Å, respectively.[72] The photodissociation threshold was determined by Mordaunt and Ashfold[99] to be D_0(HCC−H) = 46 074 ± 8 cm^{-1} (corresponding to 217.0 nm), using the rotationally resolved H-atom photofragment spectroscopy on the 211.53-nm photodissociation of jet-cooled acetylene.

The first singlet excited state ($\tilde{A}^1A_u$) arises from promotion of an electron from the $^1\pi_u(1a_u)$ to $^1\pi_g(4a_g)$ orbitals and has a trans-bent planar geometry, as discovered in the early 1950s by Ingold and King[100] and Innes.[101] This is the origin of the long progression of the ν_3 (trans-bending) mode found in the $\tilde{A}^1A_u - \tilde{X}^1\Sigma_g^+$ system (190−240 nm). The region 155−190 nm consists of a rather complex spectrum of diffuse bands ($\tilde{B}^1B_u - \tilde{X}^1\Sigma_g^+$), again with a long ν_3 progression. The $\tilde{B}^1B_u$ state has also a trans-bent geometry.[102]

The early history of photodissociation studies started from the high-energy side. Photolysis below 129.5 nm gave a fluorescence in the visible region as reported by Becker et al.[103] Okabe[104] determined the origin of this emission to be electronically excited C_2H (ethynyl). Okabe photodissociated C_2H_2 at 147[105] and 184.9 nm[106] and concluded that direct dissociation

$$HC{\equiv}CH + h\nu \rightarrow C_2H + H \qquad (17)$$

is the major primary process (with a quantum yield of 0.3) and the H_2 production process

$$HC{\equiv}CH + h\nu \rightarrow C_2 + H_2 \qquad (18)$$

is minor (quantum yield ≤0.1) at 147 nm. The remaining process was the formation of a metastable acetylene leading to diacetylene formation.

Photodissociation studies have lead to determination of the bond energy D_0 (C_2H−H). Wodtke and Y. T. Lee[107] found the reaction (eq 17) to be the major process at 193 nm. They determined D_0(C_2H−H) to be 132 ± 2 kcal by measuring the maximum release of translational energy for eq 17. After several slightly different values of D_0(C_2H−H) were reported by several groups,[108−111] Mordaunt and Ashfold[99] obtained a precise value of D_0(C_2H−H) mentioned above.

Fletcher and Leone[112] applied time-resolved FTIR emission spectroscopy to observe the nascent rotational distribution of C_2H ($\tilde{A}^2\Pi(010)$) formed at 193 nm. C_2H ($\tilde{A}^2\Pi$) is low-lying (T_0 = 3700 cm^{-1}). The average energy in rotation was found to be only 156 cm^{-1}, which was less than that in the 300 K C_2H_2 precursor. This rotational cooling was ascribed to orbital angular momentum carryaway by the tangential velocity of the leaving H atom.

The dynamics at 193 nm presents a big puzzle to solve. It was discussed by Wodtke and Y. T. Lee[107] by drawing the PES related to the $\tilde{A}^1A_u$ state as shown in Figure 18, based on the calculation of the isoelectronic molecule HCN by Vazquez.[113] The $\tilde{A}^1A_u$ state has an A″ symmetry in the C_s point group, so

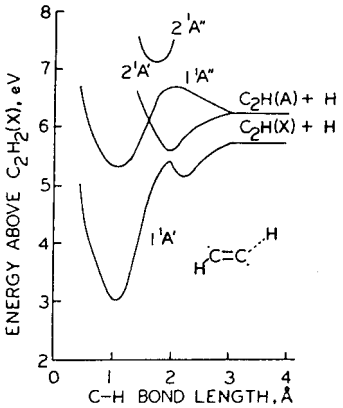

Figure 18. Potential energy curves for HC≡CH. (Reprinted with permission from ref 107. Copyright 1985 American Chemical Society.)

it is adiabatically correlated with C_2H ($\tilde{A}^2\Pi$) + H (^2S) in the planar geometry. Then photodissociation at this wavelength is likely to produce C_2H in the $\tilde{A}^2\Pi$ excited state. However, acetylene predissociates into C_2H ($\tilde{X}^2\Sigma$) + H (^2S). Does the internal conversion of the excited parent to the ground state occur before dissociation? Experimental observation of a significant release of translational energy renders this process unlikely to be an important channel. Actually, the total energy of the molecule excited onto the $\tilde{A}^1A_u-{}^1A''$ PES may be less than the barrier height in the exit channel of this surface. This slows down the C_2H ($\tilde{A}^2\Pi$) + H (^2S) process and allows the vibronic coupling from $1^1A''$ to $2^1A'$ to compete. Nonadiabatic surface hopping at the avoided crossing of $2^1A'$ and X^1A' would give the ground-state fragment pair C_2H ($\tilde{X}^2\Sigma$) + H (^2S). Later Cool et al.[114] remarked that a similar nonadiabatic transition in the corresponding triplet manifold may occur in parallel. Hsu et al.[115] probed the nascent state distribution of C_2H on the 193-nm photodissociation by LIF. Extensive bending excitation was observed. They proposed two dissociation mechanisms: (pre)-dissociation on the potential surface of the $\tilde{A}^1A_u$ state and predissociation via the low-lying dissociative triplet state. Both the $\tilde{A}$ and $\tilde{X}$ states of C_2H can be produced in the former, and only $\tilde{X}$ is formed in the latter. Hashimoto and Suzuki[116,117] and Ashfold and co-workers[118] examined translational energy release in dissociation from a number of $\tilde{A}$ state vibronic levels and found the presence of an exit barrier (~560 cm^{-1}) to dissociation. Hashimoto et al.[117] determined the upper bound for the lifetime of a metastable doorway state for dissociation (triplet precursor state) to be ≤100 ns. Recently Mordaunt et al.[119] detailed near threshold (205−220 nm) photodissociation using H-atom photofragment translational spectroscopy. C_2H ($\tilde{X}$) was found in most of the bending vibrational levels permitted by energy conservation. Its bimodal rotational distribution indicated two competing dissociation mechanisms $S_1 \rightarrow T_3 \rightarrow T_2 \rightarrow T_1$ and $S_1 \rightarrow T_1$. Most recently Suzuki and Hashimoto[120] probed the rovibrational state dependence of fluorescence and dissociation yield in the 46 295−49 108 cm^{-1} region. From the average translational energy release calculated from the Doppler profile of H atoms, they concluded that dissociation mainly occurs on the $\tilde{a}$ triplet state over a 560-cm^{-1} barrier, with a small contribution of another channel, dissociation via the ground state. Theoretical studies of C_2H were performed by Morokuma and co-workers.[121]

IR + UV photolysis (vibrationally mediated photodissociation, see also section IV.Q) of acetylene has been studied by several groups. By so doing one can excite the parent molecule in a molecular geometry far from its ground vibrational state. Propensities toward C_2H ($\tilde{A}^2\Pi$) were found by Zhang et al.[122] when they excited acetylene to the $\nu_1'' + 3\nu_3''$ (four quanta of CH stretch) vibrational level and then photodissociated at 248 nm, while direct 193-nm dissociation (only 1200 cm^{-1} less energy) gave C_2H ($\tilde{X}^2\Sigma^+$) as the primary product. Photodissociation at 121.6 nm gave C_2H ($\tilde{A}^2\Pi$) exclusively. Rosenwaks and co-workers[123−126] photodissociated vibrationally excited ($2\nu_1'' + 3\nu_3''$, five quanta of CH stretch) molecules at 243.1 nm. The rovibrational excitation leads to an enormous enhancement in CH bond cleavage. Combination bands (composed of high stretch and low bend), although very weak in absorption spectrum, showed an even larger enhancement within the action spectra. This was attributed to a better Franck−Condon overlap between the combination bands and the upper bent-electronic states that lead to photodissociation.

D. Cyanogen Iodine ICN—The I* and I Product Ratio Reflects the Linear and Bent Geometry of the Excited ICN

ICN is linear in its ground electronic state. The I−C and C−N bond lengths are 1.995 and 1.159 Å, respectively.[72] Dissociation energy D_0(I−CN) is 3.16 ± 0.05 eV.[8] A broad absorption band, the $\tilde{A}$ continuum, covers the 260−220 nm range. Another broad band ($\tilde{\alpha}$ band) is located at 180−210 nm. Rydberg states $\tilde{B}$ and $\tilde{C}$ appear near 170 and 157 nm, respectively.[127,128]

Two reaction channels in

$$ICN + h\nu \rightarrow CN\ (X^2\Sigma^+) + I\ (^2P_{3/2}),\ I^*\ (^2P_{1/2}) \quad (19)$$

are observed in the photodissociation in the $\tilde{A}$ continuum. The wavelength-dependent branching ratio I*/I leads to an interesting conjecture on the nature of excited states involved in the dynamics, that is, whether it has a linear or a bent geomety.

Ling and Wilson's photofragment spectroscopy experiment at 266 nm[129] revealed two peaks, corresponding to I* and I channels. Both were associated with the fragment angular recoil distribution peaking parallel to the electric vector of the light, indicating the dissociation process to be predominantly derived from parallel transitions. Pitts and Baronavski[130] determined the branching ratio I*/I across the $\tilde{A}$ state continuum as a function of wavelength (280−239.5 nm) by measuring the IR emission I* → I. The branching ratio increased from 0.30/0.70 at 280 nm to 0.61/0.39 at 266 nm and then decreased to 0.09/0.81 at 239.5 nm. Thus, they found contributions of three electronic states leading to CN (X) + I, CN (X) + I*, and again CN (X) + I with increasing photodissociation energy (Figure 19). Morse, Freed, and

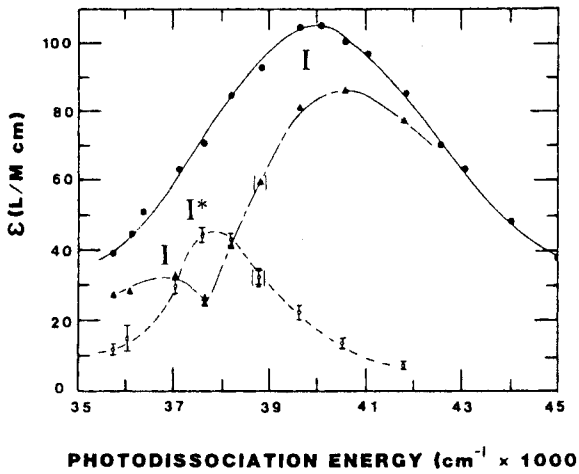

Figure 19. Contribution of I and I* channels to the absorption spectrum of ICN. (Reprinted with permission from ref 130. Copyright 1980 Elsevier Science.)

Band[131] theoretically predicted that CN (X) + I cannot be reached by a parallel transition to a linear excited state of ICN. Thus, at least one of the excited states concerned must be bent, because both I* and I are produced via excitation of parallel transitions as mentioned above. A bent ICN intermediate is likely to give rise to rotationally excited CN fragments. This reasoning led Marinelli et al. in Houston's group[132] to probe rotational distribution of CN (X) on the photodissociation of jet-cooled ICN at five wavelengths in the 290−235 nm range. Their results suggested that the ICN electronic state leading to CN + I* is linear, while two states leading to CN + I are bent. The upper of the two CN + I surfaces crosses the surface leading to CN + I*. A similar conclusion was reached in the sub-Doppler LIF study (on a flow sample) of Nadler et al.[133] at 266 nm. The CN + I* channel was associated with a rotational distribution peaked sharply at low N, while high N ($\geq$20) were selectively produced for CN + I. Apparently the low and high N are derived from linear and bent exit channel geometries, respectively.

These findings suggest the broad similarity of the dynamics of ICN to that of CH_3I. The $^3Q_0^+ \rightarrow {}^1Q_1$ curve crossing that constitutes one of the two origins of the ground-state iodine-atom I ($^2P_{3/2}$) has been the target of long, intense research. The relationship of anisotropy (β) and the internal energy (mostly rotational) imparted to the CN fragment has been extensively studied in this context.[134−137] Black[136] made a very detailed analysis of bipolar moments determined with a variety of excitation-detection geometries at 249 nm. The results were consistent with the contribution of three (one parallel and two perpendicular) optically active transitions at this wavelength. Griffiths and El-Sayed[137] studied photodissociation at 304.67 nm, where only the CN (X) + I ($^2P_{3/2}$) channel is accessible.

Alignment and orientation of the CN (X) fragment tell more about the finer details of the photodissociation dynamics. Hall et al.[138] determined rotational alignment $A_0^{(2)}$ of CN (X) at several photodissociation wavelengths in the 290−235 nm range for jet-cooled samples. At 245 nm, for example, the value of $A_0^{(2)}$ increased from −0.35 at low N (e.g., $N = 2$) toward −0.12 at high N ($N = 40$). O'Halloran et al. in Zare's group[46] determined $A_0^{(2)}$ on 248 nm photolysis of flowing ICN samples. The values ranged from −0.28 at low N to −0.12 at high N, in accordance with the results of Hall et al.[138] The $A_0^{(2)}$ values approaching the classical limit of −2/5 (corresponding to the case $\boldsymbol{J} \perp \boldsymbol{\mu}$) were indicative of the predominance of essentially a single excited electronic state with parallel absorption. Hasselbrink et al.[139] of Zare's group used circularly polarized 248-nm light for photolyzing ICN and probed the CN fragment using a counterpropagating right- or left-circularly polarized light. Very interestingly, the CN fragments were oriented. For CN (X, $v = 2$) fragments, the sense of orientation was opposite for the two fine-structure components F_1 and F_2. Spin−orbit interaction was the origin of the photofragment orientation.

North et al.[140] applied high-resolution transient frequency modulated absorption spectroscopy using A ← X LIF of CN (X) to obtain rotationally resolved anisotropy. Its value was strongly positive at 308 nm, indicating parallel transition at this long wavelength. Then Costen et al.[141] used this technique for almost the entire band photodissociation at 308, 266, 248, and 222 nm. Their results were in broad agreement with the theory. However, distinction of adiabatic and diabatic origin of I should be sought by the measurement of coherent effects on certain types of bipolar moments. They discussed the implication of coherent effects in Doppler spectra. The effects of coherence in multiple-surface reactions with mixed adiabatic and diabatic dynamics must be clarified.

ICN has been one of the target molecules of femtosecond real-time probing of photodissociation and femtosecond transition-state spectroscopy (FTS) by Zewail's group, as already described in section II.J[27,28,55−57] (see Figures 12 and 13).

On the theoretical side, Amatatsu, Yabushita, and Morokuma[142,143] published ab initio excited-state PESs. Five bright states comprise the Ã continuum. A bent $^3\Pi_0^+$ (A′) state correlates diabatically to I*. It can be populated from the ground state by a parallel transition. Bent A′ and A″ components of a $^1\Pi_1$ and a $^3\Pi_1$ state, all correlating diabatically to ground-state I atom, are populated by weaker perpendicular transitions located to the shorter and longer wavelengths of the $^3\Pi_0^+$ (A′) transition. Qian et al.[144] presented a time-dependent quantum mechanical calculation in the Ã continuum using the PESs obtained above. The calculated absorption spectrum, β parameters, the I/I* branching ratio, and the rotational distribution were in good agreement with experiment.

E. Nitrosyl Cyanide NCNO and Cyanogen NCCN

Four-atomic molecules such as NCNO and NCCN provide us a good opportunity to probe the detailed dynamics of photodissociation, since the internal energy of both diatomic fragments can be probed along with the translational energy. Doppler determination of the speed distribution of state-selected (v, J) photofragments gives us the internal energy distribution of the undetected coincident photofragments, thus leading to a total picture of energy

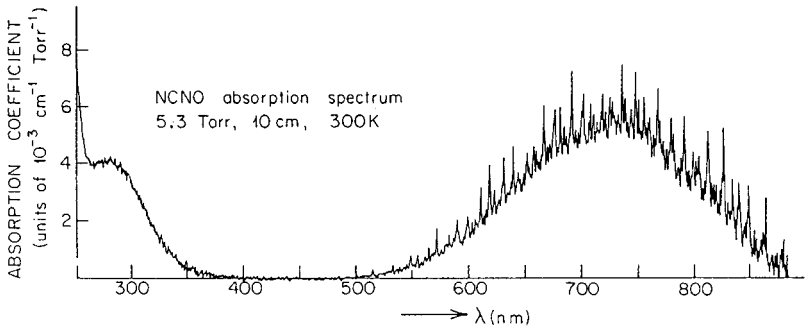

Figure 20. Absorption spectrum of NCNO. (Reprinted with permission from ref 145. Copyright 1984 American Institute of Physics.)

disposal. NCNO and NCCN are prototypes for statistical dissociation (ground-state dissociation following optical excitation), along with such molecules as CH_2CO, CF_3NO, and H_2O_2. Closer examinations of vibrational and rotational distributions revealed the more subtle nature of the energy distribution; the energy flow between vibrational and rotational degrees of freedom is not complete during the time of the dissociation event.

Nitrosyl cyanide (NCNO) has an almost linear N−C−N skeleton and a bent C−N−O bond (∠CNO = 113.6°).[6] Its $\pi^* \leftarrow$ n absorption band ($\tilde{A}^1A'' \leftarrow \tilde{X}^1A'$ is located in the very convenient visible and near-IR region (884−450 nm), as shown in Figure 20.[145] This excitation is accompanied with the opening of the CNO angle to 133°.[6] NCNO has an unusually weak central C−N bond. (Caution: It tends to explode violently when impure.) It undergoes photolysis below the threshold 585.3 nm[146]

$$\mathrm{NCNO} + h\nu \rightarrow \mathrm{CN}\ (\mathrm{X}\ ^2\textstyle\sum^+) + \mathrm{NO}\ (\mathrm{X}\ ^2\Pi)$$
$$D_0 = 17\ 085\ \mathrm{cm}^{-1} \quad (20)$$

(A much smaller dissociation energy 28.8 kcal mol^{-1} corresponding to 10 100 $cm^{-1}$was reported mass-spectrometrically.[6,145]) Pfab et al.[6] probed nascent CN (X) and NO (X) distributions by LIF, following the photodissociation at 532 nm. Both fragments were found mostly in the $v'' = 0$ state but rotationally hot. Energy partitioning was such that by far the largest portion (85%) appears as translational energy. The observed distribution of available energy into internal and translational degrees of freedom of the fragments was consistent with predissociation of bound Ã state levels into the continuum of ground-state NCNO. Nadler et al.[145] probed CN in the photolysis in the region 900−540 nm (either in the one- and two-photon) and found in the one-photon dissociation at 549 nm, $f_R = 0.33$, in good agreement with that predicted by PST (0.32). However, their closer examination in the expansion-cooled condition[146] showed the following. When CN $v = 2$ was reached, the CN rotational excitation was less than PST and CN vibrational excitation exceeded PST. They proposed the separate statistical ensemble (SSE) model, i.e., a PST modified to take into account the incomplete vibrational to rotational energy conversion during the photodissociation event. Doppler profiles of selected CN rotational lines were recorded by Qian et al.[147] in expansion-cooled conditions at several excess energies between 0 and 3000 cm^{-1}, yielding vibrational and rotational distributions of NO associated with specific CN (X) rotational states. Vibrational and rotational distributions of both products were statistical; the Doppler profiles could be fitted using the PST/SSE model.

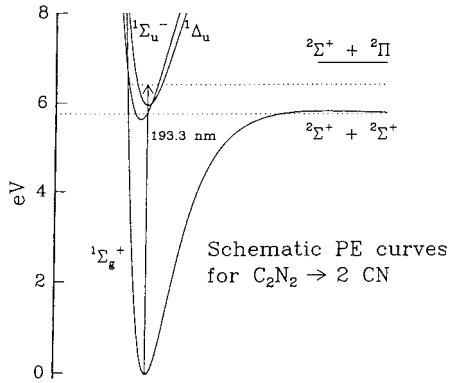

Figure 21. Schematic energy diagram for cyanogen dissociation at 193 nm. (Reprinted with permission from ref 150. Copyright 1997 American Institute of Physics.)

Knee et al. of Zewail's group[55] studied picosecond photofragmentation at two wavelengths. A relatively slow rise of CN (*N*-dependent) was observed at 611.7−604 nm, while the rise was instantaneous when a higher excited state of the parent was probed at 305.5 nm. Khundkar et al. of Zewail's group[148] measured microcanonical state-to-state rates using a picosecond laser and a molecular beam. The measured rate depended sharply on the total energy of the reactant (the characteristic time varied from ≥2.0 ns at the threshold to 10.0 ps at 690 cm^{-1} excess energy).

For cyanogen NCCN, the ground state is $\tilde{X}^1\Sigma_g^+$ of $D_{\infty h}$ symmetry.[8] A vibronically allowed $\tilde{A}^1\Sigma_u^- - \tilde{X}^1\Sigma_g^+$ transition occurs below 226 nm.[149,150] The continuum starts (i.e., threshold for dissociation into CN fragments) at 212.2 nm.[151] Below 210 nm another transition to the $\tilde{B}^1\Delta_u$ state starts.[150] Neither of these two states correlate directly to two ground-state CN fragments (Figure 21[150]). Therefore, the fragmentation

$$\mathrm{NCCN} + h\nu \rightarrow \mathrm{CN}\ (\mathrm{X}^2\textstyle\sum^+) + \mathrm{CN}\ (\mathrm{X}^2\textstyle\sum^+)$$
$$D_0 = 47\ 100\ \mathrm{cm}^{-1} \quad (21)$$

is a predissociation via internal conversion to the $\tilde{X}^1\Sigma_g^+$ ground state.

Halpern and Jackson[152] measured the vibrational and rotational distribution of the fragment CN at 193 nm. They found the same rotational temperature (900 K) for $v = 0$ and 1. This finding led them to the conjecture that the rotational motion is decoupled during the dissociation from the vibrational and translational motion of the fragments. The partition of available energy between the latter two degrees of freedom was consistent with a simple statistical model (the prior distribution). On the other hand, Eres et al.[153] found a totally nonstatistical vibrational distribution. Only 63% of that predicted by statistical calculation was observed in the $v = 1$ state and no population in the $v = 2$. Rotational distribution in each vibrational level was fairly well interpreted by simple PST. In the near-threshold (47 023−48 657 cm^{-1}) photodissociation study by Wannenmacher et al.,[149] the PST modeled the rotational structure of their PHOFEX spectra. Loss of alignment ($\boldsymbol{\mu}-\boldsymbol{J}$ correlation) suggested that C_2N_2 dissociates through a loose transition state with a small exit channel barrier and that the time for dissociation is much longer than the cyanogen rotational period. At 193 nm, however, Wu and Hall[154] observed a modest $\boldsymbol{V}-\boldsymbol{J}$ correlation with an increasing $\boldsymbol{V}\perp\boldsymbol{J}$ tendency at high N in their Doppler analyses of high-resolution transient absorption spectra. Coincident pair distribution indicated that the PST gave a reasonable fit to translational energy, but it overestimated the total internal energy of the photofragments. In North and Hall's Doppler LIF analyses[150] at 193 nm, the rotational distribution could be fitted by PST but the vibrational distribution was not, indicating that the product vibration becomes adiabatic sooner than the rotational degree of freedom (i.e., Wittig's SSE[70]). Their correlated vibrational distribution data $P(v_1, v_2)$ showed an excess of $P(0, 0)$ and a strong suppression of $v = 2$ compared to the PST prediction. The energy disposal at 157 nm was reported by Eng et al.[155]

F. Formaldehyde H_2CO—The Ground State of the Parent Molecule Has Very Nearly the Same Energy as the Products but They Are Separated by a High Barrier, S_1–S_0 Level Crossing Is Probed by the Stark Effect

Formaldehyde occupies its own niche in photodissociation studies because it is a prototypical "small and large" molecule. Moore and co-workers studied this system in great detail. In the ground state, the molecule is planar (C_{2v}) with C−H and C−O distances of 1.116 and 1.208 Å, respectively, and the angle ∠HCH 116.5°.[72] The UV absorption spectrum consists of many sharp bands in the 360−240 nm region.[8] After excitation of the $\tilde{A}^1A_2 \leftarrow \tilde{X}^1A_1$ transition (355−280 nm), molecular and radical reactions occur

$$H_2CO + h\nu \rightarrow H_2\,(^1\textstyle\sum_g^+) + CO\,(X^1\textstyle\sum^+) \quad (22)$$

$$H_2CO + h\nu \rightarrow H\,(^2S) + HCO\,(\tilde{X}) \quad (23)$$

The process given in eq 22 predominates for energies near the S_1 origin at 28 188 cm^{-1}, while eq 23 predominates above 32 250 cm^{-1}.[156]

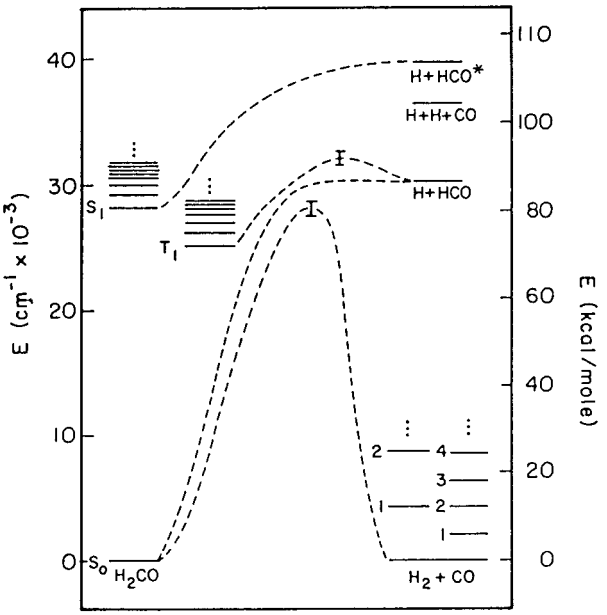

Figure 22. Potential energy diagram of photodissociation of H_2CO. (Reprinted with permission from ref 167. Copyright 1987 American Institute of Physics.)

The very interesting feature of eq 22 is that the ground state of the parent molecule has very nearly the same energy as the H_2 ($v = 0$) + CO ($v = 0$) products (Figure 22).[167] The distribution of available energy among many degrees of freedom is controlled by the *dynamics* of the fragments as they separate in the steep repulsive exit valley of the PES (a transition state with an average dissociation impact parameter of 0.9 Å).[158] Ho et al. (Moore's group with Y. T. Lee)[157] detected the molecular product CO by TOF mass spectroscopy for the photodissociation into H_2 + CO at the 2^14^1 and 4^1 vibrational bands in the S_1 state (339 and 353 nm, respectively). The product translational energy was very high; the maximum in the distribution was 65% of the total available energy. Ho and Smith[159] observed rotationally excited ($J = 26-63$) CO molecules on the 355 nm photolysis by VUV LIF. The 70 ns rise time of CO indicated *prompt* dissociation into H_2 and rotationally highly excited CO. The H_2 (v,J) distribution on the 2^14^1 of S_1 (29 500 cm^{-1}) photodissociation was probed by CARS by Pealat et al.[160] and Debarre et al.,[158] both with Moore's group. The vibrational distributions of H_2 peaked at $v = 1$.

Detailed aspects in the dissociation on the ground-state PES were clarified by Stark level-crossing spectra (Bitto et al.[161] and Polik et al.[162]). The enhanced nonradiative decay of S_1 occurs through the resonant S_0* state. Since S_1 and S_0* have different dipole moments, the S_1 state is Stark-shifted relative to the S_0* manifold as the electric field is increased, thereby tuning the individual S_0* state into and out of resonance. By monitoring S_1 fluorescence lifetimes as a function of applied electric field, the highly vibrationally excited S_0* energy levels can be mapped out. The dynamics of the intramolecular vibrational redistribution (IVR) was very nearly quantum ergodic. Vector correlations of *para*-H_2 ($v = 1$, $J = 0-8$) produced by photolysis on the $^rR_0(0)e$ line of the 2^14^1 $S_1 \leftarrow S_0$ transition were probed by Doppler-resolved

LIF.[163] Only small correlations were observed between the transition dipole moment $\boldsymbol{\mu}$ with the H_2 recoil velocity $\boldsymbol{V}$ and with the angular momentum $\boldsymbol{J}$, probably because the parent molecule rotates many times between excitation and fragmentation. H_2 rotational distributions and H_2 vector correlations were discussed through the analysis of Doppler-resolved LIF line shapes by Butenhoff et al.[164] and Carleton et al.,[165] both in Moore's group. Higher vibrational states of H_2 were correlated with lower rotational states of CO.[164] A simple impulsive model was not adequate to interpret the H_2 ($\boldsymbol{V},\boldsymbol{J}$) vector correlations.[165]

The dynamics of the radical dissociation process (eq 23) remain relatively unexplored. They were studied by Reilly, Clerk, Moore, and Pimentel.[166] Photolysis at 294.1 nm produced HCO in its ground vibrational state (~2/3) and one quantum of vibrational excitation in either the bending (~1/3) or CO stretching (10^{-1}−10^{-2}) vibrations. Chuang et al.[167] studied HDCO in the 329.5−289 nm range, detecting H or D by VUV LIF. The energy dependence H + DCO/D + HCO branching ratio showed a remarkable deviation from the statistical calculation. It was attributed to the participation of the first excited triplet (T_1) PES in dissociation in addition to the ground state (S_0) PES. They located the T_1 exit channel barrier height at 32 200 ± 200 cm^{-1}. Recently Dulligan et al.[168] studied at energies where the S_0 and T_1 radical pathways compete, by probing H by the high-n Rydberg time-of-flight (HRTOF) technique. Deduced HCO internal energy distributions revealed rotational excitation as high as $K_a = 6$ for $v = 0$. It was attributed to the contribution of the S_0 PES. Terentis et al.[169] probed HCO (N, K_a, K_c, J) distributions from near-threshold photolysis. The distributions were in general agreement with PST predictions. The deviation found within 10 cm^{-1} of the threshold was explained by inclusion of a centrifugal barrier. Valachovic et al.[170] of Wittig and Reisler's group accessed H + HCO products by both imaging and high-n Rydberg TOF spectroscopy (HR TOF) techniques at 1103−2654 cm^{-1} above the threshold (relocated at 30 328.5 cm^{-1}). The S_0 pathway dominated in the low end and the T_1 pathway in the high end.

The photochemistry of H_2CO was reviewed by Moore et al.[171,172]

G. Ketene CH_2CO

The molecular geometry of ketene in the ground state is such that the C−H, C−C, and C−O distances are 1.080, 1.317, and 1.161 Å, respectively, and the angle ∠HCH is 123.0°.[72] The absorption spectrum consists of diffuse bands in the 400−260 and 213−193 nm range.[8] Ketene in the near UV dissociates either in the singlet and triplet channel

$$CH_2CO + h\nu \rightarrow CH_2\,(\tilde{X}^3B_1) + CO\,(X^1\textstyle\sum^+) \qquad D_0 = 28\,290\ cm^{-1} \quad (24)$$

$$CH_2CO + h\nu \rightarrow CH_2\,(\tilde{a}^1A_1) + CO\,(X^1\textstyle\sum^+) \qquad D_0 = 30\,116\ cm^{-1} \quad (25)$$

Concerning the singlet channel (eq 25), the dynamics are essentially statistical. Moore's group made an extensive study near the threshold. Nesbitt et al.[173] detected CO ($v = 0$ and 1) from the 308-nm photodissociation. Their rotational state distribution was accurately matched by PST; the $v = 1/v = 0$ ratio (0.09) could be well fitted by Wittig's SSE model.[70] The barrier to dissociation was just the dissociation limit itself. The PST calculation matched the shape of PHOFEX measurement by Bitto et al.[161] Green et al.[174] determined the threshold at 30 116.2 ± 0.4 cm^{-1}.

Bitto et al.[175] dissociated ketene at 351 nm. At this low energy only the reaction in eq 24 proceeds on the triplet PES of the parent. Only $v = 0$ CO fragments were energetically allowed. Its rotational state distribution deviated drastically from PST. An impulsive model over a barrier was proposed. The appearance rate of CO from the triplet channel[176] showed a sharp increase at 28 290 cm^{-1}. The rate was compared to RRKM values with tunneling correction. The barrier height was 1330 ± 20 cm^{-1}. The rotational distribution was nonstatistical ($f_R = 0.224$), as predicted by an impulsive model.[177]

Kim et al.[178] determined the singlet/triplet branching ratio near the CH_2 ($\tilde{a}^1A_1$) threshold. Singlet yield increased from 0.15 to 0.70−0.80 at 56 and 1435−2521 cm^{-1} above the threshold. The rotational distribution of CO ($v = 0$) was bimodal between 56 and 425 cm^{-1} above the barrier. The peak at low J's due to the singlet channel was well described by PST. Rotational state distributions of fragments near the threshold (up to 2900 cm^{-1} excess energy) were probed also by Moore's group. Those of CH_2 ($\tilde{a}^1A_1$) showed good agreement with PST when probed close (within 200 cm^{-1}) to the threshold and became substantially colder for higher excess energy.[179,180] Those of CO ($v = 1$) also showed good agreement with PST up to 200 cm^{-1} excess energy and could be fitted by the constrained PST.[181]

Wodtke's group[182,183] performed quantum-state (v,J)-specific TOF measurements of CO for 308 nm dissociation. They obtained well-defined TOF peaks corresponding to three CH_2 internal state distribution ($\tilde{a}^1A_1$ (000) and (010), and $\tilde{X}\ ^3B_1$) occurring in coincidence with the chosen CO quantum state (v,J). The correlated product state distribution did not exactly follow simple PST. It could be more accurately reproduced by a PST with a restricted impact parameter. The latter model implies some restriction on the change of vibrational modes of the parent into rotational and translational motion of fragments. C−C−O bending modes in ketene may be hindered in some way at the transition state.

H. Isocyanic Acid HNCO—Very Complex Dynamics

The ground state of isocyanic acid contains an almost linear NCO group (∠NCO = 172.6°, ∠HNC = 123.9°).[184] A weak $^3A' \leftarrow {}^1A'$ absorption starts near 280 nm and is followed by a $^1A'' \leftarrow {}^1A'$ band in the 260−182.5 nm range with the maximum near 190 nm. Another $^1A'' \leftarrow {}^1A'$ band starts at 182 nm.[185,186] Absorption at shorter wavelengths was reported by

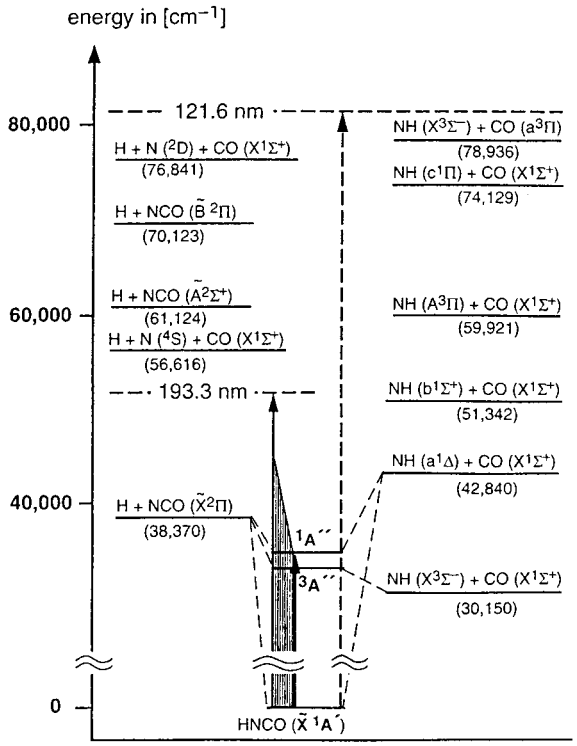

Figure 23. Energy level diagram of HNCO. (Reprinted with permission from ref 188. Copyright 1997 American Institute of Physics.)

Okabe.[187] An energy level diagram of HNCO was given by Brownsword et al.[188] (Figure 23).

The photochemistry of HNCO in the λ >190 nm range is very complex. Three reaction channels (eqs 26−28) occur on at least three PESs, S_1, S_0, and T_1.

$$\mathrm{HNCO}\ (\tilde{X}^1A') + h\nu \rightarrow \mathrm{NH}\ (X^3\textstyle\sum^-) + \mathrm{CO}\ (X^1\textstyle\sum_g^+) \qquad \Delta H = 30\ 060\ \mathrm{cm}^{-1} \quad (26)$$

$$\mathrm{HNCO}\ (\tilde{X}^1A') + h\nu \rightarrow \mathrm{NCO}\ (X^2\Pi) + \mathrm{H}\ (^2S) \qquad \Delta H = 38\ 370\ \mathrm{cm}^{-1} \quad (27)$$

$$\mathrm{HNCO}\ (\tilde{X}^1A') + h\nu \rightarrow \mathrm{NH}\ (a^1\Delta) + \mathrm{CO}\ (X^1\textstyle\sum_g^+) \qquad \Delta H = 42\ 750\ \mathrm{cm}^{-1} \quad (28)$$

The ΔH values are taken from a recent paper of Zyrianov et al.[189]

The photodissociation in the 230−190 nm range is dominated by the reaction in eq 28. Spiglanin and Chandler[190] scanned the 239−189 nm range, and the small amount of internal energy imparted for NH ($a^1\Delta$) (only $v = 0$, $f_R = 0.06-0.11$) was attributed to direct, impulsive dissociation from the nonlinear N−C−O configuration (120° in the $^1A''$ state). They[191] concluded at 230.1 nm that the threshold energy equals the dissociation energy (i.e., no barrier) from the translational energy of CO with $v = 0$, $J = 0-5$.

Concerning the channel (eq 27), Spiglanin et al.[192] reported the branching ratio NCO/NH ≤ 0.1 at 193 nm. Yi and Bersohn[193] reported $\phi(H) = 0.050$ and 0.13 at 193 and 212.6 nm, respectively. In the 193 nm photodissociation, Zhang et al.[194] detected H atoms by high-*n* Rydberg TOF spectroscopy (HR TOF) and obtained $f_T = 0.70$. This led to vibrationally excited (a long NCO bending progression was observed) but only modest rotational excitation in the counterpart, NCO. Direct dissociation was concluded from the strongly anisotropic product angular distribution. At 248 nm, eq 27 is the dominant channel with $f_T = 0.55$.[195]

Photodissociation in the near-threshold region is complex. Recent jet-cooled experiments performed by Reisler's group revealed the presence of significant barriers on the S_1 PES in the channels shown in eqs 27 and 28 that prevent direct dissociation on S_1. Zyrianov et al.[196] proposed that predissociation $S_1 \rightarrow S_0$ operates from the onset of eq 27 to at least 43 400 cm^{-1} (230 nm), although direct dissociation from S_1 cannot be excluded at higher energy. Sanov et al.[197] studied vector correlations in a photofragment imaging experiment. The value of β was close to zero at 243.1 nm in the channel given in eq 27. It was attributed to predissociation on S_1 to S_0. The substantial anisotropy $\beta = -0.66$ observed at 230.1 nm for the channel in eq 28 was attributed to direct dissociation on the S_1 PES or predissociation on S_1 to S_0. At 217.6 nm for the same channel, however, clear dynamical biases attributable to the direct dissociation were exhibited in the internal energy distributions.

The spin-forbidden triplet NH channel (eq 26) was studied rather recently. It must proceed via the triplet T_1. Jet LIF experiments of Zyrianov et al.[198] directly detected triplet NH from this reaction. They found a progressive loss of structure in its yield spectrum, at first a state-specific loss above 43 400 cm^{-1} (230 nm) and total loss above 44 000 cm^{-1}. This was attributed to the competition of intersystem crossing to T_1 with the direct reaction channels of eqs 27 and 28 which open one after the other over the respective barrier on S_1. Most recently Zyrianov et al.[189] probed the eq 27 at 17−411 cm^{-1} above threshold. Rotational state distributions of NCO could be described by PST taking a centrifugal barrier into account. Droz-Georget et al.[199] probed correlated distributions in the 230.1-nm photodissociation of NH ($X^3\Sigma^-$, $a^1\Delta$) and CO ($X^1\Sigma_g^+$) near the barrier on S_1.

Crim's group photodissociated HCNO via its C−H vibrational overtone, followed by UV excitation (vibrationally mediated photodissociation, VMP).[200−202] VMP of HNCO is described with those of other molecules in section IV.Q. Brown et al.[200] reported that the excitation of the second overtone of N−H stretching vibration ($3\nu_1$) followed by 291.5 nm excitation (Figure 24) led to a 4-fold increase of the NCO + H over NH + CO ratio compared to isoenergetic photolysis of the ground vibrational state. They[201] studied initial state (v,K) resolved photofragment yield spectra of NCO ($\tilde{X}^2\Pi$) and NH ($a^1\Delta$). They[202] observed the NH ($a^1\Delta$)/NH($X^3\Sigma^-$) branching ratio decrease using by $3\nu_1$ + UV vs UV excitation, i.e., VMP decreased the ratio. One possibility is that the N−H stretch promotes the $S_1 \rightarrow S_0$ predissociation and enhances the H + NCO channel, which competes with the NH ($a^1\Delta$) + CO channel. NH ($X^3\Sigma^-$) is likely to be formed by $S_1 \rightarrow S_0 \rightarrow T_1$.

On the theoretical side, Klossika et al.[203] of Schinke's group calculated a small barrier of about 550 cm^{-1}

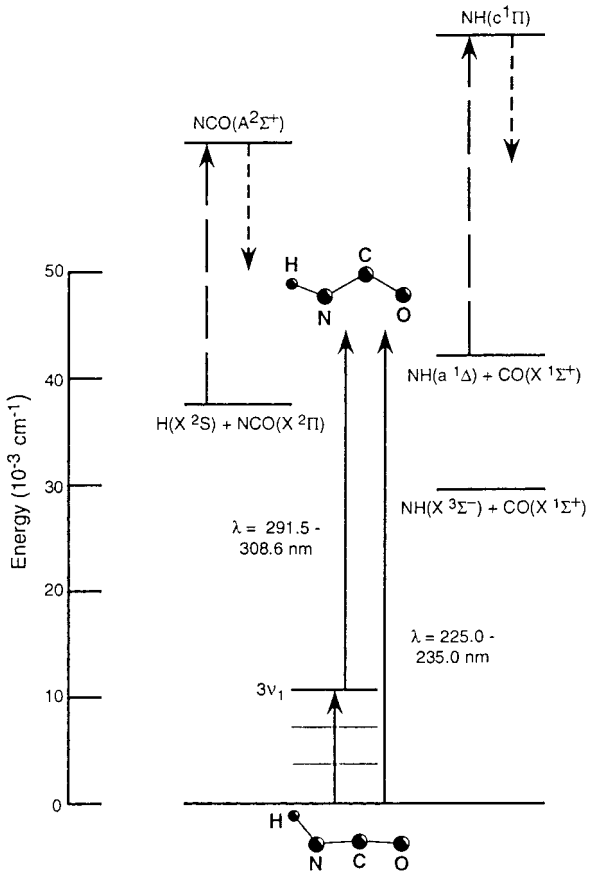

Figure 24. Vibrationally mediated photodissociation of HNCO. (Reprinted with permission from ref 200. Copyright 1996 American Institute of Physics.)

for eq 28 and a large barrier of ca. 8700 cm^{-1} for eq 27 via ab initio methods. Klossika and Schinke[204] presented a classical trajectory study using ab initio PESs. Morokuma and co-workers[205,206] presented ab initio studies on the participation of four electronic states, S_0, S_1, T_1, and T_2 in the three product channels of eqs 26−28.

I. Carbon Disulfide CS_2

CS_2 in the ground state ($\tilde{X}^1\Sigma_g^+$) is linear (R_e (CS) = 1.552$_6$ Å).[72] The first excited state (430−330 nm) is a triplet state ($^3A_2$).[8] CS_2 in the $^1B_2$ state (320−290 nm) produces no S atoms.[8] CS_2 in the S_3 ($\tilde{A}^1B_2$) band in the 230−185 nm range predissociates into CS and S fragments[207]

$$CS_2\ (\tilde{A}^1B_2) \rightarrow CS\ (X^1\Sigma) + S\ (^3P_J) \quad \lambda < 277.7\ \text{nm} \tag{29}$$

$$CS_2\ (\tilde{A}^1B_2) \rightarrow CS\ (X^1\Sigma) + S\ (^1D_2) \quad \lambda < 220.9\ \text{nm} \tag{30}$$

CS_2 in the S_3 ($\tilde{A}^1B_2$) excited state is bent.[208]

The branching ratio between eqs 29 and 30 is manifested in the S (^3P_j)/S ($^1D_2$) ratio. Waller and Hepburn[209] used VUV LIF detection of S atoms and obtained the S (^3P_j)/S ($^1D_2$) ratio of 2.8. Tzeng et al.[210] probed both fragments CS and S by TOF experiments and obtained results compatible with the ratio of 2.5. Detailed studies by Hepburn's group[211,212] in the range 214−198 nm revealed that the S (^3P_j)/S ($^1D_2$) ratio was mode-specific, as was the predissociation lifetime. They varied as a function of vibrational levels in the CS_2 ($\tilde{A}^1B_2$) state. Moreover, $K = 0$ levels gave mostly S ($^3P_2$) while $K = 1$ levels displayed a marked enhancement of S ($^1D_2$). The predissociation time of $K = 1$ levels was shorter than that of $K = 0$.

Baronavski and Owrutsky[213] measured the lifetime of the S_3 state by femtosecond MPI. The lifetime at 205 nm was 600 fs. Quite recently, Farmanara et al.[214] measured the lifetime as a function of exciting wavelength. It decreased from 620 fs at 207 nm to 180 fs at 194 nm. A nearly constant plateau at about 200 nm was attributed as representing the barrier from the bent to quasilinear geometry of the excited CS_2 molecule.

On excitation to the Rydberg states at shorter wavelengths

$$CS_2 \rightarrow CS\ (A^1\Pi) + S\ (^3P_J) \quad \lambda < 133.7\ \text{nm} \tag{31}$$

$$CS_2 \rightarrow CS\ (A^1\Pi) + S\ (^1D_2) \quad \lambda < 119\ \text{nm} \tag{32}$$

are observable. Okabe[215] detected the CS ($A^1\Pi$) fluorescence. Equation 31 is spin-forbidden. L. C. Lee and Judge[216] and later Ashfold, Simons, and others[217] reported the vibrational distribution of CS ($A^1\Pi$). Anisotropy in the two-photon (at 308 nm) excitation of CS_2 was reported by Kawasaki et al.[218,219]

J. Ammonia NH_3—Despite Its Deceptive Simplicity, the Dynamics Is Very Complicated. H Atoms Tunnel through a Barrier

Ammonia plays a major role in the chemistry of the Jovian atmosphere. This molecule in the ground state ($\tilde{X}\ ^1A_1$) is pyramidal (C_{3v} symmetry). The N−H bond distance (r_e) is 1.012 Å, and the angle ∠HNH (θ_e) = 106.7°.[72] Its UV absorption spectrum consists of $\tilde{A}^1A_2''$ (220−170 nm, with a long progression of out-of-plane umbrella bending vibration ν_2)[8] and $\tilde{B}^1E''$ (170−140 nm) bands.[220] The molecule is planar (D_{3h}) in these excited states. In the $\tilde{A}$ state, the predissociation reaction

$$NH_3 + h\nu \rightarrow NH_2\ (\tilde{X}^2B_1) + H(^2S) \quad \lambda < 280\ \text{nm} \tag{33}$$

is the primary process with essentially unit quantum yield.[8]

Despite its deceptive simplicity, the $\tilde{A}$ state dynamics of ammonia are very complicated. According to theoretical studies,[221−223] the equilibrium (D_{3h}) configuration is at the energy minimum on the $\tilde{A}$ state PES. H-atom loss then must proceed via an energy barrier, the height of which increases with increasing out-of-plane bending angle. Dissociation of $v = 1$ and 2 can occur by tunneling through this barrier. The existence of a conical intersection between $\tilde{A}$ and $\tilde{X}$ PESs of the parent molecule at larger H−NH_2 separations makes the situation even more complex (see Figure 25[222]).

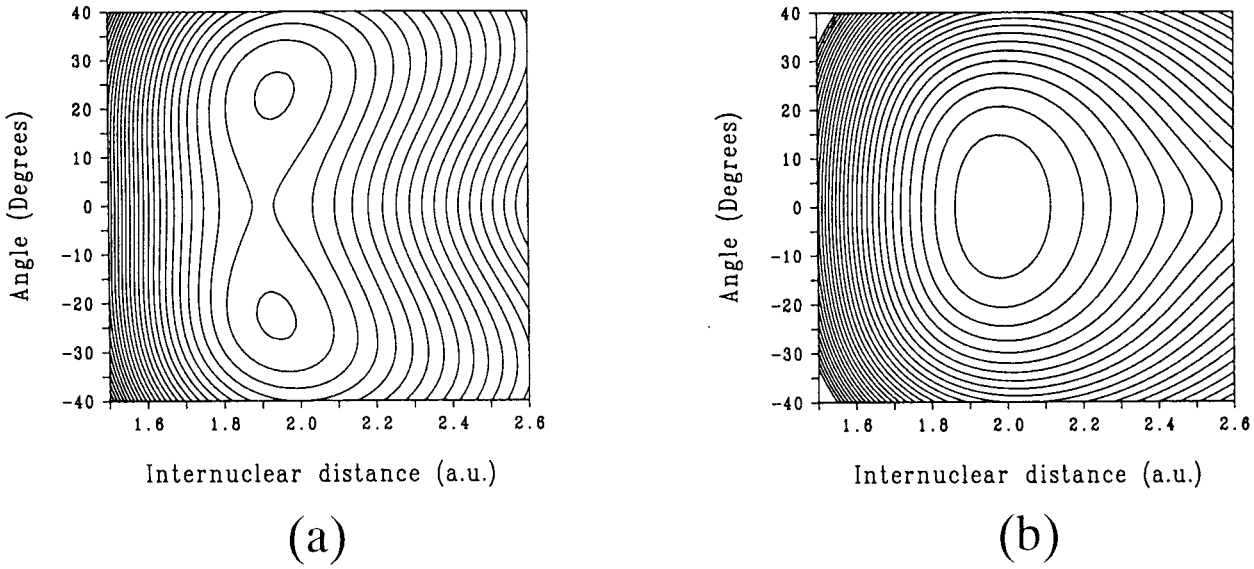

Figure 25. Potential energy surfaces of for the $\tilde{X}$ (a) and $\tilde{A}$ (b) states of NH_3 (Reprinted with permission from ref 222. Copyright 1987 American Institute of Physics.)

Ashfold et al.[224] determined the dependence of predissociation lifetimes of NH_3 and ND_3 on vibronic states of the parent $\tilde{A}$ state. Rates measured for the levels 2^0 and 2^1 in both isotopic species were interpreted in terms of H-atom loss by quantum tunneling through an exit channel barrier. Probing of the NH_2 ($\tilde{X}^2B_1$) state distributions by LIF was very difficult due to the formidable complexity of the spectrum.[225] Biesner et al. of Welge's group with Ashfold and Dixon[226,227] used H-atom Rydberg photofragment spectroscopy of jet-cooled NH_3 to extract the vibrational and rotational distribution of the counterfragment NH_2 ($\tilde{X}^2B_1$) on photodissociation from the two lowest vibrational levels ($v_2 = 0$ and 1) of the $\tilde{A}^1A_2''$ state of the parent (at 216.38 and 212.33 nm, respectively). Bands with $N = K_a$ were dominant in the rotational structure. Such high levels of *a*-axis rotational excitation accounted for the bulk of the internal energy in the NH_2 ($\tilde{X}$) fragments. The anisotropy β was negative for low N and positive for high N.[228] This means that the H atom is ejected at right angles and parallel to the C_3 top axis of NH_3 at low and high N, respectively. Velocity aligned Doppler spectroscopy (VADS) on the H-atom fragment was carried out by Xu, Koplitz, and Wittig for the 193-nm photodissociation.[229,230] Recent angle-resolved H-atom photofragment spectroscopy by Mordaunt et al.[231] revealed much finer details of the photodissociation. Dissociation from the lowest vibrational levels ($v_2 \leq 1$) occurs predominantly via H-atom tunneling through an exit channel barrier leading to $NH_2 + H$. The vector correlation of H atoms was found to be bimodal. The H atoms born in association with the counter NH_2 fragments with little rotational excitation and those born with the NH_2 fragments with high rotational excitation were shown to have very different β values, tending to -1 and $+2$ (asymptotically perpendicular and parallel $\boldsymbol{\mu}-\boldsymbol{V}$ correlation), respectively. These two must come from different origins. Mordaunt, Ashfold, and Dixon[232] showed the anisotropy of the recoiling $D + ND_2$ (X) photoproducts to be dependent upon five quantum numbers (rotational quantum numbers in the absorption of the parent (J', J'', K) and the rotational and vibrational quantum numbers of the product).

Woodbridge et al.[233] determined the rovibrational state distribution of the NH_2 ($\tilde{A}^2A_1$) fragment (threshold = 206 nm) at 193 nm by time-resolved FT IR emission spectroscopy. NH_2 ($\tilde{A}^2A_1$) fragments were observed predominantly in the vibrational ground state, with substantial rotational excitation about the *a*-inertial axis up to the limit of the available energy. Loomis et al.[234] found a bimodal $N = K_a$ rotational distribution in the $v_2 = 0$ (predominant) NH_2 ($\tilde{A}$) fragments in the 193 nm photolysis, using IR emission spectroscopy.

Kenner et al.[235] of Stuhl's group reported observation of NH ($a^1\Delta$) due to the

$$NH_3 + h\nu \rightarrow NH(a^1\Delta) + H_2\,(^1\textstyle\sum_g^+) \quad \lambda < 224\ \text{nm} \tag{34}$$

channel in a one-photon process during the 193 nm photolysis. Two-photon formation of NH ($A^3\Pi$), first observed by Donnelly et al.,[236] was studied in detail by Stuhl's group.[237−239] Sequential formation of NH ($A^3\Pi$) via the NH_2 intermediate (internally excited ground state) was shown by double-pulse experiments by Stuhl's group.[240,241]

K. Hydrazoic Acid HN_3

Hydrazoic acid (HN_3) is isoelectronic to HNCO. HN_3 in the electronic ground state $\tilde{X}^1A'$ is planar, consisting of an almost linear N_3 chain and a strongly bent NH bond.[242] Its electronic absorption spectrum starts near 320 nm[243] and has maxima near 265, 204, and 190 nm. It first maximum corresponds to the transition from the ground state to the first singlet excited state $\tilde{A}^1A''$ (Figure 26).[244] The corresponding transition moment $\boldsymbol{\mu}$ ($\tilde{A} - \tilde{X}$) is perpendicular to the symmetry plane of the parent. HN_3 is a very fragile molecule; the bond energy relative to formation of

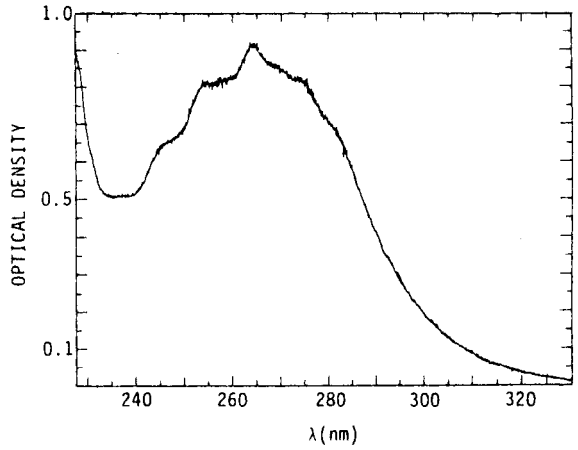

Figure 26. Absorption spectrum of HN_3. (Reprinted with permission from ref 244. Copyright 1978 Elsevier Science.)

ground-state fragments NH ($X^3\Sigma^-$) and N_2 ($X^1\Sigma_g^+$) is as small as 0.47 ± 0.06 eV (ca. 6000 cm^{-1}).[8] However, the reaction generating ground-state NH

$$HN_3\,(\tilde{X}^1A') + h\nu \rightarrow NH\,(X^3\textstyle\sum^-) + N_2\,(X^1\textstyle\sum_g^+) \quad (35)$$

is spin forbidden. Photodissociation in the near UV is dominated by the singlet-channel

$$HN_3\,(\tilde{X}^1A') + h\nu \rightarrow NH\,(a^1\Delta) + N_2\,(X^1\textstyle\sum_g^+) \quad (36)$$

as pioneered by McDonald et al.,[243] Baronavski et al.[244] at 266 nm, and Kenner et al.[235] at 193 nm. The reaction is impulsive rather than statistical. Gericke et al.[242] probed vector correlations at 266 nm. The value of β ($\boldsymbol{\mu}-\boldsymbol{V}$ correlation) was negative for low J_{NH} and positive for high J_{NH}. The $\boldsymbol{V}-\boldsymbol{J}$ correlation was positive and increased with J_{NH}, showing preferential parallel alignment of $\boldsymbol{V}_{NH}$ and $\boldsymbol{J}_{NH}$. The HN_3 distorts from a nonplanar configuration after excitation of a linear−bent electronic transition in the NNN framework, resulting in a strong N_2 rotation and relatively weak NH rotation. Nelson and McDonald[245] and Hawley et al.[246] completely characterized energy partitioning in the range 220−290 nm. The vibrational population distribution, although sometimes reported to be inverted, showed a smooth decrease with the vibrational quantum number. They found a marked wavelength dependence of the NH ($a^1\Delta$) $v = 1/v = 0$ population ratio. Its rather steep rise near 250 nm was not totally unexpected from the nonstatistical direct dissociation mechanism. The counterpart fragment N_2 ($X^1\Sigma_g^+$) was probed by Chu et al.[247] in the vicinity of 283 nm using MPI. The N_2 fragment was found only in the $v = 0$ level, rotationally highly excited. The value of $A_0^{(2)}$ ($\boldsymbol{\mu}-\boldsymbol{J}$ correlation) was positive and ca. 0.5. Gericke et al.[248] performed a detailed vector correlation study in the $1^1A''$ band at various excitation energies in the range 308−248 nm. Meier and Staemmler[249] performed ab initio and valence CI calculations on the reaction in eq 36 from the $1^1A''$ state.

Hydrogen-atom-producing channels

$$HN_3\,(\tilde{X}^1A') + h\nu \rightarrow N_3\,(\tilde{X}^2\Pi) + H(^2S) \quad (37)$$

$$HN_3\,(\tilde{X}\,^1A') + h\nu \rightarrow N(^4S) + N_2\,(X\,^1\textstyle\sum_g^+) + H\,(^2S) \quad (38)$$

were probed at 248 and 193 nm by Gericke et al.[250] H atoms were detected by VUV LIF. The quantum yield of H atom is 0.24 and 0.15 at 248 and 193 nm, respectively. The H atoms detected were attributed to the channel in eq 37. Haas et al.[251] deduced the vibrational population distribution of N_3 indirectly through the kinetic energy distribution of H detected by REMPI−TOFMS. The excitation of the symmetric stretching mode of N_3 indicated the dominating influence of the $N-N_2H$, N_2-NH, and N_3-H coordinates of the upper PES on the N_3 internal energy distribution. Zhang et al.[252] used the high-*n* Rydberg H-atom TOF (HRTOF) technique and obtained $f_T = 0.71$, $\beta = -0.8$ at 248 nm. At 193 nm, the internal energy-dependent variation of β was suggestive of multiple dissociation pathways via different electronic states.

Foy et al.[253−255] and Casassa et al.[256] studied eq 35 by vibrational overtone ($5\nu_1$, $6\nu_1$) excitation. The NH ($X^3\Sigma^-$) product had little vibrational and rotational excitation. This was considered to be the result of HN and NN bonds in the S−T crossing region possessing bond lengths equivalent to free molecule values and a small impact parameter.[253] The predissociation rates increased monotonically with vibrational energy in the ($5\nu_1 - 6\nu_1$) energy range.[255]

L. Nitrogen Dioxide NO_2—Fluctuation in the Statistical Rotational Distribution of NO Product on Near-Threshold Photodissociation

This molecule is bent in its ground state ($\tilde{X}^2A_1$) with the O−N−O angle = 134.1°.[72] The absorption spectrum of NO_2 in the near UV−visible region is extremely complex.[257,258] Two excited states $\tilde{A}^2B_2$ and $\tilde{B}^2B_1$ are involved. A long vibrational progression develops in the visible region, because these excited states have equilibrium bond angles 111° and 180°, respectively, substantially different from that in the ground state.[257,259] Moreover, there is a strong vibronic coupling between the $\tilde{A}^2B_2$ state and high vibrational levels of the ground $\tilde{X}^2A_1$ state.[258]

The photodissociation limit for the reaction

$$NO_2 + h\nu \rightarrow NO\,(X^2\Pi) + O(^3P) \quad (39)$$

is 25 132 cm^{-1}, corresponding to 397.86 nm.[260]

There has been a long-sustained controversy on the statistical/nonstatistical nature of photodecomposition of NO_2. However, recently it seems to have settled down as essentially statistical for photodissociation immediately above the threshold, and the main target of research interest has moved into the more subtle issue related to characteristic *fluctuations* observed in the rotational distribution.

Early experiments were performed well above the threshold and pointed to nonstatistical behavior. Busch and Wilson[39,261] applied photofragment spectroscopy at 347 nm and found nonstatistical behavior. The average translational energy of the fragments was about 60% of the available energy. Their angular distribution peaked in the direction of the electric vector of the light, indicating that the predominant upper state is of $^2B_2$ symmetry. Vibrational and rotational distributions of NO ($X^2\Pi$) fragments were probed at 337 nm at room temperature in bulk conditions by Zacharias et al. of Welge's group.[260] They were nonstatistical; the partitioning of available energy was about 70% into internal (51% into vibration and 16% into rotation of NO) and 30% into recoil fragment energy. The high rotational excitation of NO was attributed to the decay of NO_2 in highly excited *bending* vibrational states reached by vertical Franck−Condon transitions. Conservation of total angular momentum was attributed to a correspondingly large orbital angular momentum of the two fragments. Vibrational distributions of NO fragments were strongly inverted in the 248 nm photodissociation work of Slanger et al.[262] in a flow cell, with most of the nascent NO being in $v = 6-8$. A peculiar rotational distribution was also observed.

Mons and Dimicoli[263] determined velocity and angular distributions of photofragments in well-defined internal states by photodissociation (at 360 nm) in an effusive jet in the interaction chamber of a TOF mass spectrometer, followed by state-selective ionization in a REMPI process. They succeeded in determining E_T and E_{INT} values for $J = 29/2$, 37/2, 47/2, and 57/2 rotational levels of the NO ($X^2\Pi_{3/2}$, $v = 0$). The values of β were all close to 0.9, indicating that fragments were preferentially ejected in the direction of the polarizing vector $\boldsymbol{E}$. f_T was 80% for $J = 29/2$, decreasing to about 40% for $J = 57/2$. Then Mons and Dimicoli[264] applied the REMPI TOF MS method to the near-threshold photodissociation of NO_2 in a thermal jet at excess energies from -600 up to 1700 cm^{-1} above the NO ($X^2\Pi$, $v = 1$) + O (^3P) dissociation limit. Above the threshold, the rotational distribution was essentially statistical. Translational and rotational anisotropies, positive β, and negative A values, respectively, were consistent with the picture of the excitation toward a B_2 symmetry state in the C_{2v} configuration of the parent molecule. Below threshold, the energy for bond scission comes from parent rotation.

The main interest in the 1990s has been centered on the photodissociation in the near-threshold region. Robra, Zacharias, and Welge[265] photodissociated NO_2 in a seeded supersonic molecular beam near the threshold (redetermined to be 25 130.6 ± 0.6 cm^{-1}). Up to an excess energy of 121 cm^{-1}, about 42% of the excess energy was partitioned into rotation of NO, hence 58% into the translational degrees of freedom. Photofragment-excitation (PHOFEX) spectra for NO ($^2\Pi_{1/2,3/2}$, $v = 0$, J) exhibited characteristic structures near the threshold region of the respective channels with a different rotational quantum number J. An interesting Π^+/Π^- population alternation was found at excess energies 38 $cm^{-1} \leq E_{exc}$(over D_0) $\leq$ 59 cm^{-1}. The average rotational energy of the NO product showed a discrete (stepwise) increase when a new rotational state in the product becomes accessible, suggesting an exit channel effect.

Near-threshold photodissociation experiments performed by two groups (Tsuchiya's and Reisler's) gave product state distributions fluctuating around statistical values. Miyawaki et al. of Tsuchiya's group[266] observed the O (^3P_J)-photofragment excitation (PHOFEX) spectrum of NO_2 by detecting O (^3P_J) near the dissociation limit. The branching ratios of the spin−orbit sublevels showed a significant fluctuation. However, their averaged values were consistent with those predicted by a restricted statistical distribution model, in which the predissociation rate is proportional to the number of energetically allowed channels of an NO fragment multiplied by constant factors. Robie et al. of Reisler's group[267] studied the photodissociation near the NO $v = 1$ threshold. The vibrational populations were nonstatistical as compared with the predictions of phase space theory (PST). The rotational distributions in both NO $v = 0$ and 1 showed pronounced structures and fluctuations. However, their average could be fit fairly well by PST. The structures were interpreted as fluctuations inherent in the decomposition of an excited complex with many overlapping resonances (Ericson fluctuations). Miyawaki et al.[268] then monitored the specific quantum states of fragment NO ($^2\Pi_{1/2}$, $v = 0$, $J = 0.5-6.5$) in the energy range 0−160 cm^{-1} above the dissociation limit of NO ($^2\Pi_{1/2}$) + O ($^3P_2$) using an extremely cold (≈1 K) jet and high (≈0.05 cm^{-1}) resolution. The dissociation rate constant k (obtained from the peak width of the PHOFEX spectrum) increased stepwise when a new rotational product channel opens (e.g., $J = 1.5$ following $J = 0.5$) in accordance with the statistical theory. A loose transition state (PST-like) was assumed. State (J, Λ)-dependent product distributions fluctuated around the statistical values and were interpreted as statistical fluctuations due to the complete mixing of vibrational modes in NO_2. Hunter et al. of Reisler's group[269] examined detailed vibrational, rotational, and electronic distributions of nascent NO($X\ ^2\Pi_{1/2,3/2}$) on near-threshold (0−3100 cm^{-1} above the threshold) photolysis of expansion-cooled (T_{rot} < 10 K) NO_2. All rotational distributions of the NO ($v = 0$, 1) product followed statistical distributions on average but showed prominent fluctuations. The NO ($v = 1$) population was greater than expected by PST. The population was bounded by the predictions of the SSE[70] method (the product vibrational excitation is only from parent vibration). Variational-RRKM calculations[68] were in agreement with the experimental results. Reid et al. of Reisler's group[270] interpreted the rotational fluctuations in terms of projections of coherently excited overlapping ($\tilde{X}^2A_1/\tilde{A}^2B_2$) molecular eigenstates onto the manifold of final states via the levels of the transition state. Then Reid et al.[271,272] examined the nature of fluctuations in a more detailed way by double-resonance IR/visible photofragment yield spectra (PHOFRY).

Wittig and co-workers studied NO_2 photodissociation in the time domain.[273,274] Ionov et al. determined

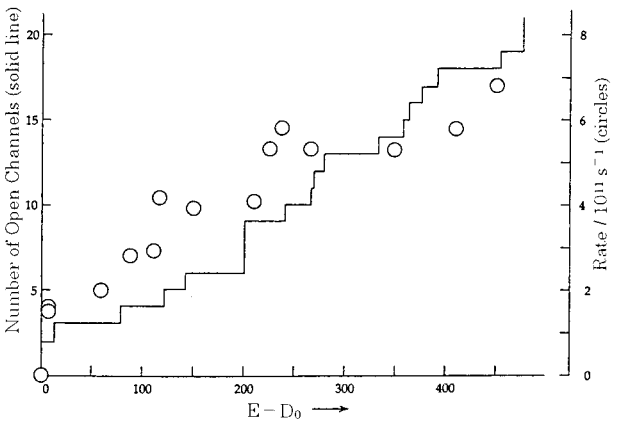

Figure 27. Decomposition rate (○) in comparison with the number of open channels from the theoretical study of NO_2. (Reprinted with permission from ref 274. Copyright 1994 American Institute of Physics.)

the unimolecular decay rates by probing the build-up of NO LIF signal from expansion-cooled (≈6 or ≈1 K beam, 0.02 cm^{-1} resolution) NO_2 following subpicosecond excitation in the range 24 894−26 656 cm^{-1} (402−375 nm). Above threshold, the rate increased "steplike" with the excitation energy. The ca. 100 cm^{-1} step was assigned to bending in the transition state. The measured rate was consistent with simple transition-state theory predictions. Its dependence on the excess energy ran parallel with the number of open channels W (see eq 13) calculated by Katagiri and Kato[275] (Figure 27). Actually they become equivalent when $\rho = 0.75/cm^{-1}$ is used. Jost et al.[276] redetermined the threshold to be 25 128.57 ± 0.05 cm^{-1}. They found that the density of vibronic levels in the threshold region was very high (2.7 levels/cm^{-1}).

Very recently, Monti et al.[277] reported on the rapidly fluctuating anisotropy parameter (β) in the near-threshold region. Ahmed et al. of Suits' group[278] presented the evidence for the coherence between parallel and perpendicular contributions to the photodissociation at 212.8 nm.

M. Ozone O_3—Many New Findings Important in Relation to the Ozone-Deficit Issue

Ozone is a strong absorber of solar radiation. Its photochemistry plays a crucial role in the upper atmosphere of the earth. Ozone in the ground state is bent.[72] The dissociation energy $D_0(O-O_2)$ is as small as 1.05 ± 0.02 eV (corresponding to 1180 nm).[8] Absorption of light starts near 900 nm. The Chappuis (850−440 nm), Huggins (360−300 nm), and Hartley bands (320−200 nm) are known.[8]

In the visible region (the Chappuis band) only

$$O_3 + h\nu \rightarrow O_2\,(X^3\textstyle\sum_g^-) + O\,(^3P) \quad \lambda < 1180\ \text{nm} \qquad (40)$$

occurs. (Thermochemical limits[8] are shown in wavelengths in this section.) Fairchild et al.[279] applied photofragment spectroscopy at 600 nm and found $O_2(X^3\Sigma_g^-)$ fragments with $v = 0$, 1, 2. Valentini and co-workers[280−282] reported collision-free CARS spectra of the $O_2(X^3\Sigma_g^-)$ fragment in the 300 K photodissociation of O_3 at 638−560, 578, and 532 nm. The nascent vibrational, rotational and translational energy distributions were (on average) 10%, 24%, and 66% of the available energy, respectively.[282] Only a narrow range of high rotational levels was populated. Vibrational distributions were such that only states $v = 0-4$ were populated. It was concluded that the dynamics were vibrationally adiabatic but rotationally impulsive. No evidence for the $O_2(^1\Delta_g)$ state was found even though it is energetically accessible.

In the 200−320 nm range (the Hartley band), in addition to the reaction in eq 40

$$O_3 + h\nu \rightarrow O_2(a^1\Delta_g) + O(^1D) \quad \lambda < 310\ \text{nm} \qquad (41)$$

occurs. Brock and Watson[283] determined the quantum yield (ϕ) of O (^{3}P) to be 0.12 ± 0.02 at 266 nm, which gives ϕ (O^1D) = 0.88. Much later, Turnipseed et al.[284] measured ϕ (O^3P) at 222 nm to be 0.13 ± 0.02. At 193 nm they determined ϕ (O^1D) by converting O (^{1}D) to OH, which was then detected by LIF, yielding ϕ (O^1D) = 0.46 ± 0.29 and $\phi(O^3P) = 0.57 \pm 0.14$. They discussed the implication of the sum being greater than unity as the presence of a channel which produces three O (^{3}P) atoms. Cooper et al.[285] directly measured the relative quantum yield of O ($^1D_2$) in the wavelength region 221.5−243.5 nm by observing the weak 630-nm fluorescence due to the spin-forbidden O ($^1D_2$) → O (^{3}P) transition.

Sparks et al.[286] applied the TOF method to ozone photolysis at 266 nm to determine the electronic/vibrational state distribution of primary products. They obtained vibrational population distributions of $v = 0-3$ levels in eq 41.

Imre, Kinsey, et al.[25,26] measured the emission spectrum of the dissociating ozone molecule. The spectrum revealed overtones and combination bands in ν_1 (symmetric stretch) and even quanta of ν_3 (antisymmetric stretch). No progression in ν_2 (bending mode) was present, indicating that the change in bond angle with excitation is very slight. Valentini and co-workers[287−289] measured the CARS spectrum of O_2 ($a^1\Delta_g$) formed on the photodissociation of O_3 at 266 and 311−230 nm. The vibrational distribution peaked very sharply at $v = 0$, while the rotational distributions were narrow with a peaking at high J. This was interpreted as a vibrationally adiabatic and rotationally impulsive dissociation. Propensity for even−J rotational states was attributed to nuclear symmetry restrictions during the O_2 ($X^3\Sigma_g^-$) + O (^{3}P)/O_2 ($a^1\Delta_g$) + O (^{1}D) curve crossing. Daniels and Wiesenfeld[290] probed rotational distributions of O_2 ($X^3\Sigma_g^-$, $v'' = 9$, 12, and 15) by LIF following ozone photolysis at 248 nm. The nascent rotational distribution peaked at 15% of the available kinetic energy. The energy release was largely impulsive. These authors gave approximate potential energy curves of O_3 (Figure 28). Photofragment vector correlations were probed using photofragment imaging techniques by Suits et al.[291] for O_2 ($a^1\Delta_g$, v, J) from the 248-nm photodissociation of ozone. The O_2 fragments were shown to recoil with substantial rotational

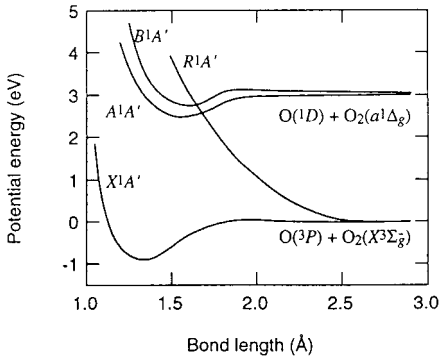

Figure 28. Approximate potential energy diagram of O_3. (Reprinted with permission from ref 290. Copyright 1993 American Institute of Physics.)

excitation and with ***J*** perpendicular to ***V***. The experimental results were reproduced assuming an impulsive dissociation from the ground-state geometry. High-resolution photofragment translational spectroscopy (PTS) was applied at 248 and 272−295 nm by Thelen et al.[292] The photofragment yield measured by PTS between 272 and 286 nm revealed a strong fluctuation on the vibrational state distribution with the dissociation wavelength.

Ozone photodissociation at the wavelengths shorter than 193 nm has attracted surprisingly little attention. Taherian and Slanger[293] studied the reaction at 157.6 nm, reporting the observation of a spin-allowed channel

$$O_3 + h\nu \rightarrow O_2\,(b^1\textstyle\sum_g^+) + O\,(^1D) \quad \lambda < 266\ \text{nm} \quad (42)$$

(the O_2 ($b^1\Sigma_g^+$) was detected by prompt emission in the 730−810 nm range), together with the dissociation into three ground-state O atoms.

There is recent interest on the following two topics, both with much relevance to the ozone-deficit problem: (1) very weak but sizable photodissociation of ozone far out to ca. 350 nm, the wavelength range hitherto believed to be unimportant to photodissociation of ozone, either due to participation of spin-forbidden channels or due to absorption by internally hot parent molecules, (2) UV photolysis of ozone to yield vibrationally hot ground-state oxygen molecules O_2 (X, $v \geq 26$) which readily react with O_2 to give O_3 + O.

First, the importance of the spin-forbidden channel

$$O_3 + h\nu \rightarrow O_2\,(X^3\textstyle\sum_g^-) + O\,(^1D) \quad \lambda < 411\ \text{nm} \quad (43)$$

in the 317−327 nm range was pointed out by Takahashi et al. of Kawasaki's group,[294,295] by Silvente et al.,[296] and by Denzer, Hancock, et al.[297] Ball, Hancock, et al.[298] directly measured the O (^{1}D) quantum yield between 300 and 328 nm using REMPI. The O (^{1}D) tail extended to at least 328 nm. Ball et al.[299] deduced from their TOF study that another spin-forbidden channel

$$O_3 + h\nu \rightarrow O_2\,(a^1\Delta_g) + O\,(^3P_j) \quad \lambda < 611\ \text{nm} \quad (44)$$

is operative at 331.52 nm. Ball et al.[300] measured the relative quantum yield of O_2 ($a^1\Delta_g$) in the 300−322 nm range at two temperatures, concluding that it is mainly due to internally excited parent for 310−319 nm and due to the spin-forbidden channel above 320 nm. O'Keefe et al. of Donovan's group[301] found the participation of

$$O_3 + h\nu \rightarrow O_2\,(b^1\textstyle\sum_g^+) + O\,(^3P_J) \quad \lambda < 463\ \text{nm} \quad (45)$$

in the 352−335 nm range.

Second, vibrational excitation of O_2 ($X^3\Sigma_g^-$) on the photodissociation of O_3 was remarked by Kinugawa et al. of Kawasaki's group[302] in the 226 nm range. They probed O (^3P_J) by REMPI−TOFMS. Vibrational excitation ($v_{av} = 12$) of the counterpart O_2 (X) was inferred. At 248 nm, Park and Slanger[303] found O_2 (X, $v = 5-22$ with a peak near $v = 8$) by quenching (with O_2) rate measurements and by LIF studies. A bimodal velocity distribution of O (^3P_J) fragment was found by photodissociation of O_3 at 226 nm by Miller, Houston, Wodtke, and co-workers.[304] The internal energy of the sibling O_2 ($X^3\Sigma_g^-$) photofragment formed in coincidence must have a bimodal distribution. Taken together with the results of pump−probe (LIF) experiments by the Wodtke's group, they demonstrated that highly vibrationally excited O_2 ($X^3\Sigma_g^-$) was produced. The vibrational distribution was bimodal with peaks at both $v = 14$ and ≥ 27. This finding is important with relevance to the ozone-deficit problem since O_2 (X, $v \geq 26$) can react rapidly with O_2 to form O_3 + O. A photofragment translational spectroscopy (PTS) study at 193 nm by Suits' group[305] revealed the production of a substantial yield (7.7%) of hot triplet states of O_2 ($X^3\Sigma_g^-$) together with 2.0% of 3O (^{3}P), 45.5% of O_2 ($a^1\Delta_g$), and 23.3% of O_2 ($b^1\Sigma_g^+$). Wilson et al. of Houston's group[306] determined speed-dependent anisotropy parameters for O_2 ($X^3\Sigma_g^-$) + O (^3P_J) products on photodissociation at 226, 230, 240, and 266 nm. At 226 and 230 nm, a strongly bimodal distribution of O ($^3P_2$) was found, in keeping with the results of Miller et al.[304] and Syage[307,308] at 226 nm and Suits et al.[291] at 193 nm. At 240 and 266 nm, however, the bimodal velocity distributions became less evident. Anisotropy parameters rise steadily as the oxygen-atom speed increases. Geiser et al. of Houston's group[309] determined the yields of O_2 product (X, $v \geq 26$) for 266, 240−226 nm.

On the theoretical side, absorption spectra, potential energy curves, and dissociation limits of several dissociation channels were calculated by Peyerimhoff and co-workers.[310] Leforestier et al.[311] presented a fully ab initio study in the Hartley band. Flöthmann, Schinke, and co-workers[312] performed time-dependent wave packet calculations employing ab initio PESs and nonadiabatic coupling elements in the Chappuis band.

N. Water H_2O—Simple Nature of the PES Makes State-to-State Photochemistry Possible

The ground state of H_2O ($\tilde{X}^1A_1$) is bent (r_e(OH) = 0.9575 Å, ∠HOH (θ_e) = 104.51°).[72] The dissociation

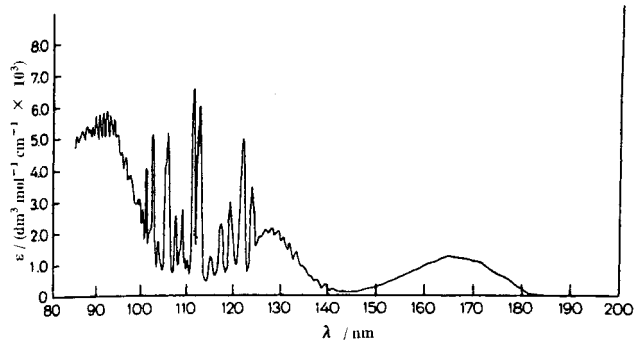

Figure 29. Absorption spectrum of H_2O. (Reprinted with permission from ref 316. Copyright 1985 Wiley VCH (Originally reprinted with permission from ref 313. Copyright 1974 Academic Press.).)

energy D_0(H−OH) is 5.118 eV (corresponding to 242 nm).[8] The absorption spectrum is shown in Figure 29.[313] Relevant electronic states are[8,314,315]

$(1a_1)^2(2a_1)^2(1b_2)^2(3a_1)^2(1b_1)^2$: ground state $\tilde{X}^1A_1$

$(1a_1)^2(2a_1)^2(1b_2)^2(3a_1)^2(1b_1)(4a_1 = 3sa_1)$:
$\tilde{A}^1B_1$ 185−140 nm (max ≈ 165 nm), bent

$(1a_1)^2(2a_1)^2(1b_2)^2(3a_1)^2(1b_1)(2b_2)$:
$^1A_2 \approx$ 135 nm (forbidden from $\tilde{X}$)

$(1a_1)^2(2a_1)^2(1b_2)^2(3a_1)(1b_1)^2(4a_1 = 3sa_1)$:
$\tilde{B}^1A_1$ 137−125 nm (max ≈ 130 nm), linear

$(1a_1)^2(2a_1)^2(1b_2)^2(3a_1)^2(1b_1)(3pa_1)$:
$\tilde{C}^1B_1 \approx$ 124 nm, bent

$(1a_1)^2(2a_1)^2(1b_2)^2(3a_1)^2(1b_1)(3pb_1)$:
$\tilde{D}^1A_1 \approx$ 121 nm, bent

Schematic potential energy curves are given in Figures 30 and 31.[315−318] The first absorption band ($\tilde{A}^1B_1 - \tilde{X}^1A_1$) is well isolated from the other bands. Between 137 and 125 nm the photodissociation proceeds directly through the $\tilde{B}^1A_1$ state. The sharper bands below 125 nm with rovibrational structure are due to $\tilde{C}^1B_1$ and $\tilde{D}^1A_1$ states.[319]

In the Ã-band photodissociation only one excited-state PES is involved. It is well isolated from higher-energy ones and strongly repulsive. The dissociation is direct (no predissociation) and prompt. This makes the photodissociation in this range one of the best understood cases. The main process is

$$H_2O\ (\tilde{A}^1B_1) \rightarrow OH\ (X^2\Pi) + H\ (^2S) \quad \lambda < 242\ \text{nm} \tag{46}$$

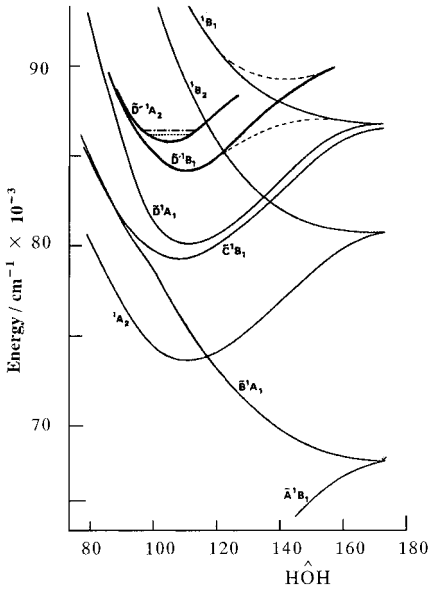

Figure 30. Schematic potential energy curves for H_2O. (Reprinted with permission from ref 316. Copyright 1985 Wiley VCH.)

The contribution of another channel

$$H_2O\ (\tilde{A}^1B_1) \rightarrow H_2\ (^1\textstyle\sum_g^+) + O\ (^1D) \quad \lambda < 177\ \text{nm} \tag{47}$$

is only minor.[8]

The simple, straightforward nature of the dynamics is clearly manifested in the photodissociation at 157 nm studied by Andresen et al.[320−323] Only the ground-state OH ($X\ ^2\Pi$) is produced. The energy disposal was that for a highly repulsive photodissociation (f_T = 0.885).[320] Very large alignment effects (strongly N-dependent) were observed, as expected from the following idea.[320,321] The transition moment $\boldsymbol{\mu}$ is perpendicular to the H_2O molecular plane. Since the probability of excitation is proportional to $|\boldsymbol{\mu}\cdot\boldsymbol{E}|^2$, the H_2O^* planes must be preferntially aligned perpendicular to the electric vector $\boldsymbol{E}$ of light. The forces acting in the dissociation lie in the H_2O^* planes, and so the $\boldsymbol{J}$ vectors of the OH must be partially aligned with $\boldsymbol{E}$. In addition, these authors found for cold H_2O a strong inversion in the Λ doublets in favor of the upper (i.e., higher in energy) Π^--component of OH, again strongly N-dependent; the unpaired electron preferentially occupies the p-lobe parallel to the OH rotation axis (perpendicular to the H_2O^* molecular plane).[322,323] This stems from symmetry constraints: the photodissociation starts from the excited state of the parent that is antisymmetric to the molecular plane.

Mikulecky et al.[324] photolyzed H_2O at 157.6 nm and detected OH ($X^2\Pi$) by LIF. The vibrational excitation was smaller than the one calculated. However, recent HRTOF results of the vibrational distribution by Hwang et al.[325] is at variance with this result. The reaction in eq 46 is reviewed by Schinke and co-workers[326,327] The simple, straightforward nature of photodissociation of H_2O in the Ã band makes it a convenient playground for the state-to-state photodissociation, as addressed in the next section (section IV.O).

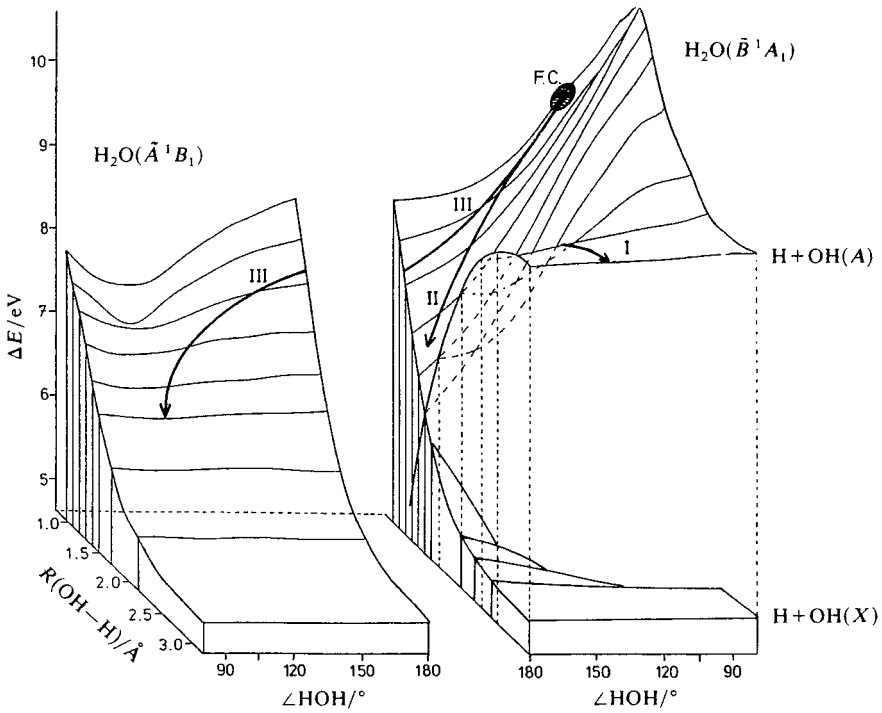

Figure 31. Three-dimensional representations of parts of PESs for the $\tilde{A}^1B_1$ and $\tilde{B}^1A_1$ states of H_2O. (Reprinted with permission from ref 317. Copyright 1986 The Royal Society of Chemistry.)

The behavior of higher excited states is rather complex. The early photodissociation studies were mostly on the OH ($A^2\Sigma^+$) emission produced by short-wavelength (<137 nm) excitation. These states produce the excited OH ($A^2\Sigma^+$) fragment by

$$H_2O\,(\tilde{B}^1A_1) \rightarrow OH\,(A^2\textstyle\sum^+) + H \quad \lambda < 135.7\ \text{nm} \tag{48}$$

together with the ground-state ($X^2\Pi$) OH fragment. The OH ($A^2\Sigma^+$) fragment was highly rotationally excited with an inverted population distribution.[328] Simons' group[314,319] studied fluorescence polarization of OH ($A^2\Sigma^+$). Then they studied rotationally resolved photofragment alignments at 121.6−130.4 nm.[329−331] They found that only $K_a' \neq 0$ or $<J_a'^2> \neq 0$ bands are effectively able to generate OH ($A^2\Sigma^+$).[331,332] This shows that "heterogeneous" predissociation from $\tilde{C}^1B_1$ to $\tilde{B}^1A_1$ is induced by Coriolis-induced *a*-axis rotation. Predissociation dynamics of the $\tilde{C}^1B_1$ state were studied using (3 + 1)-REMPI spectroscopy by Ashfold and co-workers[316,333,334] and by Kuge and Kleinermanns.[335] Comparison of the experimental spectrum with that predicted for an asymmetric top revealed that many bands were missing and the remaining ones were broadened. This is due to predissociation from a resonant intermediate state. The missing bands were those with $K_a' \neq 0$ or $<J_a'^2> \neq 0$.

Because LIF bands were diffuse due to predissociation, hydrogen-atom photofragment spectroscopy was introduced by Welge's group.[336] It proved to be a very useful means for detailed study of energy disposal in the partner OH ($A^2\Sigma^+$). At 126.2−122 nm, the OH ($A^2\Sigma^+$) were in the $v = 0$ state with a highly excited, inverted rotational distribution. This was fully addressed later by Mordaunt et al.[337] At 121.6 nm, both OH ($X^2\Pi$) and OH ($A^2\Sigma^+$) fragments were formed with little vibrational excitation but with highly inverted rotational distributions. Hwang et al.[338] proposed two different dissociation pathways to form OH ($X^2\Pi$, $v = 0$): $\tilde{B}-\tilde{X}$ conical intersection and $\tilde{B}-\tilde{A}$ Coriolis coupling. Quite recently a systematic determination of the vibrational/rotational distribution of OH/OD ($A^2\Sigma^+$) fragments was made as a function of excitation energy between 132 and 124 nm.[339]

O. Water H_2O—Bond-Selective Chemistry Is Realized by IR + UV and Vibrationally Mediated Dissociation

The simple, straightforward nature of photodissociation of H_2O in the $\tilde{A}$ band makes it a convenient playground for state-to-state photodissociation. Because the reaction starts on the repulsive PES, the quantum state preparation cannot be made on the excited state. Therefore, it is made on the ground state by IR laser excitation of to a particular rotational state within a vibrationally excited state in which a particular fundamental vibration (one quantum of either antisymmetric or symmetric stretch) is excited.

Andresen, Schinke, and co-workers[340−342] prepared H_2O molecules in a single rotational state within the *antisymmetric* stretching vibrationally excited (0,0,1) state and then photodissociated them at 193 nm. Complete characterization of product OH (rotational, Λ-doublet, and spin fine structure) was made by LIF. An increase in the population of one Λ-doublet coupled with a decrease in the population of the other, but the Λ-doublet-averaged rotational distribution was Boltzmann. The results were nicely reproduced by the Franck−Condon theory of Balint-Kurti.[343] The Franck−Condon theory essentially survived later examinations, although a small devia-

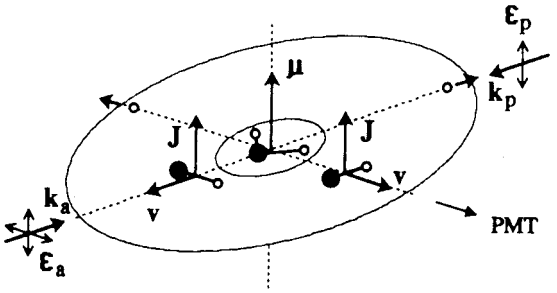

Figure 32. Vector correlation in the 193-nm photodissociation of H_2O. (Reprinted with permission from ref 346. Copyright 1993 American Chemical Society.)

tion from the theory was sometimes reported, as in the vibrational distribution of OH on excitation at 157.6 nm by Mikulecky et al.[324]

Results of 193-nm photodissociation of H_2O, prepared in particular rotational states in the fundamental *symmetric* stretch vibration (1,0,0), studied by David et al. of Rosenwaks's group,[344] were in reasonable agreement with the Franck−Condon model-based theoretical calculations. Those of Brouard et al.[345] on the 282-nm photodissociation of $|04>^-$, $|05>^-$ overtone excited molecules (see below for the notation) were also in qualitative agreement with the theory, if it is assumed that the dissociation occurred preferentially from the H−OH extended configurations. Rosenwaks' group[346−348] probed vector correlations of the OH fragments ejected from the photodissociation at 193 nm of the $J_{KaKc} = 3_{03}$ in-plane rotational state of the H_2O (1,0,0) by Doppler polarization spectroscopy (Figure 32). The results were close to the limiting values expected for an idealized orientation where the transition dipole moment of the parent ($\boldsymbol{\mu}$) is parallel to the fragment angular momentum ($\boldsymbol{J}$) and perpendicular to its velocity ($\boldsymbol{V}$). Such a simple picture stems from the shape of the Ã-state PES, on which dissociation occurs with little exit channel torque.

Crim's group used vibrational *overtone* excitation followed by another laser excitation to a dissociative state to control the pathways in molecular decomposition. They named the process vibrationally mediated photodissociation (VMP).[349−352] In the overtone excitation one can make good use of its local-mode nature; the vibrational excitation can be localized in one chemical bond, particularly in the one to be dissociated. Because the excited- and ground-state PESs approach each other for extended O−H bonds, a second photon with insufficient energy to photodissociate the ground vibrational state can dissociate the vibrationally excited molecule. The preparation of different initial vibrational states having similar energy but very different nuclear motion gave quite different vibrational distributions of the resulting OH products. While the $|04>^-$ state produced less than 1% of the OH fragment in $v = 1$, the $|13>^-$ gave a 5-fold excess of OH ($v = 1$) over OH ($v = 0$) on the 239.5-nm excitation.[350] (The notation of overtone excited states $|mn>^-$ is that of the local mode such that m and n quanta are in nonbreaking and breaking bonds, respectively. The symbols + and − are plus and minus combinations of the wave function.)

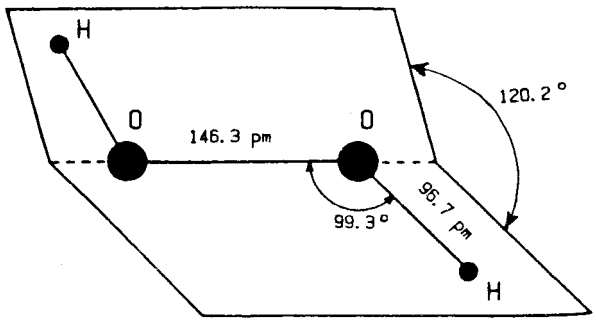

Figure 33. Molecular structutre of H_2O_2 in the ground state. (Reprinted with permission from ref 359. Copyright 1988 Wiley VCH.)

Bond-selected photodissociation of HOD was studied by Crim et al. Dissociation of HOD ($4\nu_{OH}$) with 266- or 239.5-nm photons favored O−H bond fission: it produced OD fragments with at least a 15-fold excess over OH.[350,353,354] Bar et al. of Rosenwaks' group[355,356] reported preferential O−H bond fission, favoring OD formation (the increase of OD relative to (0,0,0) was 2.5 times more than OH) by one quantum of ν_3 OH stretch of HOD on the subsequent 193-nm photodissociation.

Bond-selective dissociation is even more pronounced in the bimolecular reaction

$$H + HOD \rightarrow H_2 + OD,\ HD + OH \qquad (49)$$

Metz et al.[357] showed that excitation of $4\nu_{OH}$ and $5\nu_{OD}$ of HOD favored O−H and O−D bond breaking by a factor of ∼200 and ∼220, respectively. Preferential O−D bond breaking in the photodissociation was realized by Cohen et al.[358] by the 193-nm photolysis of HOD ($3\nu_{OD}$), in which the OH/OD branching ratio was 2.6 ± 0.5.

P. Hydrogen Peroxide H_2O_2—The Cartwheel Motion of Two OH Fragments

The ground state of H_2O_2 is nonplanar (point group C_2), as shown in Figure 33.[359] The O−O distance is 1.463 Å. The OOH angle is 99.3°. The dihedral angle between the two OOH planes is 120.2°. The O−O bond is unusually weak (the thermochemical limit corresponding to 555 nm).[360] However, the absorption band of H_2O_2 is found in the UV. It is a continuum starting near 300 nm to the beginning of a Rydberg transition.[8] The two lowest excited states, $\tilde{A}^1A$ and $\tilde{B}^1B$, are excited at 193 nm, while only $\tilde{A}^1A$ is excited at 266 or 248 nm.

At 266 and 248 nm, the reaction

$$H_2O_2(\tilde{X}^1A) + h\nu \rightarrow 2OH\ (X^2\Pi) \qquad (50)$$

gives two ground-state OH radicals. The "cartwheel" motion of two sibling OH fragments is characteristic of photodissociation of this molecule (see Figure 4). If the force acting in the dissociation event is the torsion of two OH "wheels", rotational axes of the two OH fragments will be parallel to the wheel axis (i.e., $\boldsymbol{J}//\boldsymbol{V}$). Two wheels should rotate in the same angular velocity but in the opposite direction (i.e., $N_A = -N_B$) to keep with the rule of angular momentum conservation, if no other rotation is present.

Docker et al. in Simons' group[361,362] and Klee et al. in Comes' group[363] probed OH fragments formed at 248 and 266 nm, respectively, by polarization-dependent Doppler spectroscopy. OH radicals were vibrationally and rotationally cold ($f_V + f_R = 0.11$ from $f_T = 0.89$). The high translational anisotropy ($\beta = -1$ at low N) indicated a prompt repulsion along the O−O axis. The Doppler line shapes were interpreted by $\boldsymbol{V}-\boldsymbol{J}$ correlation ($\boldsymbol{J}$ tends to be parallel to $\boldsymbol{V}$), with the fragment rotation predominantly generated by torsion about the O−O axis. At 193 nm, Grunewald et al., in Comes' group,[364,365] and Gerlach-Meyer et al.[366] and Jacobs et al.,[367] in Wolfrum 's group, found $f_T = 0.84$, $f_R = 0.16$. Rotational distributions of OH radicals are strongly inverted ($N_{peak} = 12$). Grunewald et al.[365] attributed $\beta \approx 0$ to the contribution of two excited states of the parent (62% $\tilde{A}^1A$ and 38% $\tilde{B}^1B$).

Correlations between angular momenta of coincident pairs were probed by Gericke et al. in Comes' group.[368] A strong correlation between the two rotational vectors ($|N_A| = |N_B|$)was observed for higher rotational states ($N > 10$) for 193 nm photodissociation of jet-cooled molecules. The partner molecules of species generated at low rotational states were formed in a rotational state significantly higher than expected from the above relationship. The former tendency is supported by highly positive $\boldsymbol{V}-\boldsymbol{J}$ correlation indicating preferentially parallel $\boldsymbol{V}$ and $\boldsymbol{J}$, which is only possible by the torsional motion of the OH rotors during the photodissociation act. Then conservation of angular momentum requires $N_A = -N_B$ (sibling OH must rotate in the opposite direction). For low rotational states the decrease in the $\boldsymbol{V}-\boldsymbol{J}$ correlation implied a negative correlation, corresponding to OH angular momenta perpendicular to $\boldsymbol{V}$. This can be caused by symmetric or antisymmetric bending vibration. In this case the conservation of angular momenta can be always fulfilled by the O_A-O_B rotation on the dissociation act. Later, Gericke et al.[369] probed coincidently generated pairs generated at 193 nm in a cold beam. Two OH partner radicals were formed with comparable angular momenta. For a specific rotation of one OH, the partner rotational state distribution was centered at about the same rotation with a width of only a few rotational quanta.

Near-threshold photodissociation, far out to the very weak long wavelength absorption edge (465−308 nm), was probed by Brouard et al. in Simons' group.[370] Quite contrary to the excitation to the Franck−Condon zone on the excited-state PES (266−193 nm cases), $\boldsymbol{\mu}-\boldsymbol{V}$ correlation was positive ($\beta = +1.7$ at 440−465 nm, +0.83 at 390 nm) and $\boldsymbol{V}-\boldsymbol{J}$ and $\boldsymbol{\mu}-\boldsymbol{J}$ correlations were nearly zero or slightly negative. The participating excited state was not specified, but contributions of at least two single-photon electronic transitions were suggested.

Overtone vibration-induced dissociation at the fifth overtone of the OH stretch ($6\nu_{OH}$) was studied by Rizzo et al. of Crim's group[371,372] Excitation of $6\nu_{OH}$ adds 54.2 kcal mol^{-1} (larger than the dissociation energy = 49.6 kcal mol^{-1}) to the initial thermal energy. Time evolution of OH decomposition product was monitored for $N = 9$ to $N = 1$ (0−2 μs). The excitation spectrum for the product OH showed an activity of $6\nu_{OH} + \nu_X$ in addition to $6\nu_{OH}$. The rotational distribution of OH was statistical for excitation of a purely local mode vibration ($6\nu_{OH}$) but not so for the $6\nu_{OH} + \nu_X$ excitation. Ticich et al.[373] studied overtone vibration-induced dissociation at the fourth overtone of the OH stretch ($5\nu_{OH}$). In this case the deficit of energy was supplied by initial thermal energy. Scherer et al. in Zewail's group[374,375] reported the picosecond time-resolved measurement on the overtone ($5\nu_{OH}$) initiated dissociation. The quasi-biexponential rise of OH LIF intensity was sensitive to the exact excitation wavelength.

Vibrationally mediated photodissociation (VMP) of H_2O_2 is described in the next section (section IV.Q).

Q. Vibrationally Mediated Photodissociation (VMP) of H_2O_2 and Other Molecules—Photodissociation Starting from Molecular Geometry Much Different from that in the Vibrationally Ground State

Vibrationally mediated photodissociation (VMP) as pioneered by Crim's group[376] involves the one-photon excitation to a high-energy *bound overtone* vibration state followed by another one-photon excitation to a dissociative electronic state. Vibrational overtone and UV photolysis work on C_2H_2 by Wittig's group[122] and Rosenwaks group,[123−126] VMP of HNCO by Crim's group,[200−202] and VMP of H_2O and HOD by Crim's group[349−354] are already described in the section on each molecule. VMP studies of other molecules, including H_2O_2, are addressed here.

Crim's group[376−379] applied the VMP technique to other OH-containing molecules, H_2O_2, $HONO_2$, and t-C_4H_9OOH. These molecules were excited in the region of $4\nu_{OH}$ (the third overtone of O−H stretching vibration) at 740−765 nm. A time-delayed second photon, either of the same as or different energy than the first one, dissociated the molecule. The dynamics in the VMP were substantially different from those observed for dissociation by single photons of comparable energy. In the case of H_2O_2, more than 11% of the OH fragments were vibrationally excited ($v = 1$) as compared to almost none in the single-photon UV dissociation. For t-C_4H_9OOH,[379] the VMP produced slowly recoiling fragments with substantially more energy in internal excitation, compared to the single-photon photolysis at 376 nm which gave fragments with large recoil velocities. Simons, Brouard, et al.[380−382] studied photofragment vector correlations in $4\nu_{OH}$ VMP of H_2O_2. The low value of $\beta(\boldsymbol{\mu}-\boldsymbol{V}$ correlation) was attributed, among other possibilities, to the participation of two excited states, $\tilde{A}^1A$ and $\tilde{B}^1B$, which are nearly degenerate in the O−O extended configuration that the second photon probes. Substantial values of ($\boldsymbol{V}-\boldsymbol{J}$) correlation indicated the important role played by torsional motion.

High-resolution VMP not only supplies the high-resolution spectroscopy of the intermediate overtone states, but also unravels finer details of intramolecular rotation−vibration interaction which enhances photodissociation. Brouard and Mabbs[383] reinvestigated the VMP of $4\nu_{OH}$ of H_2O_2 in jet-cooled conditions

and found the rotational state (J_{KaKc} of the intermediate overtone state) dependent photodissociation cross sections: $K_a = 1$ gave about a 10-fold increase of dissociation cross section compared to $K_a = 0$. Delocalization of the overtone state wave function into wide-amplitude O−O stretching regions of the ground state is profoundly influenced by parent molecular rotation.

Another approach to mode-selective chemistry is to selectively populate different vibrational modes in a predissociative *excited* electronic state. Bishenden and Donaldson[384] demonstrated vibrational mode selectivity in photodissociation of OClO in the Ã excited state: the ratio of OCl + O over Cl + O_2 was significantly enhanced when combination bands associated with antisymmetric stretching were excited in the OClO Ã electronic state.

Vibrational state control of photodissociation and bimolecular reaction is reviewed by Crim.[385]

R. Molecules Containing Metal and Metalloid Atoms

Molecules containing metal (or metalloid) atoms are studied partly from interest related to semiconductor technology. Beuermann and Stuke[386] photodissociated trimethylaluminum $Al_2(CH_3)_6$ in the 320−200 nm range and at 193 nm and measured by REMPI the relative yields of Al and $AlCH_3$ fragments as a function of wavelength. They[387] emphasized the important role of vibrationally excited $Al(CH_3)_2$ fragments ($Al(CH_3)_2^{\ddagger}$) which spontaneously dissociate into Al and C_2H_6. Zhang and Stuke[388] detected the AlH fragment in the dissociation of triethylaluminum and tri(*i*-butyl)aluminum at 248 and 193 nm. Beuermann and Stuke[387] indicated the important role of the $Ga(CH_3)_2^{\ddagger}$ intermediate in the dissociation (310−190 nm) of trimethylgallium. Braun, Okabe, and coworkers[389] measured quantum yields for production of CH_3 and C_2H_6 in the photodissociation of trimethylgallium at 193 nm. They found a long-lived reaction intermediate ($GaCH_3$ or $Ga(CH_3)_2$ they did not specify) absorbing at 215 and 220 nm. Sato et al.[390] photodissociated trimethylgallium in the range 227−209 nm, and wavelength-dependent relative yields of $Ga(CH_3)_3$, $Ga(CH_3)_2$, $GaCH_3$, and Ga were measured by REMPI. Dips in the yield of parent ion $Ga(CH_3)_3^+$ appeared at 220 and 216 nm (Figure 34), in agreement with the positions of absorption bands of the unidentified intermediate of Braun et al.[389] Sato et al.[390] identified the absorbing intermediate as $GaCH_3$ by comparison to the results of solid-surface photodissociation. A consistent view of photodissociation of alkylaluminum and alkylgallium emerged from these studies. Photodissociation of silane SiH_4 using synchrotron radiation by Washida et al.,[391] Suto and L. C. Lee,[392] and Itoh et al.[393] gave SiH ($A^2\Delta$). Kasatani et al.[394] and Mori et al.[395] detected CdI ($X^2\Sigma$) and ZnI ($X^2\Sigma$) by the 308-nm photodissociation of CdI_2 and ZnI_2, respectively. Kawasaki et al.[396] dissociated $Sn(CH_3)_4$ at 193 nm and found two reaction channels, $Sn(CH_3)_3 + CH_3$ and $Sn(CH_3)_2 + 2CH_3$. Photodissociation dynamics of metal-atom-containing cluster ions is discussed in the next section (section IV.S).

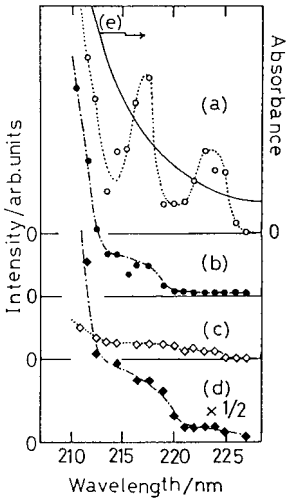

Figure 34. Dips in the wavelength-dependent yield of $Ga(CH_3)_3^+$ ions. (Reprinted with permission from ref 390. Copyright 1993 American Chemical Society.)

S. Photodissociation of van der Waals Molecules and Clusters—A van der Waals Complex Can Be Thought of as a Model of the Collision Complex in a Chemical Reaction

Binding energies of van der Waals molecules are small (typically hundreds of wavenumbers or less). Therefore, states of van der Waals molecules in which a vibrational mode in the parent moiety is excited are isoenergetic with continuum states corresponding to unbound fragments. These bound and unbound states are mixed, and the van der Waals molecules undergo vibrational predissociation. Their study can reveal the nature of various intramolecular interactions. Levy's group began such a study around 1980. In the vibronic excitation of I_2-He_n, $n = 1, 2, 3$,[397] and I_2-Ne_n,[398] vibrational predissociation product state distributions were probed. All complexes required at least one I_2 stretching quantum per rare-gas atom for dissociation. A very strong propensity to use one vibrational quantum per dissociated rare-gas atom was observed even though a single vibrational quantum contains enough energy to break several van der Waals bonds. Vibrational predissociation of ICl−Ne was probed in real time by the optical−optical double resonance technique. A vibrational predissociation lifetime between 2.3 and 50 ps was indicated by the homogeneous broadening of the ICl−Ne feature (Lester's group[399,400]). Rotational analysis of well-resolved state-to-state data of He−Cl_2 (Janda's group[401]) allowed determination of a T-shaped structure in which the He atom lies along the perpendicular bisector of the Cl−Cl bond axis. Rotational distributions of products strongly reflect the interaction potential (e.g., between ICl and Ne,[402] Cl_2 and Ar,[403] see below).

Photodissociation dynamics of metal-atom-containing cluster ions have been the target of intensive research. Both vibrational and electronic spectroscopy have been applied to the study of solvation processes in ionic clusters. Lisy and co-workers[404] examined solvation of Cs^+ in $Cs^+(CH_3OH)_n$, $n = 4-25$, by vibrational predissociation spectroscopy in conjunction with Monte Carlo simulations. Analysis

of the vibrational spectra indicated that the first solvation shell about the cesium ion consists of 10 methanol molecules. Infrared photodissociation spectra of $Ag_n(C_2H_4)_m$, $Ag_n(C_2H_4O)_m$, and $Fe_n(CH_3OH)_m$ complexes were measured by Knickelbein et al.[405,406]

Electronic spectroscopy in mass-selected clusters has also been employed for metal-containing cluster ions. Donnelly, Farrar, and co-workers[407,408] studied $Sr^+(H_2O)_n$, $Sr^+(NH_3)_n$, and $Sr^+(CH_3OH)_n$. Kleiber and Stwalley with others[409,410] studied $MgD_2^+ \rightarrow MgD^+ + D$ reaction and $MgCH_4^+ \rightarrow MgH^+ + CH_3$ and $MgCH_3^+ + H$ reactions.

For most of the van der Waals molecules of the molecule−rare-gas-atom type, the strongest electronic transition is the $\Delta v = 0$ transition. The spectral shift between the $\Delta v = 0$ band of the complex and the corresponding band of the uncomplexed substrate molecule is small, indicating that the van der Waals potential does not significantly change upon electronic excitation. However, Langridge-Smith et al. (with Levy and others)[411] found a case (NO−Ar) where the excited-state potential is shifted outward and the electronic excitation occurs to the repulsive wall of the excited-state potential leading to direct photodissociation of the complex.

In the van der Waals complexes the reactive partners have more or less fixed geometry and impact parameter (although recent spectroscopic studies have come to conclude that they are very floppy molecules). Indeed, "the direct observation of the collision complex in a chemical reaction is a long-sought-after goal since M. Polanyi's first experiment[412] designed to grasp directly the reaction dynamics", as Jouvet and Soep remarked.[413] Jouvet and Soep with others studied photodissociation of van der Waals complexes frozen in a supersonic jet.[413−417] They used complexes of mercury $Hg-Cl_2$, $Hg-N_2$, $Hg-H_2$, etc., excited at the Hg $6^3P_1-6^1S_0$ transition. In a "Harpoon-type" reaction

$$Hg-Cl_2 + h\nu \rightarrow Hg-Cl_2^*/Hg^+-Cl_2^- \rightarrow HgCl\,(B^2\Sigma^+) + Cl \quad (51)$$

they monitored the formation of the product HgCl ($B^2\Sigma^+$). Its action spectrum was very broad and structureless, extending to the red and to the blue (up to the UV cutoff corresponding to the $Hg-Cl_2^*/Hg^+Cl_2^- \rightarrow Hg\,(6^3P_1) + Cl_2$ dissociation limit (Figure 35)). In the $Hg-H_2$ case,[415−417] the action spectrum of HgH formation consisted of a continuum extending to the red of the mercury $^3P_1 \rightarrow {}^1S_0$ line, corresponding to the $^3\Pi$ ($\Omega = 0$) potential region of the complex, and of two bands appearing to the blue of the mercury line, corresponding to a slower than 3 ps dissociation from the $^3\Sigma(\Omega = 1)$ region of the complex.

Wittig et al. studied the reaction of H with a molecule under a "precursor geometry limited" conditions using van der Waals complexes such as $HBr-CO_2$,[418,419] $DBr-OCS$,[420] $DBr-CO_2$,[421] H_2S-CO_2,[422] and $HBr-N_2O$.[423] These authors[424] used CO_2-HBr, CO_2-HCl, and N_2O-HI complexes to probe the entrance channel stereospecificity of photoinitiated H-atom reactions in these weakly bonded complexes. Structures of these complexes are known. CO_2-HBr is asymmetric with the Br−C line essentially perpendicular to the CO_2 axis, and the H atom is probably located near one of the oxygen atoms, while CO_2-HCl is nearly linear with the hydrogen bonded to the oxygen. LIF detection of OH photofragments in comparison with bulk bimolecular reaction revealed a striking decrease by a factor of 60 for CO_2-HCl in going from bulk to complexed conditions, that is, the broadside H-atom approaches in CO_2-HBr complexes are greatly favored over the relatively end-on approaches of CO_2-HCl complexes (Figure 36). For the N_2O-HI complex, for which a T-shaped structure was assumed, much lower [NH]/[OH] ratios were obtained for the complex in comparison with the single-collision conditions at the same photolysis wavelength. In addition, rotational distributions of OH were markedly different between bulk and complexed conditions (the amount of rotational excitation was dramatically reduced in the case of complexed precursors), while NH rotational distributions were similar. Photoinitiated processes of the CO_2-HI complex were studied by Wittig 's group.[425,426]

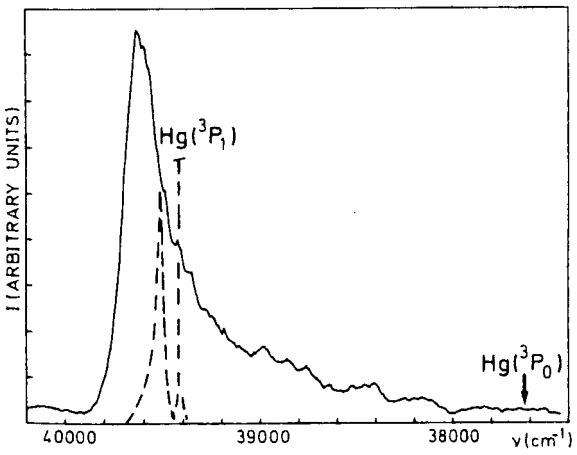

Figure 35. Action spectrum of $HgCl(B^2\Sigma^+)$ formation from $Hg-Cl_2$. (Reprinted with permission from ref 413. Copyright 1983 Elsevier Science.)

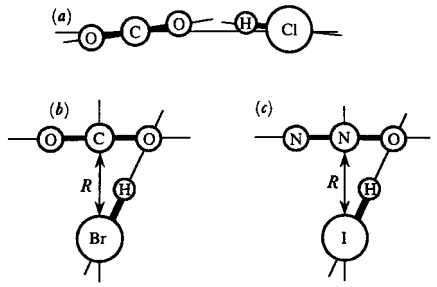

Figure 36. Photodissociation of "precursor geometry limited" conditions, $HCl-CO_2$ and $HBr-CO_2$. (Reprinted with permission from ref 424. Copyright 1990 The Royal Society.)

Honma et al.[427] studied the reaction

$$O\,(^1D) + N_2O \rightarrow 2NO \quad (52)$$

in a van der Waals molecule and compared the result with the reaction in the bulk. They prepared the O (^1D)−N_2O pair by photodissociating $(N_2O)_2$ in a molecular beam at 193 nm and detected the product NO by LIF. The vibrational distribution of NO was

bimodal, composed of cold and hot components. From isotopically labeled experiments they ascribed these components, respectively, to those originally in the $O(^1D)-N_2O$ complex and those formed by eq 52. The rotational temperature of NO formed in the reaction was very low (70−80 K), in contrast to high rotational excitation found in the bulk reaction. This was ascribed to a difference in the geometry of the $O(^1D)-N_2O$ approach in the van der Waals molecule and in the bulk reaction.

Vibrationally excited nitric oxide dimer $(NO)_2$ was studied by Casassa et al.[428] Results for the ν_1 ($v = 1$) symmetric NO stretching mode and the ν_4 ($v = 1$) antisymmetric NO stretching mode were compared, and a dramatic mode dependence of the predissociation lifetime was observed.

The photodissociation of van der Waals molecules and clusters has been reviewed by many authors.[429−434]

V. Conclusions

Investigations on the dynamics of photodissociation reactions of simple molecules have been reviewed, compiling the data on some typical molecules as well as van der Waals molecules. The coverage is from 1970 up to approximately the end of 1999.

A photodissociation reaction is a unimolecular reaction driven by light energy. It corresponds to the latter half of a bimolecular reaction, where the parent molecule in the excited state takes the role of the transition state. Photodissociation reactions occur under the constraint of energy and angular momentum conservation. On photodissociation, the available energy is distributed to various degrees of freedom, both translational and internal (electronic, vibrational, rotational). Vector correlations reveal the interrelations between many directional properties relevant to the photodissociation reaction.

Photodissociation dynamics have now become a new form of molecular spectroscopy full of detailed information on the nature of chemical bonding both in static and dynamic contexts. The nature of various intramolecular interactions, sometimes very subtle, can be unraveled through the study of the dynamics of photodissociation reactions. Such a study has also much practical relevance, such as those related to the ozone-deficit problem or the automobile exhaust gas issues, together with much significance related to astronomical (intergalactic) chemistry.

VI. Acknowledgments

The author thanks anonymous reviewers for many valuable suggestions. He is grateful to Professor J. M. Lisy, University of Illinois, for correcting and improving the English usage.

VII. Supporting Information

Tables containing more complete listings of compounds discussed in this paper. This material is available free of charge via the Internet at http://pubs.acs.org.

VIII. References

(1) Eyring, H. *J. Chem. Phys.* **1935**, *3*, 107.
(2) Evans, M. G.; Polanyi, M. *Trans. Faraday Soc.* **1935**, *31*, 875.
(3) Polanyi, J. C.; Wong, W. H. *J. Chem. Phys.* **1969**, *51*, 1439.
(4) Riley, S. J.; Wilson, K. R. *Faraday Discuss. Chem. Soc.* **1972**, *53*, 132.
(5) Kroger, P. M.; Demou, P. C.; Riley, S. J. *J. Chem. Phys.* **1976**, *65*, 1823.
(6) Pfab, J.; Häger, J.; Krieger, W. *J. Chem. Phys.* **1983**, *78*, 266.
(7) Simons, J. P. *J. Phys. Chem.* **1987**, *91*, 5378.
(8) Okabe, H. *Photochemistry of Small Molecules*; Wiley: New York, 1978.
(9) Ashfold, M. N. R.; Macpherson, M. T.; Simons, J. P. *Top. Curr. Chem.* **1979**, *86*, 1.
(10) Bersohn, R. *IEEE J. Quantum Electron.* **1980**, *QE−16*, 1208.
(11) Leone, S. R. In *Dynamics of the Excited State*; Lawley, K. P., Ed.; Advances in Chemical Physics; Wiley: New York, 1982; Vol. 50, 255.
(12) Simons, J. P. *J. Phys. Chem.* **1984**, *88*, 1287.
(13) Jackson, W. M.; Okabe, H. *Adv. Photochem.* **1986**, *13*, 1.
(14) *Faraday Discuss. Chem. Soc.*, No. 82, *Dynamics of Molecular Photofragmentation*; The Faraday Division of the Royal Society of Chemistry, 1986.
(15) Reisler, H.; Wittig, C. *Annu. Rev. Phys. Chem.* **1986**, *37*, 307.
(16) *Molecular Photodissociation Dynamics*; Ashfold, M. N. R., Baggott, J. E., Eds.; Royal Society of Chemistry: London, 1987.
(17) Schinke, R. *Photodissociation Dynamics*; Cambridge University Press: Cambridge, 1993.
(18) Butler, L. J.; Neumark, D. M. *J. Phys. Chem.* **1996**, *100*, 12801.
(19) Sato, H. *Photodissociation of Simple Molecules in the Gas Phase*; Bunshin: Mitaka, Tokyo, 1992. *Photodissociation of Simple Molecules in the Gas Phase*; Mie University Press: Tsu, 2000; Vol. II.
(20) Sato, H. *Res. Rep. Fac. Eng., Mie Univ.* **1986**, *11*, 123; **1987**, *12*, 103; **1988**, *13*, 79; **1989**, *14*, 93; **1990**, *15*, 91; **1991**, *16*, 89; **1992**, *17*, 123; **1993**, *18*, 81; **1994**, *19*, 161; **1995**, *20*, 119; **1996**, *21*, 45; **1997**, *22*, 109; **1998**, *23*, 71; **1999**, *24*, 45.
(21) Butler, L. J. *Annu. Rev. Phys. Chem.* **1998**, *49*, 125.
(22) Kash, P. W.; Waschewsky, G. C. G.; Butler, L. J.; Francl, M. M. *J. Chem. Phys.* **1993**, *99*, 4479.
(23) Brooks, P. R. *Chem. Rev.* **1988**, *88*, 407.
(24) Imre, D. G.; Kinsey, J. L.; Field, R. W.; Katayama, D. H. *J. Phys. Chem.* **1982**, *86*, 2564.
(25) Imre, D.; Kinsey, J. L.; Sinha, A.; Krenos, J. *J. Phys. Chem.* **1984**, *88*, 3956.
(26) Johnson, B. R.; Kittrell, C.; Kelly, P. B.; Kinsey, J. L. *J. Phys. Chem.* **1996**, *100*, 7743.
(27) Dantus, M.; Rosker, M. J.; Zewail, A. H. *J. Chem. Phys.* **1987**, *87*, 2395.
(28) Dantus, M.; Rosker, M. J.; Zewail, A. H. *J. Chem. Phys.* **1988**, *89*, 6128.
(29) Dantus, M.; Bowman, R. M.; Gruebele, M.; Zewail, A. H. *J. Chem. Phys.* **1989**, *91*, 7437.
(30) Butler, L. J. *Chem. Phys. Lett.* **1991**, *182*, 393.
(31) Person, M. D.; Lao, K. Q.; Eckholm, B. J.; Butler, L. J. *J. Chem. Phys.* **1989**, *91*, 812.
(32) Weaver, A.; Metz, R. B.; Bradforth, S. E.; Neumark, D. M. *J. Phys. Chem.* **1988**, *92*, 5558.
(33) Waller, I. M.; Kitsopoulos, T. N.; Neumark, D. M. *J. Phys. Chem.* **1990**, *94*, 2240.
(34) Metz, R. B.; Kitsopoulos, T.; Weaver, A.; Neumark, D. M. *J. Chem. Phys.* **1988**, *88*, 1463.
(35) Metz, R. B.; Weaver, A.; Bradforth, S. E.; Kitsopoulos, T. N.; Neumark, D. M. *J. Phys. Chem.* **1990**, *94*, 1377.
(36) Faist, J.; Capasso, F.; Sivco, D. L.; Sirtori, C.; Hutchinson, A. L.; Cho, A. Y. *Science* **1994**, *264*, 553.
(37) Zare, R.N.; Dagdigian, P. J. *Science* **1974**, *185*, 739.
(38) Ashfold, M. N. R.; Lambert, I. R.; Mordaunt, D. H.; Morley, G. P.; Western, C. M. *J. Phys. Chem.* **1992**, *96*, 2938.
(39) Busch, G. E.; Wilson, K. R. *J. Chem. Phys.* **1972**, *56*, 3638.
(40) Ashfold, M. N. R.; Mordaunt, D. H.; Wilson, S. H. S. *Adv. Photochem.* **1996**, *21*, 217.
(41) Zare, R. N. Ph.D. Thesis, Harvard University, 1964; *Mol. Photochem.* **1972**, *4*, 1.
(42) Jonah, C.; Chandra, P.; Bersohn, R. *J. Chem. Phys.* **1971**, *55*, 1903.
(43) Yang, S.-C.; Bersohn, R. *J. Chem. Phys.* **1974**, *61*, 4400.
(44) Jonah, C. *J. Chem. Phys.* **1971**, *55*, 1915.
(45) Greene, C. H.; Zare, R. N. *J. Chem. Phys.* **1983**, *78*, 6741.
(46) O'Halloran, M. A.; Joswig, H.; Zare, R. N. *J. Chem. Phys.* **1987**, *87*, 303.
(47) Dixon, R. N. *J. Chem. Phys.* **1986**, *85*, 1866.
(48) Houston, P. L. *J. Phys. Chem.* **1987**, *91*, 5388.
(49) Hall, G. E.; Sivakumar, N.; Chawla, D.; Houston, P. L.; Burak, I. *J. Chem. Phys.* **1988**, *88*, 3682.
(50) Chandler, D. W.; Houston, P. L. *J. Chem. Phys.* **1987**, *87*, 1445.
(51) Chandler, D. W.; Janssen, M. H. M.; Stolte, S.; Stickland, R. N.; Thoman, J. W. Jr.; Parker, D. H. *J. Phys. Chem.* **1990**, *94*, 4839.
(52) Thoman, J. W. Jr.; Chandler, D. W.; Parker, D. H.; Janssen, M. H. M. *Laser Chem.* **1988**, *9*, 27.
(53) Houston, P. L. *J. Phys. Chem.* **1996**, *100*, 12757.
(54) Chandler, D. W.; Parker, D. H. *Adv. Photochem.* **1999**, *25*, 59.

(55) Knee, J. L.; Khundkar, L. R.; Zewail, A. H. *J. Phys. Chem.* **1985**, *89*, 4659.
(56) Scherer, N. F.; Knee, J. L.; Smith, D. D.; Zewail, A. H. *J. Phys. Chem.* **1985**, *89*, 5141.
(57) Rosker, M. J.; Dantus, M.; Zewail, A. H. *Science* **1988**, *241*, 1200.
(58) Rosker, M. J.; Dantus, M.; Zewail. A. H. *J. Chem. Phys.* **1988**, *89*, 6113.
(59) Bernstein, R. B.; Zewail, A. H. *J. Chem. Phys.* **1989**, *90*, 829.
(60) Zewail, A. H. *J. Chem. Soc., Faraday Trans. 2* **1989**, *85*, 1221.
(61) Dantus, M.; Bowman, R. M.; Baskin, J. S.; Zewail, A. H. *Chem. Phys. Lett.* **1989**, *159*, 406.
(62) Zewail, A. H. *J. Phys. Chem.* **1993**, *97*, 12427.
(63) Zewail, A. H. *J. Phys. Chem.* **1996**, *100*, 12701.
(64) Alexander, M. H.; Andresen, P.; Bacis, R.; Bersohn, R.; Comes, F. J.; Dagdigian, P. J.; Dixon, R. N.; Field, R. W.; Flynn, G. W.; Gericke, K.-H.; Grant, E. R.; Howard, B. J.; Huber, J. R.; King, D. S.; Kinsey, J. L.; Kleinermanns, K.; Kuchitsu, K.; Luntz, A. C.; McCaffery, A. J.; Pouilly, B.; Reisler, H.; Rosenwaks, S.; Rothe, E. W.; Shapiro, M.; Simons, J. P.; Vasudev, R.; Wiesenfeld, J. R.; Wittig, C.; Zare, R. N. *J. Chem. Phys.* **1988**, *89*, 1749.
(65) Marcus, R. A. *J. Chem. Phys.* **1952**, *20*, 359.
(66) Pechukas, P.; Light, J. C. *J. Chem. Phys.* **1965**, *42*, 3281.
(67) Klots, C. E. *J. Phys. Chem.* **1971**, *75*, 1526.
(68) Marcus, R. A. *J. Chem. Phys.* **1986**, *85*, 5035.
(69) Quack, M.; Troe, J. *Ber. Bunsen-Ges. Phys. Chem.* **1974**, *78*, 240; **1975**, *79*, 170; *Int. Rev. Phys. Chem.* **1981**, *1*, 97.
(70) Wittig, C.; Nadler, I.; Reisler, H.; Noble, M.; Catanzarite, J.; Radhakrishnan, G. *J. Chem. Phys.* **1985**, *83*, 5581.
(71) Kasper, J. V. V.; Pimentel, G. C. *Appl. Phys. Lett.* **1964**, *5*, 231.
(72) *Kagaku Benran* (*Handbook of Chemistry*); Maruzen: Tokyo, 1984; Chapter 15.
(73) Pence, W. H.; Baughcum, S. L.; Leone, S. R. *J. Phys. Chem.* **1981**, *85*, 3844.
(74) Wang, P. G.; Ziegler, L. D. *J. Chem. Phys.* **1991**, *95*, 288.
(75) Mulliken, R. S. *Phys. Rev.* **1936**, *50*, 1017; *J. Chem. Phys.* **1940**, *8*, 382.
(76) Gedanken, A.; Rowe, M. D. *Chem. Phys. Lett.* **1975**, *34*, 39.
(77) Fairbrother, D. H.; Briggman, K. A.; Weitz, E.; Stair, P. C. *J. Chem. Phys.* **1994**, *101*, 3787.
(78) Baughcum, S. L.; Leone, S. R. *J. Chem. Phys.* **1980**, *72*, 6531.
(79) Sparks, R. K.; Shobatake, K.; Carlson, L. R.; Lee, Y. T. *J. Chem. Phys.* **1981**, *75*, 3838.
(80) Loo, R. O.; Haerri, H.-P.; Hall, G. E.; Houston, P. L. *J. Chem. Phys.* **1989**, *90*, 4222.
(81) Suzuki, T.; Kanamori, H.; Hirota, E. *J. Chem. Phys.* **1991**, *94*, 6607.
(82) Zahedi, M.; Harrison, J. A.; Nibler, J. W. *J. Chem. Phys.* **1994**, *100*, 4043.
(83) Eppink, A. T. J. B.; Parker, D. H. *J. Chem. Phys.* **1999**, *110*, 832.
(84) Janssen, M. H. M.; Mastenbroek, J. W. G.; Stolte, S. *J. Phys. Chem. A* **1997**, *101*, 7605.
(85) Black, J. F.; Powis, I. *Chem. Phys.* **1988**, *125*, 375.
(86) Black, J. F.; Powis, I. *Laser Chem.* **1988**, *9*, 339.
(87) Lao, K. Q.; Person, M. D.; Xayariboun, P.; Butler, L. J. *J. Chem. Phys.* **1990**, *92*, 823.
(88) Campbell, D. J.; Ziegler, L. D. *Chem. Phys. Lett.* **1993**, *201*, 159.
(89) Syage, J. A. *Chem. Phys. Lett.* **1993**, *212*, 124.
(90) Knee, J. L.; Khundkar, L. R.; Zewail, A. H. *J. Chem. Phys.* **1985**, *83*, 1996.
(91) Dantus, M.; Janssen, M. H. M.; Zewail, A. H. *Chem. Phys. Lett.* **1991**, *181*, 281.
(92) Guo, H.; Zewail, A. H. *Can. J. Chem.* **1994**, *72*, 947.
(93) Shapiro, M. *J. Phys. Chem.* **1986**, *90*, 3644.
(94) Amatatsu, Y.; Morokuma, K.; Yabushita, S. *J. Chem. Phys.* **1991**, *94*, 4858.
(95) Amatatsu, Y.; Yabushita, S.; Morokuma, K. *J. Chem. Phys.* **1996**, *104*, 9783.
(96) Lee, S. J.; Bersohn, R. *J. Phys. Chem.* **1982**, *86*, 728.
(97) Butler, L. J.; Hintsa, E. J.; Lee, Y. T. *J. Chem. Phys.* **1986**, *84.* 4104.
(98) Butler, L. J.; Hintsa, E. J.; Shane, S. F.; Lee, Y. T. *J. Chem. Phys.* **1987**, *86*, 2051.
(99) Mordaunt, D. H.; Ashfold, M. N. R. *J. Chem. Phys.* **1994**, *101*, 2630.
(100) Ingold, C. K.; King, G. W. *J. Chem. Soc.* **1953**, 2702.
(101) Innes, K. K. *J. Chem. Phys.* **1954**, *22*, 863.
(102) Foo, P. D.; Innes, K. K. *Chem. Phys. Lett.* **1973**, *22*, 439.
(103) Becker, K. H.; Haaks, D.; Schürgers, M. *Z. Naturforsch.* **1971**, *26a*, 1770.
(104) Okabe, H. *J. Chem. Phys.* **1975**, *62*, 2782.
(105) Okabe, H. *J. Chem. Phys.* **1981**, *75*, 2772.
(106) Okabe, H. *J. Chem. Phys.* **1983**, *78*, 1312.
(107) Wodtke, A. M.; Lee, Y. T. *J. Phys. Chem.* **1985**, *89*, 4744.
(108) Segall, J.; Lavi, R.; Wen, Y.; Wittig, C. *J. Phys. Chem.* **1989**, *93*, 7287.
(109) Baldwin, D. P.; Buntine, M. A.; Chandler, D. W. *J. Chem. Phys.* **1990**, *93*, 6578.
(110) Balko, B. A.; Zhang, J.; Lee, Y. T. *J. Chem. Phys.* **1991**, *94*, 7958.
(111) Segall, J.; Wen, Y.; Lavi, R.; Singer, R.; Wittig, C. *J. Phys. Chem.* **1991**, *95*, 8078.
(112) Fletcher, T. R.; Leone, S. R. *J. Chem. Phys.* **1989**, *90*, 871.
(113) Vazquez, G. J. *Nuovo Cimento* **1981**, *63B*, 446.
(114) Cool, T. A.; Goodwin, P. M.; Otis, C. E. *J. Chem. Phys.* **1990**, *93*, 3714.
(115) Hsu, Y.-C.; Chen, F.-T.; Chou, L.-C.; Shiu, Y.-J. *J. Chem. Phys.* **1996**, *105*, 9153.
(116) Hashimoto, N.; Suzuki, T. *J. Chem. Phys.* **1996**, *104*, 6070.
(117) Hashimoto, N.; Yonekura, N.; Suzuki, T. *Chem. Phys. Lett.* **1997**, *264*, 545.
(118) Wilson, S. H. S.; Reed, C. L.; Mordaunt, D. H.; Ashfold, M. N. R.; Kawasaki, M. *Bull. Chem. Soc. Jpn.* **1996**, *69*, 71.
(119) Mordaunt, D. H.; Ashfold, M. N. R.; Dixon, R. N.; Löffler, P.; Schnieder, L.; Welge, K. H. *J. Chem. Phys.* **1998**, *108*, 519.
(120) Suzuki, T.; Hashimoto, N. *J. Chem. Phys.* **1999**, *110*, 2042.
(121) Cui, Q.; Morokuma, K. *J. Chem. Phys.* **1998**, *108*, 626.
(122) Zhang, J.; Riehn, C. W.; Dulligan, M.; Wittig, C. *J. Chem. Phys.* **1995**, *103*, 6815.
(123) Arusi-Parpar, T.; Schmid, R. P.; Li, R.-J.; Bar, I.; Rosenwaks, S. *Chem. Phys. Lett.* **1997**, *268*, 163.
(124) Schmid, R. P.; Arusi-Parpar, T.; Li, R.-J.; Bar, I.; Rosenwaks, S. *J. Chem. Phys.* **1997**, *107*, 385.
(125) Arusi-Parpar, T.; Schmid, R. P.; Ganot, Y.; Bar, I.; Rosenwaks, S. *Chem. Phys. Lett.* **1998**, *287*, 347.
(126) Schmid, R. P.; Ganot, Y.; Bar, I.; Rosenwaks, S. *J. Chem. Phys.* **1998**, *109*, 8959.
(127) Sabety-Dzvonik, M. J.; Cody, R. J. *J. Chem. Phys.* **1977**, *66*, 125.
(128) Macpherson, M. T.; Simons, J. P. *J. Chem. Soc., Faraday Trans. 2* **1979**, *75*, 1572.
(129) Ling, J. H.; Wilson, K. R. *J. Chem. Phys.* **1975**, *63*, 101.
(130) Pitts, W. M.; Baronavski, A. P. *Chem. Phys. Lett.* **1980**, *71*, 395.
(131) Morse, M. D.; Freed, K. F.; Band, Y. B. *J. Chem. Phys.* **1979**, *70*, 3620.
(132) Marinelli, W. J.; Sivakumar, N.; Houston, P. L. *J. Phys. Chem.* **1984**, *88*, 6685.
(133) Nadler, I.; Mahgerefteh, D.; Reisler, H.; Wittig, C. *J. Chem. Phys.* **1985**, *82*, 3885.
(134) Black, J. F.; Waldeck, J. R.; Zare, R. N. *J. Chem. Phys.* **1990**, *92*, 3519.
(135) Kash, P. W.; Butler, L. J. *J. Chem. Phys.* **1992**, *96*, 8923.
(136) Black, J. F. *J. Chem. Phys.* **1993**, *98*, 6853; **1994**, *100*, 5392.
(137) Griffiths, J. A.; El-Sayed, M. A. *J. Chem. Phys.* **1994**, *100*, 4910.
(138) Hall, G. E.; Sivakumar, N.; Houston, P. L. *J. Chem. Phys.* **1986**, *84*, 2120.
(139) Hasselbrink, E.; Waldeck, J. R.; Zare, R. N. *Chem. Phys.* **1988**, *126*, 191.
(140) North, S. W.; Mueller, J.; Hall, G. E. *Chem. Phys. Lett.* **1997**, *276*, 103.
(141) Costen, M. L.; North, S. W.; Hall, G. E *J. Chem. Phys.* **1999**, *111*, 6735.
(142) Yabushita, S.; Morokuma, K. *Chem. Phys. Lett.* **1990**, *175*, 518.
(143) Amatatsu, Y.; Yabushita, S.; Morokuma, K. *J. Chem. Phys.* **1994**, *100*, 4894.
(144) Qian, J.; Tannor, D. J.; Amatatsu, Y.; Morokuma, K. *J. Chem. Phys.* **1994**, *101*, 9597.
(145) Nadler, I.; Pfab, J.; Reisler, H.; Wittig, C. *J. Chem. Phys.* **1984**, *81*, 653.
(146) Nadler, I.; Noble, M.; Reisler, H.; Wittig, C. *J. Chem. Phys.* **1985**, *82*, 2608.
(147) Qian, C. X. W.; Ogai, A.; Reisler, H.; Wittig, C. *J. Chem. Phys.* **1989**, *90*, 209.
(148) Khundkar, L. R.; Knee, J. L.; Zewail, A. H. *J. Chem. Phys.* **1987**, *87*, 77.
(149) Wannenmacher, E. A. J.; Lin, H.; Jackson, W. M. *J. Phys. Chem.* **1990**, *94*, 6608.
(150) North, S. W.; Hall, G. E. *J. Chem. Phys.* **1997**, *106*, 60.
(151) Huang, Y.; Barts, S. A.; Halpern, J. B. *J. Phys. Chem.* **1992**, *96*, 425.
(152) Halpern, J. B.; Jackson, W. M. *J. Phys. Chem.* **1982**, *86*, 973.
(153) Eres, D.; Gurnick, M.; McDonald, J. D. *J. Chem. Phys.* **1984**, *81*, 5552.
(154) Wu, M.; Hall, G. E. *J. Photochem. Photobiol. A: Chem.* **1994**, *80*, 45.
(155) Eng, R.; Lambert, H. M.; Fei, R.; Carrington, T.; Filseth, S. V. *Chem. Phys. Lett.* **1996**, *261*, 651.
(156) Houston, P. L.; Moore, C. B. *J. Chem. Phys.* **1976**, *65*, 757.
(157) Ho, P.; Bamford, D. J.; Buss, R. J.; Lee, Y. T.; Moore, C. B. *J. Chem. Phys.* **1982**, *76*, 3630.
(158) Debarre, D.; Lefebvre, M.; Péalat, M.; Taran, J.-P. E.; Bamford, D. J.; Moore, C. B. *J. Chem. Phys.* **1985**, *83*, 4476.
(159) Ho, P.; Smith, A. V. *Chem. Phys. Lett.* **1982**, *90*, 407.
(160) Pealat, M.; Debarre, D.; Marie, J.-M.; Taran, J.-P. E.; Tramer, A.; Moore, C. B. *Chem. Phys. Lett.* **1983**, *98*, 299.
(161) Bitto, H.; Guyer, D. R.; Polik, W. F.; Moore, C. B. *Faraday Discuss. Chem. Soc.* **1986**, *82*, 149.
(162) Polik, W. F.; Guyer, D. R.; Miller, W. H.; Moore, C. B. *J. Chem. Phys.* **1990**, *92*, 3471.

(163) Butenhoff, T. J.; Carleton, K. L.; Chuang, M.-C.; Moore, C. B. *J. Chem. Soc., Faraday Trans. 2* **1989**, *85*, 1155.
(164) Butenhoff, T. J.; Carleton, K. L.; Moore, C. B. *J. Chem. Phys.* **1990**, *92*, 377.
(165) Carleton, K. L.; Butenhoff, T. J.; Moore, C. B. *J. Chem. Phys.* **1990**, *93*, 3907.
(166) Reilly, J. P.; Clark, J. H.; Moore, C. B.; Pimentel, G. C. *J. Chem. Phys.* **1978**, *69*, 4381.
(167) Chuang, M.-C.; Foltz, M. F.; Moore, C. B. *J. Chem. Phys.* **1987**, *87*, 3855.
(168) Dulligan, M. J.; Tuchler, M. F.; Zhang, J.; Kolessov, A.; Wittig, C. *Chem. Phys. Lett.* **1997**, *276*, 84.
(169) Terentis, A. C.; Waugh, S. E.; Metha, G. F.; Kable, S. H. *J. Chem. Phys.* **1998**, *108*, 3187.
(170) Valachovic, L. R.; Tuchler, M. F.; Dulligan, M.; Droz-Georget, Th.; Zyrianov, M.; Kolessov, A.; Reisler, H.; Wittig, C. *J. Chem. Phys.* **2000**, *112*, 2752.
(171) Moore, C. B.; Weisshaar, J. C. *Annu. Rev.Phys. Chem.***1983**, *34*, 525.
(172) Green, W. H. Jr.; Moore, C. B.; Polik, W. F. *Annu. Rev. Phys. Chem.* **1992**, *43*, 591.
(173) Nesbitt, D. J.; Petek, H.; Foltz, M. F.; Filseth, S. V.; Bamford, D. J.; Moore, C. B. *J. Chem. Phys.* **1985**, *83*, 223.
(174) Green, W. H., Jr.; Chen, I.-C.; Moore, C. B. *Ber. Bunsen-Ges. Phys. Chem.* **1988**, *92*, 389.
(175) Bitto, H.; Chen, I −C.; Moore, C. B. *J. Chem. Phys.* **1986**, *85*, 5101.
(176) Chen, I.-C.; Moore, C. B. *J. Phys. Chem.* **1990**, *94*, 263.
(177) Chen, I.-C.; Moore, C. B. *J. Phys. Chem.* **1990**, *94*, 269.
(178) Kim, S. K.; Choi, Y. S.; Pibel, C. D.; Zheng, Q.-K.; Moore, C. B. *J. Chem. Phys.* **1991**, *94*, 1954.
(179) Garcia-Moreno, I.; Lovejoy, E. R.; Moore, C. B. *J. Chem. Phys.* **1994**, *100*, 8890.
(180) Garcia-Moreno, I.; Lovejoy, E. R.; Moore, C. B. *J. Chem. Phys.* **1994**, *100*, 8902.
(181) Wade, E. A.; Clauberg, H.; Kim, S. K.; Mellinger, A.; Moore, C. B. *J. Phys. Chem. A* **1997**, *101*, 732.
(182) Drabbels, M.; Morgan, C. G.; McGuire, D. S.; Wodtke, A. M. *J. Chem. Phys.* **1995**, *102*, 611.
(183) Morgan, C. G.; Drabbels, M.; Wodtke, A. M. *J. Chem. Phys.* **1996**, *104*, 7460.
(184) Yamada, K. *J. Mol. Spectrosc.* **1980**, *79*, 323.
(185) Rabalais, J. W.; McDonald, J. R.; McGlynn, S. P. *J. Chem. Phys.* **1969**, *51*, 5103.
(186) Drozdoski, W. S.; Baronavski, A. P.; McDonald, J. R. *Chem. Phys. Lett.* **1979**, *64*, 421.
(187) Okabe, H. *J. Chem. Phys.* **1970**, *53*, 3507.
(188) Brownsword, R. A.; Laurent, T.; Hillenkamp, M.; Vatsa, R. K.; Volpp, H.-R. *J. Chem. Phys.* **1997**, *106*, 9563.
(189) Zyrianov, M.; Sanov, A.; Droz-Georget, Th.; Reisler, H. *J. Chem. Phys.* **1999**, *110*, 10774.
(190) Spiglanin, T. A.; Chandler, D. W. *J. Chem. Phys.* **1987**, *87*, 1577.
(191) Spiglanin, T. A.; Chandler, D. W. *Chem. Phys. Lett.* **1987**, *141*, 428.
(192) Spiglanin, T. A.; Perry, R. A.; Chandler, D. W. *J. Phys. Chem.* **1986**, *90*, 6184.
(193) Yi, W.; Bersohn, R. *Chem. Phys. Lett.* **1993**, *206*, 365.
(194) Zhang, J.; Dulligan, M.; Wittig, C. *J. Phys. Chem.* **1995**, *99*, 7446.
(195) Brownsword, R. A.; Laurent, T.; Vatsa, R. K.; Volpp, H.-R.; Wolfrum, J. *Chem. Phys. Lett.* **1996**, *258*, 164.
(196) Zyrianov, M.; Droz-Georget, Th.; Sanov, A.; Reisler, H. *J. Chem. Phys.* **1996**, *105*, 8111.
(197) Sanov, A.; Droz-Georget, Th.; Zyrianov, M.; Reisler, H. *J. Chem. Phys.* **1997**, *106*, 7013.
(198) Zyrianov, M.; Droz-Georget, Th.; Reisler, H. *J. Chem. Phys.* **1997**, *106*, 7454.
(199) Droz-Georget, Th.; Zyrianov, M.; Reisler, H.; Chandler, D. W. *Chem. Phys. Lett.* **1997**, *276*, 316.
(200) Brown, S. S.; Metz, R. B.; Berghout, H. L.; Crim, F. F. *J. Chem. Phys.* **1996**, *105*, 6293.
(201) Brown, S. S.; Berghout, H. L.; Crim, F. F. *J. Chem. Phys.* **1997**, *107*, 8985.
(202) Berghout, H. L.; Brown, S. S.; Delgado, R.; Crim, F. F. *J. Chem. Phys.* **1998**, *109*, 2257.
(203) Klossika, J.-J.; Flöthmann, H.; Beck, C.; Schinke, R.; Yamashita, K. *Chem. Phys. Lett.* **1997**, *276*, 325.
(204) Klossika, J.-J.; Schinke, R. *J. Chem. Phys.* **1999**, *111*, 5882.
(205) Stevens, J. E.; Cui, Q.; Morokuma, K. *J. Chem. Phys.* **1998**, *108*, 1452.
(206) Kaledin, A. L.; Cui, Q.; Heaven, M. C.; Morokuma, K. *J. Chem. Phys.* **1999**, *111*, 5004.
(207) Butler, J. E.; Drozdoski, W. S.; McDonald, J. R. *Chem. Phys.* **1980**, *50*, 413.
(208) Yang, S. C.; Freedman, A.; Kawasaki, M.; Bersohn, R. *J. Chem. Phys.* **1980**, *72*, 4058.
(209) Waller, I. M.; Hepburn, J. W. *J. Chem. Phys.* **1987**, *87*, 3261.
(210) Tzeng, W.-B.; Yin, H.-M.; Leung, W.-Y.; Luo, J.-Y.; Nourbakhsh, S.; Flesch, G. D.; Ng, C. Y. *J. Chem. Phys.* **1988**, *88*, 1658.
(211) Starrs, C.; Jego, M. N.; Mank, A.; Hepburn, J. W. *J. Phys. Chem.* **1992**, *96*, 6526.
(212) Mank, A.; Starrs, C.; Jego, M. N.; Hepburn, J. W. *J. Chem. Phys.* **1996**, *104*, 3609.
(213) Baronavski, A. P.; Owrutsky, J. C. *Chem. Phys. Lett.* **1994**, *221*, 419.
(214) Farmanara, P.; Stert, V.; Radloff, W. *J. Chem. Phys.* **1999**, *111*, 5338.
(215) Okabe, H. *J. Chem. Phys.* **1972**, *56*, 4381.
(216) Lee, L. C.; Judge, D. L. *J. Chem. Phys.* **1975**, *63*, 2782.
(217) Ashfold, M. N. R.; Quinton, A. M.; Simons, J. P. *J. Chem. Soc., Faraday Trans. 2* **1980**, *76*, 905.
(218) Kawasaki, M.; Sato, H.; Kikuchi, T.; Fukuroda, A.; Kobayashi, S.; Arikawa, T. *J. Chem. Phys.* **1987**, *86*, 4425.
(219) Kawasaki, M.; Sato, H.; Kobayashi, S.; Arikawa, T. *Chem. Phys. Lett.* **1988**, *146*, 101.
(220) Douglas, A. E.; Hollas, J. M. *Can. J. Phys.* **1961**, *39*, 479.
(221) Ashfold, M. N. R.; Bennett, C. L.; Dixon, R. N. *Chem. Phys.* **1985**, *93*, 293.
(222) Rosmus, P.; Botschwina, P.; Werner, H.-J.; Vaida, V.; Engelking, P. C.; McCarthy, M. I. *J. Chem. Phys.* **1987**, *86*, 6677.
(223) McCarthy, M. I.; Rosmus, P.; Werner, H.-J.; Botschwina, P.; Vaida, V. *J. Chem. Phys.* **1987**, *86*, 6693.
(224) Ashfold, M. N. R.; Bennett, C. L.; Dixon, R. N. *Faraday Discuss. Chem. Soc.* **1986**, *82*, 163.
(225) Fuke, K.; Yamada, H.; Yoshida, Y.; Kaya, K. *J. Chem. Phys.* **1988**, *88*, 5238.
(226) Biesner, J.; Schnieder, L.; Schmeer, J.; Ahlers, G.; Xie, X.; Welge, K. H.; Ashfold, M. N. R.; Dixon, R. N. *J. Chem. Phys.* **1988**, *88*, 3607.
(227) Biesner, J.; Schnieder, L.; Ahlers, G.; Xie, X.; Welge, K. H.; Ashfold, M. N. R.; Dixon, R. N. *J. Chem. Phys.* **1989**, *91*, 2901.
(228) Ashfold, M. N. R.; Dixon, R. N.; Irving, S. J.; Koeppe, H.-M.; Meier, W.; Nightingale, J. R.; Schnieder, L.; Welge, K. H. *Philos. Trans. R. Soc. London A* **1990**, *332*, 375.
(229) Koplitz, B.; Xu, Z.; Wittig, C. *Chem. Phys. Lett.* **1987**, *137*, 505.
(230) Xu, Z.; Koplitz, B.; Wittig, C. *J. Chem. Phys.* **1989**, *90*, 2692.
(231) Mordaunt, D. H.; Ashfold, M. N. R.; Dixon, R. N. *J. Chem. Phys.* **1996**, *104*, 6460.
(232) Mordaunt, D. H.; Ashfold, M. N. R.; Dixon, R. N. *J. Chem. Phys.* **1998**, *109*, 7659.
(233) Woodbridge, E. L.; Ashfold, M. N. R.; Leone, S. R. *J. Chem. Phys.* **1991**, *94*, 4195.
(234) Loomis, R. A.; Reid, J. P.; Leone, S. R. *J. Chem. Phys.* **2000**, *112*, 658.
(235) Kenner, R. D.; Rohrer, F.; Stuhl, F. *J. Chem. Phys.* **1987**, *86*, 2036.
(236) Donnelly, V. M.; Baronavski, A. P.; McDonald, J. R. *Chem. Phys.* **1979**, *43*, 271.
(237) Haak, H. K.; Stuhl, F. *J. Phys. Chem.* **1984**, *88*, 2201.
(238) Hofzumahaus, A.; Stuhl, F. *J. Chem. Phys.* **1985**, *82*, 3152.
(239) Hofzumahaus, A.; Stuhl, F. *J. Chem. Phys.* **1985**, *82*, 5519.
(240) Kenner, R. D.; Rohrer, F.; Stuhl, F. *Chem. Phys. Lett.* **1985**, *116*, 374.
(241) Kenner, R. D.; Rohrer, F.; Browarzik, R. K.; Kaes, A.; Stuhl, F. *Chem. Phys.* **1987**, *118*, 141.
(242) Gericke, K.-H.; Theinl, R.; Comes, F. J. *J. Chem. Phys.* **1990**, *92*, 6548.
(243) McDonald, J. R.; Miller, R. G.; Baronavski, A. P. *Chem. Phys. Lett.* **1977**, *51*, 57.
(244) Baronavski, A. P.; Miller, R. G.; McDonald, J. R. *Chem. Phys.* **1978**, *30*, 119.
(245) Nelson, H. H.; McDonald, J. R. *J. Chem. Phys.* **1990**, *93*, 8777.
(246) Hawley, M.; Baronavski, A. P.; Nelson, H. H. *J. Chem. Phys.* **1993**, *99*, 2638.
(247) Chu, J.-J.; Marcus, P.; Dagdigian, P. J. *J. Chem. Phys.* **1990**, *93*, 257.
(248) Gericke, K.-H.; Haas, T.; Lock, M.; Theinl, R.; Comes, F. J. *J. Phys. Chem.* **1991**, *95*, 6104.
(249) Meier, U.; Staemmler, V. *J. Phys. Chem.* **1991**, *95*, 6111.
(250) Gericke, K.-H.; Lock, M.; Comes, F. J. *Chem. Phys. Lett.* **1991**, *186*, 427.
(251) Haas, T.; Gericke, K.-H.; Maul, C.; Comes, F. J. *Chem. Phys. Lett.* **1993**, *202*, 108.
(252) Zhang, J.; Xu, K.; Amaral, G. *Chem. Phys. Lett.* **1999**, *299*, 285.
(253) Foy, B. R.; Casassa, M. P.; Stephenson, J. C.; King, D. S. *J. Chem. Phys.* **1988**, *89*, 608.
(254) Foy, B. R.; Casassa, M. P.; Stephenson, J. C.; King, D. S. *J. Chem. Phys.* **1989**, *90*, 7037.
(255) Foy, B. R.; Cassasa, M. P.; Stephenson, J. C.; King, D. S. *J. Chem. Phys.* **1990**, *92*, 2782.
(256) Casassa, M. P.; Foy, B. R.; Stephenson, J. C.; King, D. S. *J. Chem. Phys.* **1991**, *94*, 250.
(257) Stevens, C. G.; Zare, R. N. *J. Mol. Spectrosc.* **1975**, *56*, 167.
(258) Delon, A.; Jost, R.; Lombardi, M. *J. Chem. Phys.* **1991**, *95*, 5701.
(259) Gillispie, G. D.; Khan, A. U.; Wahl; A. C.; Hosteny, R. P.; Krauss, M. *J. Chem. Phys.* **1975**, *63*, 3425.
(260) Zacharias, H.; Geilhaupt, M.; Meier, K.; Welge, K. H. *J. Chem. Phys.* **1981**, *74*, 218.

(261) Busch, G. E.; Wilson, K. R. *J. Chem. Phys.* **1972**, *56*, 3626.
(262) Slanger, T. G.; Bischel, W. K.; Dyer, M. J. *J. Chem. Phys.* **1983**, *79*, 2231.
(263) Mons, M.; Dimicoli, I. *Chem. Phys. Lett.* **1986**, *131*, 298.
(264) Mons, M.; Dimicoli, I. *Chem. Phys.* **1989**, *130*, 307.
(265) Robra, U.; Zacharias, H.; Welge, K. H. *Z. Phys. D* **1990**, *16*, 175.
(266) Miyawaki, J.; Yamanouchi, K.; Tsuchiya, S. *Chem. Phys. Lett.* **1991**, *180*, 287.
(267) Robie, D. C.; Hunter, M.; Bates, J. L.; Reisler, H. *Chem. Phys. Lett.* **1992**, *193*, 413.
(268) Miyawaki, J.; Yamanouchi, K.; Tsuchiya, S. *J. Chem. Phys.* **1993**, *99*, 254.
(269) Hunter, M.; Reid, S. A.; Robie, D. C.; Reister, H. *J. Chem. Phys.* **1993**, *99*, 1093.
(270) Reid, S. A.; Robie, D. C.; Reisler, H. *J. Chem. Phys.* **1994**, *100*, 4256.
(271) Reid, S. A.; Brandon, J. T.; Hunter, M.; Reisler, H. *J. Chem. Phys.* **1993**, *99*, 4860.
(272) Reid, S. A.; Reisler, H. *J. Chem. Phys.* **1994**, *101*, 5683.
(273) Ionov, S. I.; Brucker, G. A.; Jaques, C.; Chen, Y.; Wittig, C. *J. Chem. Phys.* **1993**, *99*, 3420.
(274) Ionov, S. I.; Davis, H. F.; Mikhaylichenko, K.; Valachovic, L.; Beaudet, R. A.; Wittig, C. *J. Chem. Phys.* **1994**, *101*, 4809.
(275) Katagiri, H.; Kato, S. *J. Chem. Phys.* **1993**, *99*, 8805.
(276) Jost, R.; Nygård, J.; Pasinski, A.; Delon, A. *J. Chem. Phys.* **1996**, *105*, 1287.
(277) Monti, O. L. A.; Dickinson, H.; Mackenzie, S. R.; Softley, T. P. *J. Chem. Phys.* **2000**, *112*, 3699.
(278) Ahmed, M.; Peterka, D. S.; Bracker, A. S.; Vasyutinskii, O. S.; Suits, A. G. *J. Chem. Phys.* **1999**, *110*, 4115.
(279) Fairchild, C. E.; Stone, E. J.; Lawrence, G. M. *J. Chem. Phys.* **1978**, *69*, 3632.
(280) Valentini, J. J.; Moore, D. S.; Bomse, D. S. *Chem. Phys. Lett.* **1981**, *83*, 217.
(281) Moore, D. S.; Bomse, D. S.; Valentini, J. J. *J. Chem. Phys.* **1983**, *79*, 1745.
(282) Levene, H. B.; Nieh, J.-C.; Valentini, J. J. *J. Chem. Phys.* **1987**, *87*, 2583.
(283) Brock, J. C.; Watson, R. T. *Chem. Phys. Lett.* **1980**, *71*, 371.
(284) Turnipseed, A. A.; Vaghjiani, G. L.; Gierczak, T.; Thompson, J. E.; Ravishankara, A. R. *J. Chem. Phys.* **1991**, *95*, 3244.
(285) Cooper, I. A.; Neill, P. J.; Wiesenfeld, J. R. *J. Geophys. Res.* **1993**, *98*, 12795.
(286) Sparks, R. K.; Carlson, L. R.; Shobatake, K.; Kowalczyk, M. L.; Lee, Y. T. *J. Chem. Phys.* **1980**, *72*, 1401.
(287) Valentini, J. J. *Chem. Phys. Lett.* **1983**, *96*, 395.
(288) Nieh, J.-C.; Valentini, J. J. *J. Phys. Chem.* **1987**, *91*, 1370.
(289) Valentini, J. J.; Gerrity, D. P.; Phillips, D. L.; Nieh, J.-C.; Tabor, K. D. *J. Chem. Phys.* **1987**, *86*, 6745.
(290) Daniels, M. J.; Wiesenfeld, J. R. *J. Chem. Phys.* **1993**, *98*, 321.
(291) Suits, A. G.; Miller, R. L.; Bontuyan, L. S.; Houston, P. L. *J. Chem. Soc., Faraday Trans.* **1993**, *89*, 1443.
(292) Thelen, M.-A.; Gejo, T.; Harrison, J. A.; Huber, J. R. *J. Chem. Phys.* **1995**, *103*, 7946.
(293) Taherian, M. R.; Slanger, T. G. *J. Chem. Phys.* **1985**, *83*, 6246.
(294) Takahashi, K.; Kishigami, M.; Matsumi, Y.; Kawasaki, M.; Orr-Ewing, A. J. *J. Chem. Phys.* **1996**, *105*, 5290.
(295) Takahashi, K.; Kishigami, M.; Taniguchi, N.; Matsumi, Y.; Kawasaki, M. *J. Chem. Phys.* **1997**, *106*, 6390.
(296) Silvente, E.; Richter, R. C.; Zheng, M.; Saltzman, E. S.; Hynes, A. J. *Chem. Phys. Lett.* **1997**, *264*, 309.
(297) Denzer, W.; Hancock, G.; Pinot de Moira, J. C.; Tyley, P. L. *Chem. Phys.* **1998**, *231*, 109.
(298) Ball, S. M.; Hancock, G.; Martin, S. E.; Pinot de Moira, J. C. *Chem. Phys. Lett.* **1997**, *264*, 531.
(299) Ball, S. M.; Hancock, G.; Pinot de Moira, J. C.; Sadowski, C. M.; Winterbottom, F. *Chem. Phys. Lett.* **1995**, *245*, 1.
(300) Ball, S. M.; Hancock, G.; Winterbottom, F. *Faraday Discuss.* **1995**, *100*, 215.
(301) O'Keeffe, P.; Ridley, T.; Wang, S.; Lawley, K. P.; Donovan, R. J. *Chem. Phys. Lett.* **1998**, *298*, 368.
(302) Kinugawa, T.; Sato, T.; Arikawa, T.; Matsumi, Y.; Kawasaki, M. *J. Chem. Phys.* **1990**, *93*, 3289.
(303) Park, H.; Slanger, T. G. *J. Chem. Phys.* **1994**, *100*, 287.
(304) Miller, R. L.; Suits, A. G.; Houston, P. L.; Toumi, R.; Mack, J. A.; Wodtke, A. W. *Science* **1994**, *265*, 1831.
(305) Stranges, D.; Yang, X.; Chesko, J. D.; Suits, A. G. *J. Chem. Phys.* **1995**, *102*, 6067.
(306) Wilson, R. J.; Mueller, J. A.; Houston, P. L. *J. Phys. Chem. A* **1997**, *101*, 7593.
(307) Syage, J. A. *J. Phys. Chem.* **1995**, *99*, 16530; (E) **1996**, *100*, 13885.
(308) Syage, J. A. *J. Chem. Phys.* **1996**, *105*, 1007.
(309) Geiser, J. D.; Dylewski, S. M.; Mueller, J. A.; Wison, R. J.; Toumi, R.; Houston, P. L. *J. Chem. Phys.* **2000**, *112*, 1279.
(310) Banichevich, A.; Peyerimhoff, S. D.; Grein, F. *Chem. Phys.* **1993**, *178*, 155.
(311) Leforestier, C.; LeQuéré, F.; Yamashita, K.; Morokuma, K. *J. Chem. Phys.* **1994**, *101*, 3806.
(312) Flöthmann, H.; Schinke, R.; Woywod, C.; Domcke, W. *J. Chem. Phys.* **1998**, *109*, 2680.
(313) Robin, M. B. *Higher excited states of polyatomic molecules*; Academic Press: NewYork, 1974.
(314) Chamberlain, G. A.; Simons, J. P. *Chem. Phys. Lett.* **1975**, *32*, 355.
(315) Theodorakopoulos, G.; Petsalakis, I. D.; Buenker, R. J.; Peyerimhoff, S. D. *Chem. Phys. Lett.* **1984**, *105*, 253.
(316) Ashfold, M. N. R.; Bayley, J. M.; Dixon, R. N.; Prince, J. D. *Ber. Bunsen-Ges.Phys. Chem.* **1985**, *89*, 254.
(317) Krautwald, H. J.; Schnieder, L.; Welge, K. H.; Ashfold, M. N. R. *Faraday Discuss. Chem. Soc.* **1986**, *82*, 99.
(318) Weide, K.; Schinke, R. *J. Chem. Phys.* **1987**, *87*, 4627.
(319) Macpherson, M. T.; Simons, J. P. *Chem. Phys. Lett.* **1977**, *51*, 261.
(320) Andresen, P.; Rothe, E. W. *J. Chem. Phys.* **1983**, *78*, 989.
(321) Andresen, P.; Ondrey, G. S.; Titze, B.; Rothe, E. W. *J. Chem. Phys.* **1984**, *80*, 2548.
(322) Andresen, P.; Ondrey, G. S.; Titze, B. *Phys. Rev. Lett.* **1983**, *50*, 486.
(323) Andresen, P. *Ber. Bunsen-Ges. Phys. Chem.* **1985**, *89*, 245.
(324) Mikulecky, K.; Gericke, K.-H.; Comes, F. J. *Chem. Phys. Lett.* **1991**, *182*, 290.
(325) Hwang, D. W.; Yang, X.; Yang, X. *J. Chem. Phys.* **1999**, *110*, 4119.
(326) Schinke, R.; Engel, V.; Hennig, S.; Weide, K.; Untch, A. *Ber. Bunsen-Ges. Phys. Chem.* **1988**, *92*, 295.
(327) Engel, V.; Staemmler, V.; Vander Wal, R. L.; Crim, F. F.; Sension, R. J.; Hudson, B.; Andresen, P.; Henning, S.; Weide, K.; Schinke, R. *J. Phys. Chem.* **1992**, *96*, 3201.
(328) Okabe, H. *J. Chem. Phys.* **1980**, *72*, 6642.
(329) Simons, J. P.; Smith, A. J. *Chem. Phys. Lett.* **1983**, *97*, 1.
(330) Simons, J. P.; Smith, A. J.; Dixon, R. N. *J. Chem. Soc., Faraday Trans. 2* **1984**, *80*, 1489.
(331) Hodgson, A.; Simons, J. P.; Ashfold, M. N. R.; Bayley, J. M.; Dixon, R. N. *Chem. Phys. Lett.* **1984**, *107*, 1.
(332) Hodgson, A.; Simons, J. P.; Ashfold, M. N. R.; Bayley, J. M.; Dixon, R. N. *Mol. Phys.* **1985**, *54*, 351.
(333) Ashfold, M. N. R.; Bayley, J. M.; Dixon, R. N. *Chem. Phys.* **1984**, *84*, 35.
(334) Ashfold, M. N. R.; Bayley, J. M.; Dixon, R. N. *Can. J. Phys.* **1984**, *62*, 1806.
(335) Kuge, H.-H.; Kleinermanns, K. *J. Chem. Phys.* **1989**, *90*, 46.
(336) Schmiedl, R.; Dugan, H.; Meier, W.; Welge, K. H. *Z. Phys. A* **1982**, *304*, 137.
(337) Mordaunt, D. H.; Ashfold, M. N. R.; Dixon, R. N. *J. Chem. Phys.* **1994**, *100*, 7360.
(338) Hwang, D. W.; Yang, X. F.; Harich, S.; Lin, J. J.; Yang, X. *J. Chem. Phys.* **1999**, *110*, 4123.
(339) Zanganeh, A. H.; Fillion, J. H.; Ruiz, J.; Castillejo, M.; Lamaire, J. L.; Shafizadeh, N.; Rostas, F. *J. Chem. Phys.* **2000**, *112*, 5660.
(340) Andresen, P.; Beushausen, V.; Hä"usler, D.; Lülf, H. W.; Rothe, E. W.*J. Chem. Phys.* **1985**, *83*, 1429.
(341) Schinke, R.; Engle, V.; Andresen, P.; Häusler, D.; Balint-Kurti, G. G. *Phys. Rev. Lett.* **1985**, *55*, 1180.
(342) Häusler, D.; Andresen, P.; Schinke, R. *J. Chem. Phys.* **1987**, *87*, 3949.
(343) Balint-Kurti, G. G. *J. Chem. Phys.* **1986**, *84*, 4443.
(344) David, D.; Strugano, A.; Bar, I.; Rosenwaks, S. *J. Chem. Phys.* **1993**, *98*, 409.
(345) Brouard, M.; Langford, S. R.; Manolopoulos, D. E. *J. Chem. Phys.* **1994**, *101*, 7458.
(346) David, D.; Bar, I.; Rosenwaks, S. *J. Phys. Chem.* **1993**, *97*, 11571.
(347) David, D.; Bar, I.; Rosenwaks, S. *J. Photochem. Photobiol. A: Chem.* **1994**, *80*, 23.
(348) Bar, I.; David, D.; Rosenwaks, S. *Chem. Phys.* **1994**, *187*, 21.
(349) Vander Wal, R. L.; Crim, F. F. *J. Phys. Chem.* **1989**, *93*, 5331.
(350) Crim, F. F.; Hsiao, M. C.; Scott, J. L.; Sinha, A.; Vander Wal, R. L. *Philos. Trans. R. Soc. London A* **1990**, *332*, 259.
(351) Vander Wal, R. L.; Scott, J. L.; Crim, F. F. *J. Chem. Phys.* **1991**, *94*, 1859.
(352) Schinke, R.; Vander Wal, R. L.; Scott, J. L.; Crim, F. F. *J. Chem. Phys.* **1991**, *94*, 283.
(353) Vander Wal, R. L.; Scott, J. L.; Crim, F. F. *J. Chem. Phys.* **1990**, *92*, 803.
(354) Vander Wal, R. L.; Scott, J. L.; Crim, F. F.; Weide, K.; Schinke, R. *J. Chem. Phys.* **1991**, *94*, 3548.
(355) Bar, I.; Cohen, Y.; David, D.; Rosenwaks, S.; Valentini, J. J. *J. Chem. Phys.* **1990**, *93*, 2146.
(356) Bar, I.; Cohen, Y.; David, D.; Arusi-Parpar, T.; Rosenwaks, S.; Valentini, J. J. *J. Chem. Phys.* **1991**, *95*, 3341.
(357) Metz, R. B.; Thoemke, J. D.; Pfeiffer, J. M.; Crim, F. F. *J. Chem. Phys.* **1993**, *99*, 1744.
(358) Cohen, Y.; Bar, I.; Rosenwaks, S. *J. Chem. Phys.* **1995**, *102*, 3612.
(359) Comes, F. J.; Gericke, K. H.; Grunewald, A. U.; Klee, S. *Ber. Bunsen-Ges. Phys. Chem.* **1988**, *92*, 273.
(360) Vaghjiani, G. L.; Turnipseed, A. A.; Warren, R. F.; Ravishankara, A. R. *J. Chem. Phys.* **1992**, *96*, 5878.

(361) Docker, M. P.; Hodgson, A.; Simons, J. P. *Chem. Phys. Lett.* **1986**, *128*, 264.
(362) Docker, M. P.; Hodgson, A.; Simons, J. P. *Faraday Discuss. Chem. Soc.* **1986**, *82*, 25.
(363) Klee, S.; Gericke, K.-H.; Comes, F. J. *J. Chem. Phys.* **1986**, *85*, 40.
(364) Grunewald, A. U.; Gericke, K.-H.; Comes, F. J. *Chem. Phys. Lett.* **1986**, *132*, 121.
(365) Grunewald, A. U.; Gericke, K.-H.; Comes, F. J. *J. Chem. Phys.* **1987**, *87*, 5709.
(366) Gerlach-Meyer, U.; Linnebach, E.; Kleinermanns, K.; Wolfrum, J. *Chem. Phys. Lett.* **1987**, *133*, 113.
(367) Jacobs, A.; Wahl, M.; Weller, R.; Wolfrum, *J. Appl. Phys. B* **1987**, *42*, 173.
(368) Gericke, K.-H.; Grunewald, A. U.; Klee, S.; Comes, F. J. *J. Chem. Phys.* **1988**, *88*, 6255.
(369) Gericke, K.-H.; Gläser, H. G.; Maul, C.; Comes, F. J. *J. Chem. Phys.* **1990**, *92*, 411.
(370) Brouard, M.; Martinez, M. T.; Milne, C. J.; Simons, J. P.; Wang, J.-X. *Chem. Phys. Lett.* **1990**, *165*, 423.
(371) Rizzo, T. R.; Hayden, C. C.; Crim, F. F. *Faraday Discuss. Chem. Soc.* **1983**, *75*, 223.
(372) Rizzo, T. R.; Hayden, C. C.; Crim, F. F. *J. Chem. Phys.* **1984**, *81*, 4501.
(373) Ticich, T. M.; Rizzo, T. R.; Dübal, H.-R.; Crim, F. F. *J. Chem. Phys.* **1986**, *84*, 1508.
(374) Scherer, N. F.; Doany, F. E.; Zewail, A. H.; Perry, J. W. *J. Chem. Phys.* **1986**, *84*, 1932.
(375) Scherer, N. F.; Zewail, A. H. *J. Chem. Phys.* **1987**, *87*, 97.
(376) Ticich, T. M.; Likar, M. D.; Dübal, H.-R.; Butler, L. J.; Crim, F. F. *J. Chem. Phys.* **1987**, *87*, 5820.
(377) Likar, M. D.; Sinha, A.; Ticich, T. M.; Vander Wal, R. L.; Crim, F. F. *Ber. Bunsen-Ges. Phys. Chem.* **1988**, *92*, 289.
(378) Likar, M. D.; Baggott, J. E.; Sinha, A.; Ticich, T. M.; Vander Wal, R. L.; Crim, F. F. *J. Chem. Soc., Faraday Trans. 2* **1988**, *84*, 1483.
(379) Likar, M. D.; Baggott, J. E.; Crim, F. F. *J. Chem. Phys.* **1989**, *90*, 6266.
(380) Brouard, M.; Martinez, M. T.; O'Mahony, J.; Simons, J. P. *Chem. Phys. Lett.* **1988**, *150*, 6.
(381) Brouard, M.; Martinez, M. T.; O'Mahony, J.; Simons, J. P. *J. Chem. Soc., Faraday Trans. 2* **1989**, *85*, 1207.
(382) Brouard, M.; Martinez, M. T.; O'Mahony, J.; Simons, J. P. *Mol. Phys.* **1990**, *69*, 65.
(383) Brouard, M.; Mabbs, R. *Chem. Phys. Lett.* **1993**, *204*, 543.
(384) Bishenden, E.; Donaldson, D. J. *J. Chem. Phys.* **1993**, *99*, 3129.
(385) Crim, F. F. *J. Phys. Chem.* **1996**, *100*, 12725.
(386) Beuermann, Th.; Stuke, M. *Appl. Phys. B* **1989**, *49*, 145.
(387) Beuermann, Th.; Stuke, M. *Chem. Phys. Lett.* **1991**, *178*, 197.
(388) Zhang, Y.; Stuke, M. *Chem. Phys. Lett.* **1988**, *149*, 310.
(389) Braun, W.; Klein, R.; Fahr, A.; Okabe, H.; Mele, A. *Chem. Phys. Lett.* **1990**, *166*, 397.
(390) Sato, A.; Tanaka, Y.; Tsunekawa, M.; Kobayashi, M.; Sato, H. *J. Phys. Chem.* **1993**, *97*, 8458.
(391) Washida, N.; Matsumi, Y.; Hayashi, T,; Ibuki, T.; Hiraya, A.; Shobatake, K. *J. Chem. Phys.* **1985**, *83*, 2769.
(392) Suto, M.; Lee, L. C. *J. Chem. Phys.* **1986**, *84*, 1160.
(393) Itoh, U.; Toyoshima, Y.; Onuki, H.; Washida, N.; Ibuki, T. *J. Chem. Phys.* **1986**, *85*, 4867.
(394) Kasatani, K.; Mori, K.; Kawasaki, M.; Sato, H. *Laser Chem.* **1987**, *7*, 95.
(395) Mori, K.; Kasatani, K.; Kawasaki, M.; Ishitani, E.; Kobayashi, M.; Shiniohara, H,; Sato, H. *J. Photochem. Photobiol., A Chem.* **1992**, *65*, 345.
(396) Kawasaki, M.; Sato, H.; Shinohara, H.; Nishi, N. *Laser Chem.* **1987**, *7*, 109.
(397) Sharfin, W.; Johnson, K. E.; Wharton, L.; Levy, D. H. *J. Chem. Phys.* **1979**, *71*, 1292.
(398) Kenny. J. E.; Johnson, K. E.; Sharfin, W.; Levy, D. H. *J. Chem. Phys.* **1980**, *72*, 1109.
(399) Drobits, J. C.; Skene, J. M.; Lester, M. I. *J. Chem. Phys.* **1986**, *84*, 2896.
(400) Drobits, J. C.; Lester, M. I. *J. Chem. Phys.* **1988**, *88*, 120.
(401) Cline, J. I.; Sivakumar, N.; Evard, D. D.; Janda, K. C. *Phys. Rev. A* **1987**, *36*, 1944.
(402) Drobits, J. C.; Lester, M. I. *J. Chem. Phys.* **1988**, *89*, 4716.
(403) Evard, D. D.; Bieler, C. R.; Cline, J. I.; Sivakumar, N.; Janda, K. C. *J. Chem. Phys.* **1988**, *89*, 2829.
(404) Draves, J. A.; Luthey-Schulten, Z.; Liu, W.-L.; Lisy, J. M. *J. Chem. Phys.* **1990**, *93*, 4589.
(405) Knickelbein, M. B. *J. Chem. Phys.* **1996**, *104*, 3517.
(406) Koretsky, G. M.; Knickelbein, M. B. *J. Chem. Phys.* **1997**, *107*, 10555.
(407) Donnelly, S. G.; Schmuttenmaer, C. A.; Qian, J.; Farrar, J. M. *J. Chem. Soc., Faraday Trans.* **1993**, *89*, 1457.
(408) Donnelly, S. G.; Farrar, J. M. *J. Chem. Phys.* **1993**, *98*, 5450.
(409) Ding, L. N.; Young, M. A.; Kleiber, P. D.; Stwalley, W. C.; Lyyra, A. M. *J. Phys. Chem.* **1993**, *97*, 2181.
(410) Cheng, Y. C.; Chen, J.; Ding, L. N.; Wong, T. H.; Kleiber, P. D.; Liu, D.-K. *J. Chem. Phys.* **1996**, *104*, 6452.
(411) Langridge-Smith, P. R. R.; Carrasquillo, E. M.; Levy, D. H. *J. Chem. Phys.* **1981**, *74*, 6513.
(412) Polanyi, M. *Z. Phys.* **1920**, *3*, 31.
(413) Jouvet, C.; Soep, B. *Chem. Phys. Lett.* **1983**, *96*, 426.
(414) Jouvet, C.; Soep, B. *J. Chem. Phys.* **1984**, *80*, 2229.
(415) Jouvet, C.; Soep, B. *Laser Chem.* **1985**, *5*, 157.
(416) Breckenridge, W. H.; Jouvet, C.; Soep, B. *J. Chem. Phys.* **1986**, *84*, 1443.
(417) Jouvet, C.; Boivineau, M.; Duval, M. C.; Soep, B. *J. Phys. Chem.* **1987**, *91*, 5416.
(418) Buelow, S.; Radhakrishnan, G.; Catanzarite, J.; Wittig, C. *J. Chem. Phys.* **1985**, *83*, 444.
(419) Radhakrishnan, G.; Buelow, S.; Wittig, C. *J. Chem. Phys.* **1986**, *84*, 727.
(420) Häusler, D.; Rice, J.; Wittig, C. *J. Phys. Chem.* **1987**, *91*, 5413.
(421) Buelow, S.; Radhakrishnan, G.; Wittig, C. *J. Phys. Chem.* **1987**, *91*, 5409.
(422) Rice, J.; Hoffman, G.; Wittig, C. *J. Chem. Phys.* **1988**, *88*, 2841.
(423) Hoffmann, G.; Oh, D.; Wittig, C. *J. Chem. Soc., Faraday Trans 2* **1989**, *85*, 1141, 1292.
(424) Shin, S. K.; Chen, Y.; Oh, D.; Wittig, C. *Philos. Trans. R. Soc. London A* **1990**, *332*, 361.
(425) Hoffmann, G.; Oh, D.; Chen, Y.; Engel, Y. M.; Wittig, C. *Isr. J. Chem.* **1990**, *30*, 115.
(426) Jaques, C.; Valachovic, L.; Ionov, S.; Böhmer, E.; Wen, Y.; Segall, J.; Wittig, C. *J. Chem. Soc., Faraday Trans.* **1993**, *89*, 1419.
(427) Honma, K.; Fujimura, Y.; Kajimoto, O.; Inoue, G. *J. Chem. Phys.* **1988**, *88*, 4739.
(428) Casassa, M. P.; Stephenson, J. C.; King, D. S. *J. Chem. Phys.* **1988**, *89*, 1966.
(429) Celii, F. G.; Janda, K. C. *Chem. Rev.* **1986**, *86*, 507.
(430) Vaida, V.; Donaldson, D. J.; Sapers, S. P.; Naaman, R.; Child, M. S. *J. Phys. Chem.* **1989**, *93*, 513.
(431) Miller, R. E. *J. Phys. Chem.* **1986**, *90*, 3301.
(432) Buelow, S.; Noble, M.; Radhakrishnan, G.; Reisler, H.; Wittig, C.; Hancock, G. *J. Phys. Chem.* **1986**, *90*, 1015.
(433) Shin, S. K.; Chen, Y.; Nickolaisen, S.; Sharpe, S. W.; Beaudet, R. A.; Wittig, C. *Adv. Photochem.* **1991**, *16*, 249.
(434) Takayanagi, M.; Hanazaki, I. *Chem. Rev.* **1991**, *91*, 1193.

CR990403L